Design and Analysis of Fiber-optic Mach-Zehnder Interferometers for Highly Sensitive Refractive Index Measurement

by

Vahid Ahsani

M.Sc., Aachen University of Applied Sciences, 2013
B.Sc., Azad University-Mashhad Branch, 2009

A Dissertation Submitted in Partial Fulfillment of
the Requirements for the Degree of

DOCTOR OF PHILOSOPHY

in the Department of Mechanical Engineering

Supervisory Committee

Design and Analysis of Fiber-optic Mach-Zehnder Interferometer for Highly Sensitive Refractive Index Measurement

by

Vahid Ahsani

M.Sc., Aachen University of Applied Sciences, 2013

B.Sc., Azad University-Mashhad Branch, 2009

Supervisory Committee

Dr. Colin Bradley, Department of Mechanical Engineering, University of Victoria
Supervisor

Dr. Peter Wild, Department of Mechanical Engineering, University of Victoria
Departmental Member

Dr. Tao Lu, Department of Electrical and Computer Engineering, University of Victoria
Outside Member

Dr. Martin B. G. Jun, School of Mechanical Engineering, Purdue University
Additional Member

Abstract

Supervisory Committee

Dr. Colin Bradley, Department of Mechanical Engineering, University of Victoria
Supervisor
Dr. Peter Wild, Department of Mechanical Engineering, University of Victoria
Departmental Member
Dr. Tao Lu, Department of Electrical and Computer Engineering, University of Victoria
Outside Member
Dr. Martin B. G. Jun, School of Mechanical Engineering, Purdue University
Additional Member

The development of reliable, affordable, and efficient sensors is a key step forward in providing tools for efficient monitoring of critical environmental parameters. Fiber-optic sensors are already widely used in various industrial sensing fields. They have proven themselves reliable in harsh environments and can measure different physical quantities, such as temperature, pressure, strain, refractive index (RI), and humidity. Fiber-optic Mach-Zehnder Interferometer (MZI) is a well-studied optical fiber interferometer that has proven capacity for sensing ambient refractive index.

In this dissertation, we present Fiber Bragg grating (FBG) embedded in a microfiber Mach-Zehnder Interferometer designed for sensing temperature and refractive index. The MZI is constructed by splicing a short length of 40-μm-diameter microfiber between standard single mode fibers. A one-millimeter-long FBG is then written in the microfiber using a direct, point-by-point, ultrafast laser inscription method. The microfiber MZI shows only moderate sensitivity to ambient refractive index and temperature changes. In contrast, the microfiber FBG is insensitive to ambient refractive index change, while it exhibits typical sensitivity to temperature variation. These distinct characteristics of the FBG and MZI sensors enable the simultaneous measurement of refractive index and temperature as well as

temperature compensation in ambient refractive index measurement.

Further, we report the use of a fiber-optic Mach-Zehnder Interferometer to measure core refractive index changes written by femtosecond laser irradiation. The core-offset interferometer was constructed by splicing a lightly misaligned stub of standard single-mode fiber between the device's lead-in and lead-out optical fibers. When the core refractive index of an in-fiber interferometer is altered, that process changes the phase of the core light. Since the phase of light propagating in the cladding (reference arm) remains unchanged, the transmission fringe pattern of the interferometer undergoes a spectral shift. In the present research, that spectral shift was used to quantify the effective core refractive index change in a standard single-mode fiber.

In addition, we designed and developed a custom flame-based tapering machine that is used to fabricate miniaturized Mach–Zehnder interferometers (MZIs) using sharply tapered photonic crystal fiber (PCF). This technique produces sensors capable of highly sensitive ambient refractive index (RI) measurements. The sensor is fabricated by fusion splicing a small stub of PCF between standard single-mode fibers with fully collapsed air holes of the PCF in a splicing region. Tiny flame geometry enables the sharp tapering of the PCF, resulting in a short fiber length and high RI sensitivity. It appears that sharp tapering has a great impact on RI sensitivity enhancement, when compared with methods that decrease taper waist diameter. The tapering technique is further used to construct the Mach-Zehnder Interferometer-based fiber-optic refractive index (RI) sensor by uniformly tapering standard single mode fibers (SMF) for RI measurement. The fabricated MZI device does not require any splicing of fibers and shows excellent RI sensitivity.

Table of Contents

List of Tables

List of Figures

List of Abbreviations and Symbols

Abbreviation or Symbol	Definition
SMF	Single Mode Fiber
FBG	Fiber Bragg Grating
LPG	Long Period Grating
MZI	Mach-Zehnder Interferometer
RI	Refractive Index
PCF	Photonics Crystal Fiber
TOF	Tapered Optical Fiber
FPI	Fabry-Perot interferometer
MI	Michelson Interferometer
MNF	Micro or Nanofiber
RIU	Refractive Index Unit
TDW	Taper Waist Diameter
OPD	Optical Path Difference
CCD	Charge-coupled Device
RIP	Refractive Index Profile
RNF	Refracted Near-field
DIC	Differential Interference Contrast
CT	Computerized Tomography
SPR	Surface Plasmon Resonance
CAD	Computer Aided Design
FWHM	Full Width at Half Maximum
HC-PCF	Hollow Core Photonic Crystal Fiber

Acknowledgments

In this acknowledgement I would like to gratefully thank all people who helped me to complete this dissertation.

First and foremost, I would like to express my deep and sincere gratitude to my supervisors Dr. Colin Bradley and Dr. Martin B.G. Jun for their continuous support, patience, motivation, enthusiasm, and friendly help in various ways. It was a great privilege and honor to work and study under their supervisions.

I would also like to thank my committee members, Dr. Peter Wild and Dr. Tao Lu for letting my defense be an enjoyable moment, and for their brilliant comments and suggestions.

I would also like to thank my dear friends and colleagues in the Laboratory of Advanced Multi-scale Manufacturing (LAMM), Dr. Farid Ahmed, Kaveh Nazeri, Yonghyun Cho, Dr. Ahmad Esmailirad, Dr. Mohammad Pelaschi, Dr. Vahid Moradi, Dr. Max Rukosuyev, and many others. Their company, advice and friendship helped me to confront the challenges and difficulties faced during my PhD.

I want to especially express my deepest sense of gratitude to my mother for her lifetime support, sacrifices, encouragement and love, to my father who was always there for me and inspired me with his strength, hard work, and energy and to my brother Dr. Vesal Ahsani for all the great moments we have had through these times. Words cannot express how much I love them and how grateful I am for their support.

Finally, most importantly, I would like to express the profound gratitude from my deep heart to my beloved wife, Golnaz, and our lovely daughter Asal. I could never have

accomplished my PhD without their wonderful support, encouragement, quiet patience, and continued love. Golnaz has been extremely supportive of me throughout entire life and has made countless sacrifices to help me get to this point.

Dedication

To my wonderful and lovely mother and father for always supporting, helping, guiding, unconditionally loving, and standing by me. Without your guidance and love I would not be the man I am.

To my best friend and beloved wife Golnaz for all of her love and supports. I am forever thankful for having you in my life.

To my precious baby, Asal: I hope my work inspires you on day. I want nothing in the world but your long life, happiness and prosperity. Your presence in my life is the best thing that has happened to me.

Chapter 1 Introduction

Fiber-optic sensors have absorbed a lot of attention as a hot research topic since low loss optical fibers were first introduced in the 1960s. Because of their outstanding properties such as compact structure, low loss, immunity to electromagnetic waves, and wide bandwidth, fiber-optic devices have been extensively used in numerous fields ranging from optical sensing to optical communication [1]. Over the past several decades, various types of fiber-optic structures were investigated with the help of development of sophisticated optical fiber fabrication techniques. Others include fiber Bragg grating (FBG), long period grating (LPG), and photonic crystal fiber (PCF), as well as more targeted structures such as tapered optical fiber (TOF), side polished fibers, interference devices and rare earth doped fibers [2].

Fiber-optic refractive index (RI) sensors have been found as a reliable sensor for chemical and biochemical monitoring applications over the past couple of years [3, 4] due to their interesting characteristics such as: small size, high-resolution detection, excellent aging characteristics, ability to operate in chemically hazardous environments, and immunity to electromagnetic noise. Gratings and interferometers are the two main configurations studied for fiber-optic RI sensing [5]. Fiber gratings are usually fabricated by modifying the refractive index (RI) along the fiber axis. Various approaches have been developed to manufacture them: to name two, the phase mask technique and the point-by-point technique [6-8]. Although fiber gratings show numerous unique properties such as compact size, wavelength selectivity, and developed fabrication

technique, they have their own limitations, especially for high-precision sensing measurement [2]. Inscribed gratings could be damaged if the sensor works at high temperature, so industrial application is limited. Long period gratings (LPGs) are one of the broadly used RI sensors [9-13]. Writing gratings are usually expensive and function only in narrow wavelength bands due to fiber gratings phase matching phenomenon. Thus, in-fiber interferometers such as Fabry-Perot interferometer (FPI), Michelson interferometer (MI), and Mach-Zehnder interferometer (MZI) have been introduced as alternative and viable approaches for RI sensing [14]. Also, the combination of interferometers and gratings has been reported in the literature; for instance, MZI has been constructed based on a pair of LPGs to increase RI sensitivity further [14, 15]. Additionally, to increase sensing performance, research based on an integration of fiber grating structures, interferometers, and fiber taper techniques has been reported [15-18].

Compared with the abovementioned typical fiber structures, tapered optical fibers (TOF) can offer the following interesting features such as large evanescent field, strong mode confinement capability, and extra small diameter. Thus, TOFs show great potential in measurement of ambient RI [19, 20]. Initially, tapered optical fibers were used for the development of directional couplers. Two or more tapers are fused together, as they provide efficient light coupling between fibers [21]. Lately, tapered optical fibers have also found applications in sensor development [22], polarizers, submicron wire [5], light amplifiers [23], and near and far field microscopy [24].

Different types of tapering machines have been developed and investigated over the last two decades [25, 26]. They are mainly categorized into arc-based [27-29], laser-based [30, 31], and flame-based machines [32-34]. Each design has its own advantages

and disadvantages. Arc and laser machines can provide a minuscule and fixed heating volume, which leads to a small tapering region, thus limiting fabrication of different sensor configurations [28, 29]. Heating the fiber with a laser beam is neither easy nor cheap [31, 35]. Another limitation with arc and laser-based tapering machines is temperature measurement and control [26, 36], which is a crucial parameter for an adiabatic tapering. To make an adiabatically tapered fiber and reduce the amount of losses, perfect control over the generated heat is required [37]. The temperature of the heating volume can be measured by a thermocouple with excellent accuracy when heated by torch [38]; however, this simple measurement is not feasible in arc or laser-based tapering machines [27, 39]. Another specific limitation of CO_2 laser-based tapering machines is the complexity of directly heating the fiber when its diameter is less than 1 µm because of the inverse square relationship between fiber radius and heating for a CO_2 laser [40]. This issue can be resolved by using a flame as a heat source, which has an inverse relationship with fiber radius. Thus fibers can be tapered down to smaller diameters with flame-based tapering machines [41, 42]. Controlling the temperature gradient and fiber geometry are the challenges when tapering fibers below 1 µm, due to the turbulence of the flame and convection [19]. It is even more challenging when miniature tapering with a flame smaller than 1 mm or tapering using oscillating flame is performed than a time arc or laser-based tapering machines are used [40].

There are three main configurations in which flame-based tapering machines are typically set up for optical micro or nanofiber (MNF) fabrication: (i) Stacked pulling stages with a fixed flame [34], (ii) independent pulling stages with a fixed flame [43], and (iii) independent pulling stages and an oscillating flame [33, 44]. The idea of

designing a custom flame-based tapering machine based on independent pulling stages with fixed flames were considered to be able to fabricate RI sensors with better sensing performances. Thus, a dual flame-based tapering system with micro-scale nozzles was designed and developed. A shutter mechanism with millisecond-scale actuation time was integrated into the system to provide better control over the heat transferred to the optical fiber.

This research started with the design and fabrication of an optical fiber sensor capable of simultaneously measuring RI and temperature [45]. Since MZIs are widely used as RI sensors in various industries, it is critical to ensure that the measurement of the RI change using an MZI sensor is accurate. Therefore, the inevitable problem of temperature and refractive index cross-sensitivity of MZI sensors were considered. The proposed MZI was fabricated by fusion splicing a stub of single mode microfiber between two standard SMFs. A femtosecond laser was then used to inscribe the Fiber Brag Grating (FBG), employing point-by-point inscription method to attain the required refractive index modulation in the fiber core. The constructed sensor was not only capable of measuring RI or temperature but also could measure temperature compensated RI changes [45].

Since Femtosecond laser was used in the first research study, and core index modulation was done to fabricate FBG on microfiber, the question of how much in-fiber refractive index change occurred during FBG fabrication remained unanswered. Therefore, the idea of using fiber-optic MZI sensors to measure the effective refractive index change in the core of SMF was examined for the first time [46]. A stub of single mode fiber was spliced between two SMFs with a slight lateral offset to enable splitting and recombining of a light. This produced a Mach-Zehnder Interferometer (MZI). The

fringe shift of the MZI, due to the fiber core refractive index alteration caused by femtosecond laser pulses was used for measurement of effective refractive index change inside the core of the single mode fiber.

The research continued with a focus on fabrication of MZI with enhanced RI sensitivity. Therefore, the potential for integrating photonic crystal fibers (PCFs) with optical fiber tapering technique was investigated. Thus, tapered PCF-based MZI sensors that revealed high ambient RI sensitivity were proposed [47]. With the help of the customized flame-based tapering machine, a short length of a PCF (3.88 mm) was sharply tapered from 125 µm to 65 µm. The fabricated sensor presented an RI sensitivity of ~1427 nm/RIU in the RI range of 1.3900 to 1.4200. In contrast, another PCF-based MZI sensor with the PCF length of 8 mm was tapered adiabatically from 125 µm to 50 µm. This sensor showed an RI sensitivity of ~ 990 nm/RIU in the similar RI range. Therefore, a compact yet highly sensitive PCF-based MZI refractive index sensor was constructed [47].

In continuation of developing MZI for sensing ambient RI changes, the fabrication of simple, inexpensive, and yet ultra-high sensitivity RI sensor was investigated. The design and fabrication of an MZI refractive index sensor with a standard single mode fiber using the custom flame-based tapering machine was presented [48]. The tapering machine was controlled such that sharp taper transitions and a uniform long taper waist in an SMF were formed to construct the Mach-Zehnder Interferometer. A maximum RI sensitivity of 4234 nm/RIU was attained in the RI range of 1.4204 to 1.4408 for a taper waist diameter (TWD) 35.5 µm and taper waist length of 19.8 mm.

1.1. Dissertation Outline

This dissertation includes the current introductory chapter that provides the context and framework to link the following Chapters in accordance to research and background information. This dissertation consists of four papers that have already been published in different peer-reviewed journals, and so far cited by other researchers more than 50 times. Information on each publication is located at the beginning of each chapter.

Chapter two presents the research and development of an optical fiber sensor for simultaneous measurement of an ambient refractive index and temperature changes. The proposed sensor was constructed with Fiber Bragg Grating (FBG) embedded in a microfiber Mach-Zehnder Interferometer. The fabricated sensor can be characterized for use in an environment where refractive index and temperature are changing, so that each variable can be measured separately.

Chapter three focusses on the studying and finding a measurement technique to measure the amount of in-fiber refractive index change during the ultrafast laser irradiation on the core of an optical fiber. Ultrafast laser is widely used for fabrication of Long Period Grating (LPG) or Fiber Bragg Grating (FBG). A fiber-optic Mach-Zehnder interferometer (MZI) device was used to measure the effective refractive index change in the core of a standard SMF during the index modification performed by a 120 femtosecond laser.

Chapter four details the fabrication techniques used to create a miniaturized Mach-Zehnder Interferometer using sharply tapered photonic crystal fiber (PCF) for ambient refractive index measurement. The custom flame-based tapering machine was presented and its unique fabrication capabilities were discussed. The fabricated compact MZI

sensor exhibited a high RI sensitivity of about 1426 nm/RIU within the RI range of 1.3917 to 1.4204. The chapter further discusses the effect of sharply tapering PCF in comparison to a smooth and adiabatic tapering.

Chapter five illustrates the continuation of the research toward improving the sensitivity of the MZIs for ambient refractive index measurement. Fabrication of an MZI using one standard single mode fiber without any fusion splicing is shown. The unique properties of the custom fame-based tapering machine essential for fabrication of the ultra-high sensitivity MZI based RI sensor are presented.

Finally, Chapter six summarizes the main results and contributions of the present research work and also suggests directions for possible future research.

1.2. Research Contributions

The presented research in this dissertation shows a gradual development in fabrication techniques used to produce highly sensitivity fiber-optic Mach-Zehnder Interferometers for ambient refractive index sensing. The main objectives of the research work were to focus on inexpensive, simple, highly sensitive, reliable, accurate, repeatable, and custom manufacturing techniques for fabricating fiber-optic MZI sensors that measure RI changes. The main contributions of this dissertation are summarized as follows:

1. After reviewing existing tapering machines, and in particular flame-based ones [40], the parameters were defined for designing and developing a unique and inexpensive flame-based tapering machine, which has the capability to taper optical fibers with wider ranges of taper lengths than has been previously achieved. The machine was designed to enable simple nozzle exchange, and various micro

nozzles were designed and laser-machined to have different flame sizes. Moreover, a novel flame shutter mechanism was designed and integrated into the system to provide excellent accuracy in the geometry of tapered profile when tapering very short lengths of fiber. The current design of the machine provides the capacity for adiabatic and uniform tapering of optical fibers with a broad range of lengths (from 0.8 mm to a couple of centimeters).

2. This research sought to design and fabricate a fiber-optic sensor that concurrently measures RI and temperature changes with moderate sensitivity, while keeping the sensor package compact, robust, and cost-effective. An MZI sensor with an embedded Fiber Brag Grating on a 4 mm microfiber with a diameter of 40 μm was fabricated and characterized for simultaneous RI and temperature sensing.
3. Having studied the design of a compact and highly sensitive RI sensor, I then considered possibilities for combining alternative fiber-optic material into an MZI configuration. Also, I wanted to utilize the designed tapering machine to further enhance the RI sensitivity of the fabricated RI sensor. The custom tapering machine was controlled so that a short length (3.8 mm) of photonic crystal fiber was tapered with a sharp tapering angle (from 125 μm to 65 μm in diameter). This process generated an MZI sensor with RI sensitivities of 334.03 nm/RIU, 673.91 nm/RIU, and 1426.70 nm/RIU within the RI ranges of 1.3327 to 1.3634, 1.3634 to 1.3917, and 1.3917 to 1.4204, respectively.
4. The research outline above raised the question of how to quantify the amount of RI index modulation on the core of standard single mode fiber (SMF) during the laser irradiation process. A basic MZI device seemed a promising solution, and

one was constructed using a stub of an SMF spliced with a slight lateral offset between two SMFs. On the core of standard single mode fiber, several identical small sections of the fiber core within the MZI were scanned with different pulse energies to study the influence of femtosecond laser pulse energy, which can be used for FBG and LPG fabrication. For the first time, the amount of gradual spectral shift in the MZI signal was considered as a means for quantifying the laser pulse energy and, thus, the effective refractive index change on the fiber core.

5. Research on fabricating ultra-high sensitivity RI sensors for the measurement of ambient refractive index changes has advanced through this project. It successfully investigated the idea of controlling a tapering machine so that it can produce an MZI sensor using a standard single mode fiber. This process results in low levels insertion loss, requires low cost, and produces mechanically robust and easy to fabricate sensors. The best sensors fabricated showed the remarkable RI sensitivity of 4234 nm/RIU in the RI range of 1.4204 to 1.4408.

Chapter 2 Bragg Grating Embedded in Mach-Zehnder Interferometer for Refractive Index and Temperature Sensing

This paper was published in Journal of IEEE Photonics Technology Letters in 2016.

Farid Ahmed, Vahid Ahsani, Akram Saad, and Martin B. G. Jun. "Bragg Grating Embedded in Mach-Zehnder Interferometer for Refractive Index and Temperature Sensing", IEEE PHOTONICS TECHNOLOGY LETTERS, VOL. 28, NO. 18, SEPTEMBER 15, 2016.

Abstract

Fiber Bragg grating (FBG) embedded in a microfiber Mach-Zehnder interferometer (MZI) is presented for sensing multi-parameters such as temperature and refractive index. The MZI is constructed by splicing a short length of 40 μm diameter microfiber between standard single mode fibers. A millimeter long FBG is then written in the microfiber using direct point-by-point ultrafast laser inscription method. The microfiber MZI shows moderate sensitivity to ambient refractive index and temperature changes. In contrast, the microfiber FBG is insensitive to ambient refractive index change while it exhibits typical sensitivity to temperature variation. These distinct characteristics of the FBG and MZI sensors enable simultaneous measurement of refractive index and temperature, and temperature compensation in ambient refractive index measurement.

2.1 Introduction

Measurement of ambient temperature and refractive index (RI) is crucial to many in-situ environmental monitoring applications. Temperature cross-sensitivity in fiber-optic sensors may lead to incorrect quantification of ambient RI. It is therefore essential to

measure both temperature and RI simultaneously and unambiguously. Novel fiber-optic measurement systems have been constantly offered to achieve application specific quantification of these parameters. Interferometric fiber-optic sensors have been widely studied due to their excellent RI sensitivity and moderate temperature sensitivity [49, 50]. Diverse Mach-Zehnder interferometers are constructed using structures such as core offset [51, 52], tapered fiber [53], and multimode microfiber [54] for simultaneous measurement of temperature and RI. Various configurations of MZI combined with fiber Bragg grating have also been explored to measure ambient refractive index and temperature simultaneously, including peanut-shape and core-offset structure [55], and only core-offset MZI [56]. Formation of MZI has also been illustrated using a pair of long period gratings [57] and splicing a piece of photonic crystal fiber between single mode fibers [58]. However, extended sensor length reported in some work may provide inaccurate sensing location and is undesirable in concurrent measurement of parameters.

Miniaturization of optical sensors is highly desirable in point-sensing of temperature and RI. Direct inscription of miniature FBG in microfiber is presented recently for enhanced temperature sensitivity [59]. A compact femtosecond laser micromachined cavity in single mode fiber is proposed to form a MZI for sensing ambient RI [60]. A miniature MZI embedded in fiber Bragg grating is also reported for simultaneous RI and temperature measurement [61]. Although the sensor demonstrates good sensitivity, the fragile structure and fabrication complexity make it difficult for many applications. Besides, it is challenging to remove solution residue from the narrow in-fiber cavity and reuse the sensor without hassle. In general, the key sensing characteristics such as moderate RI and temperature sensitivity, compactness, and robustness are hard to

achieve simultaneously.

In this study, we present an in-fiber sensor that incorporates a 1 mm long FBG in a 4 mm long MZI structure for measurement of both RI and temperature. The MZI is constructed by simply fusion splicing a single mode microfiber between standard SMFs. Pulsed femtosecond laser radiation is then used to inscribe the FBG employing point-by-point inscription method to achieve desired index modulation in fiber core. Because of inherent good RI sensitivity of MZI [60, 62] and RI insensitivity of FBG, while both are moderately sensitive to temperature, a simultaneous and unambiguous RI and temperature measurement can be achieved. The sensor is also used to demonstrate temperature compensated ambient RI measurement.

2.2 Sensor Fabrication

Fabrication schematic of the combined MZI and FBG sensor is shown in Figure 2.1. The MZI structure was fabricated by splicing a stub of single mode microfiber (core diameter: 3.75 μm, cladding diameter: 40 μm) between two standard SMFs as shown in Figure 2.2. The Fujikura (FSM 40PM) fusion splicer was used to splice standard SMF to microfiber with an arc power of 5 bit exposed for 1000 millisecond. Afterward, a FBG was inscribed in the microfiber using a femtosecond pulsed laser.

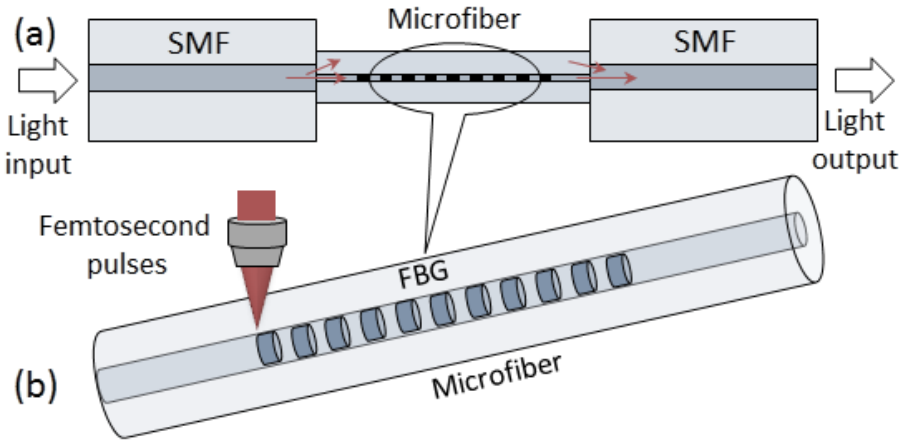

Figure 2.1 Schematic of integrated MZI and FBG sensor: Structural configuration of the sensor (a) and schematic of point-by-point fabrication of FBG in microfiber spliced between SMFs (b).

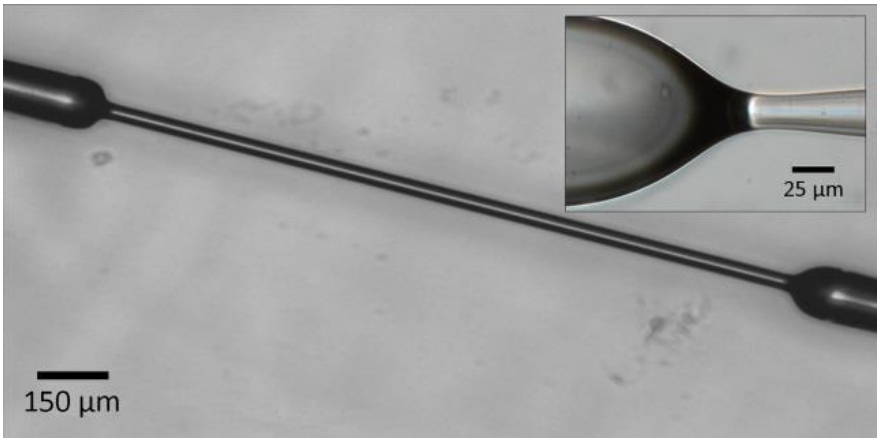

Figure 2.2 Microfiber sandwiched between SMFs to construct MZI. Inset shows the splicing of microfiber with SMF.

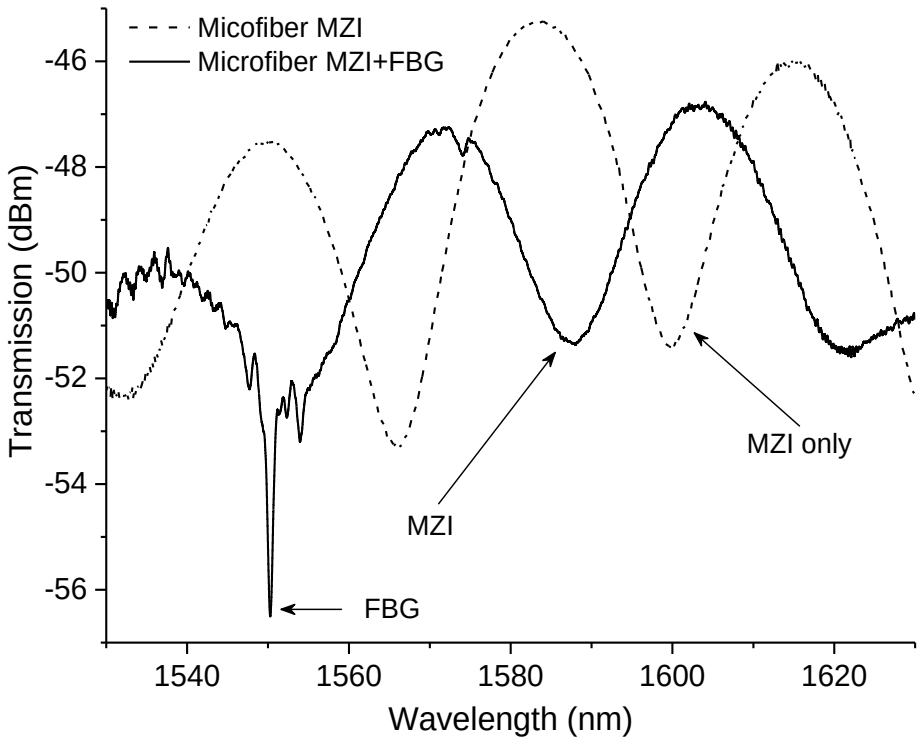

Figure 2.3 MZI transmission spectrum before and after inscription of FBG in microfiber.

The femtosecond laser system operates at center wavelength of 800 nm, pulse duration of 120 fs, and repetition rate of 1 kHz. Using an iris diaphragm, the laser beam diameter was reduced to 1.5 mm (initial diameter: 6 mm). The beam was focused by an achromatic objective lens (Numerical aperture: 0.75) into a small focal volume to elevate pulse peak power necessary for writing filamentary voids in fiber core. The fiber was coupled with a broad band light source and a spectrum analyzer to monitor and record the in-situ growth of FBG's transmission valley during fabrication. The 1 mm FBG was fabricated by scanning the microfiber with the kilohertz pulse train (pulse energy: 42.5 μJ) along its propagation axis. The scanning speed of 0.534 mm/sec was used to achieve the index modulation period of 534 nm necessary to form FBG's rejection band at 1550.28 nm. Both the transmission spectra before and after the inscription of FBG in microfiber MZI

is shown in Figure 2.3. The overall change in core refractive index in FBG inscription process alters the existing phase difference between core and cladding modes of the MZI that accounts for the spectral shift in Figure 2.3.

2.3 Results and Discussion

2.3.1 Ambient RI and temperature characterization

In ambient refractive index measurement, temperature cross-sensitivity plays a significant role, because the RI of most solutions is a function of temperature. Therefore, it is crucial to measure both RI and temperature of a system to get rid of the effect of temperature in RI measurement. This work proposes a compact fiber-optic sensor which was fabricated by integrating a microfiber FBG in microfiber MZI for both RI and temperature measurement applications.

As illustrated in Figure 2.1 (a), the incident light when interacts with the first interface (SMF and microfiber), it splits into both core and cladding of the microfiber and then recombines at the second interface (microfiber and SMF). Therefore, the core and the cladding of the microfiber act as the two arms of a typical MZI. The core mode is confined in the core while the propagation characteristic of the cladding modes depends on the RI difference at cladding-ambient interface. Small fiber diameter allows the cladding modes to extend much closer to the surrounding solution; hence, the MZI sensor shows good sensitivity to any change of RI in the surrounding environment. In contrast, the FBG couples light from forward propagating core mode to the backward propagating core mode in the microfiber. The core mode cannot reach out to the cladding and ambient interface and that explains FBG's very low sensitivity to ambient index change.

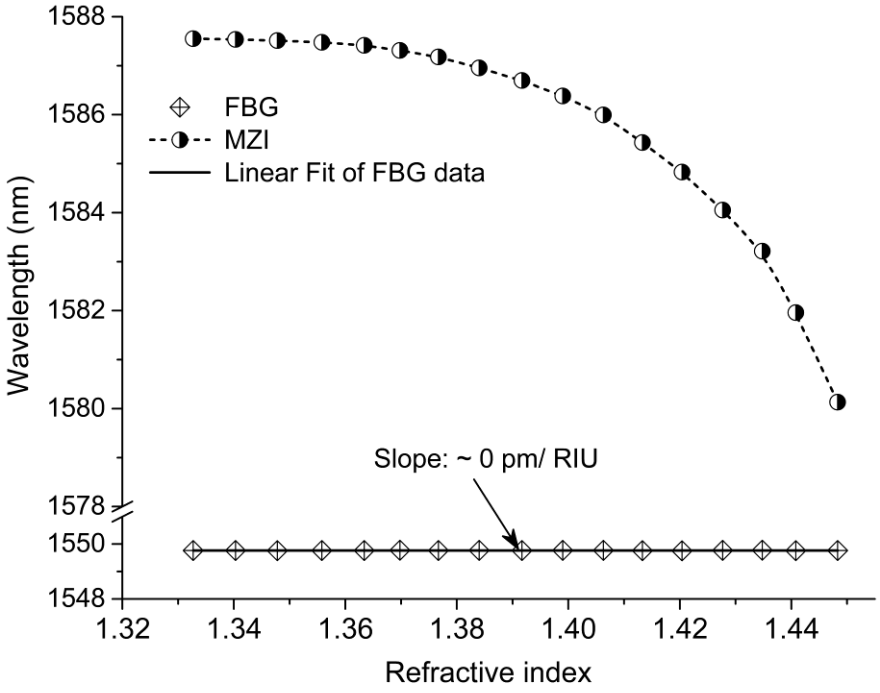

Figure 2.4 Characterization of the sensors to ambient refractive index change. The MZI shows significant RI sensitivity while the FBG is insensitive to ambient RI change.

The shift of interference pattern as a function of surrounding RI change was monitored for the MZI length of 4 mm. The sensor was characterized with different concentration of glycerin solutions at ambient temperature of 22 °C. To achieve characterization data, the device was immersed in glycerin solutions of varying RI ranging from 1.332 to 1.448. After each test, the sensor was thoroughly cleaned prior to immersing it in a subsequent higher concentration of glycerin solution. Figure 2.4 shows the wavelength shifts for both MZI and FBG due to the changes in surrounding refractive index. As the ambient RI increases, the wavelength of the transmission dip of the MZI experiences a blue-shift. In contrast, FBG's resonance transmission spectrum shows insignificant index sensitivity as shown by the flat line in Figure 2.4 The ambient RI sensitivities of the MZI and FBG are summarized in Table 2.1.

Table 2.1 Ambient RI Sensitivity of FBG and MZI

Sensor	RI range: 1.332-1.1384	RI range: 1.384- 1.420	RI range: 1.420-1.448
FBG sensitivity (nm/RIU)	0	0	0
MZI sensitivity (nm/RIU)	-10.65	-58.13	-166.30

The temperature response was examined by placing the sensor in an oven, in which the temperature was varied from 25 ˚C to 95 ˚C. Temperature dependent spectral responses of both FBG and MZI are illustrated in Figure 2.5. The MZI shows clearly dominant temperature sensitivity compared to that of FBG. A linear fit to the measured data gives the temperature sensitivities ($d\lambda/dT$) of 11.80 pm/ ˚C and 51.10 pm/ ˚C, for FBG and MZI, respectively. The experimental results show that the MZI is 4.33 times more sensitive than the FBG in temperature measurement.

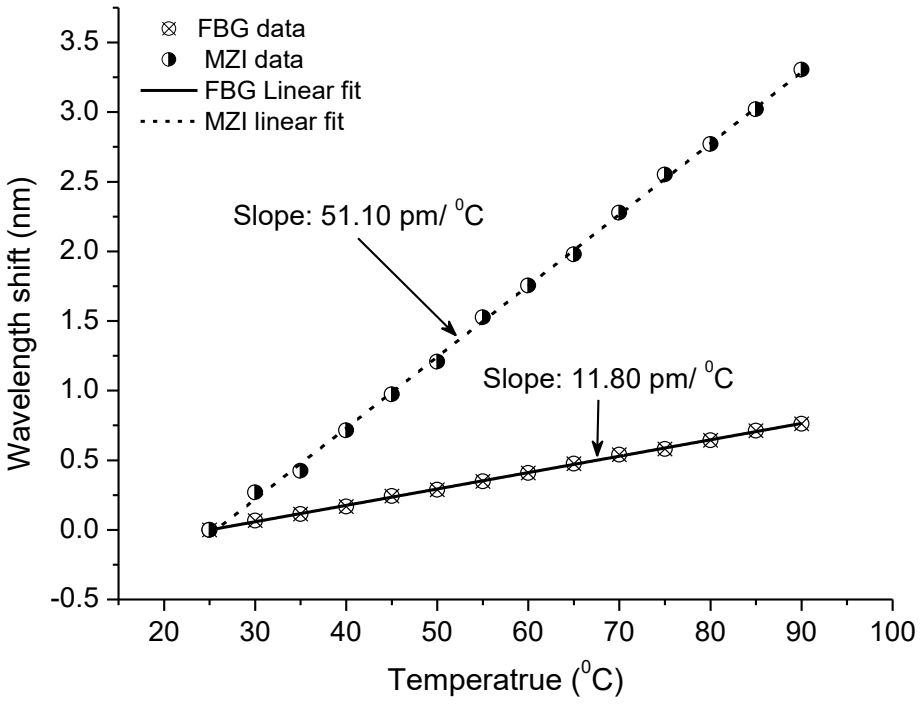

Figure 2.5 Temperature characterization of micro-fiber Bragg grating and microfiber MZI.

2.3.2 Simultaneous measurement of RI and temperature

Based on sensing characteristics of the MZI and FBG sensors, the RI and temperature can be measured simultaneously using the following matrix equation [62]:

$$\begin{bmatrix} \Delta T \\ \Delta n \end{bmatrix} = \frac{1}{k_{FBGT} \times k_{MZIn} - k_{FBGn} \times k_{MZIT}} \times \begin{bmatrix} k_{MZIn} & k_{FBGn} \\ k_{MZIT} & k_{FBGT} \end{bmatrix} \times \begin{bmatrix} \Delta\lambda_{FBG} \\ \Delta\lambda_{MZI} \end{bmatrix} \quad \textbf{(Eq. 2.1)}$$

where, ΔT is the variation of ambient temperature, Δn is the variation of ambient RI. $\Delta\lambda_{FBG}$ and $\Delta\lambda_{MZI}$ are the wavelength change corresponding to the FBG and microfiber MZI, respectively. k_{MZIn} and k_{MZIT} are the index and temperature coefficients of the microfiber MZI sensor. k_{FBGn} and k_{FBGT} are the index and temperature coefficients of the microfiber FBG. Now let's consider the $k_{MZIn} = -58.13$ and $k_{FBGn} = 0$ (RI range: 1.384 - 1.420) from the Table 2.1. As shown in Figure 2.5, the values of k_{MZIT} and k_{FBGT} are 0.0511 and 0.0118, respectively. Therefore, the Eq. (2.1) can be rewritten as follows:

$$\begin{bmatrix} \Delta T \\ \Delta n \end{bmatrix} = -\frac{1}{0.68} \begin{bmatrix} -58.13 & 0 \\ 0.0511 & 0.0118 \end{bmatrix} \begin{bmatrix} \Delta\lambda_{FBG} \\ \Delta\lambda_{MZI} \end{bmatrix} \quad \textbf{(Eq. 2.2)}$$

If the resonance wavelength shifts of the FBG and MZI are known, the temperature and RI changes can easily be calculated using Eq. (2.2).

2.3.3 Temperature compensated RI measurement

For temperature compensated refractive index measurement using point sensors, it is vital to achieve both temperature and ambient RI information at a particular point of interest. Often an FBG connected in parallel or in series is used to quantify the temperature change. It raises operation cost, and increases system complexity. In addition, due to the lack of close proximity, it may require the temperature of the whole chamber to stabilize before obtaining temperature reading. The miniature FBG

embedded in microfiber MZI appears to minimize the issues explained above. However, the temperature compensation is limited by the resolution of the FBG. Temperature compensation using embedded microfiber Bragg grating is exemplified in Figure 2.6.

Temperature compensation job in the Figure 2.6 was done following the simple steps provided bellow:

- Examine FBG's spectral response. No shift in FBG's transmission dip indicates constant temperature and no need for compensation. Read the temperature change from FBG (if there is any), and go to step 2.
- Temperature sensitivity of MZI is 4.33 times higher than that of FBG. Therefore, if there is any shift in FBG spectrum in step 1, the MZI's temperature reading can be achieved easily by taking FBG as the reference.
- As shown in characterization plots (Figure 2.4 and 2.5), the MZI spectrum displays blue and red shift with increase in ambient RI and temperature, respectively. The FBG dip shows red shift with increase in temperature and no shift for RI change. Therefore, the following two-step observation can be made to isolate the effect of temperature in MZI based RI measurement:
  a) If both the direction and amount of spectral shift for MZI and FBG are equal to the proportion of their sensitivities, it can be stated that the ambient RI is constant.
  b) If MZI's spectral shift does not correspond to the spectral response of FBG, the individual spectral shift of both MZI and FBG has to be calculated. Then using the following equation, the MZI index response (temperature

compensated) can be calculated:

MZI (RI response) = MZI (Total response) – MZI (Temperature response)

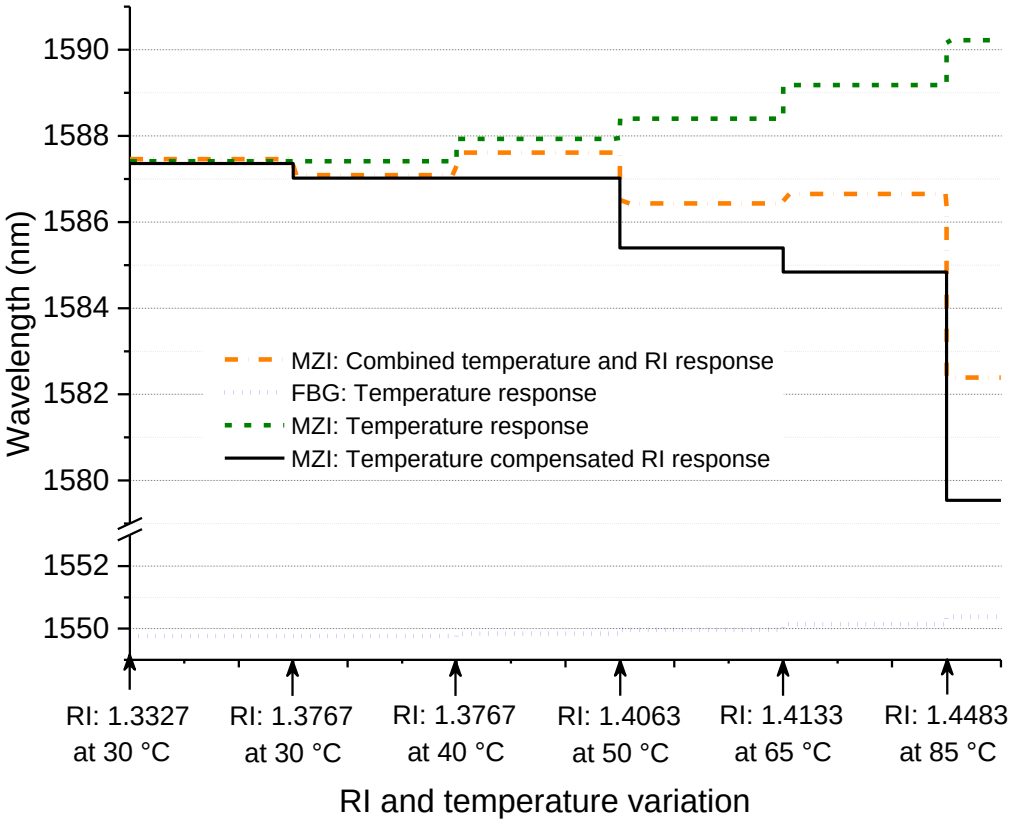

Figure 2.6 Exemplification of temperature compensation using an embedded miniature FBG for ambient RI measurement of microfiber MZI interferometer.

2.4 Conclusion

A novel optical fiber sensor based on integration of a miniature Bragg grating in microfiber MZI has been proposed for ambient RI and temperature measurement. The MZI is constructed by fusion splicing a 4 mm long microfiber between standard SMFs. The FBG is then fabricated in microfiber by the femtosecond pulse radiation using point-by-point inscription technique. The tiny fiber-optic sensor is demonstrated as a suitable device for both simultaneous RI and temperature measurement, and temperature compensated RI measurement applications.

Chapter 3 Measurement of In-fiber Refractive Index Change Using a Mach-Zehnder Interferometer

This paper was published in Journal of IEEE Photonics Technology Letter in 2019.

Farid Ahmed, Vahid Ahsani, Seunghwan Jo, Colin Bradley, Ehsan Toyserkani and Martin B. G. Jun. “Measurement of In-fiber Refractive Index Change Using a Mach-Zehnder Interferometer”, IEEE PHOTONICS TECHNOLOGY LETTERS, VOL. 31, NO. 1, JANUARY 1, 2019

Abstract

We report, for the first time, the use of a fiber-optic Mach-Zehnder interferometer to measure core refractive index changes written by an ultrafast laser irradiation. The core-offset interferometer was constructed by splicing a slightly misaligned stub of standard single mode fiber between lead-in and lead-out optical fibers. When the core refractive index of an in-fiber interferometer is altered, it changes the phase of the core light. Since the phase of light propagating in the cladding (reference arm) remains unchanged, the transmission fringe pattern of the interferometer observes a spectral shift. The spectral shift was used to quantify the effective core refractive index change in a standard single mode fiber. Measurement of effective refractive index changes as high as 0.01356 and as low as 0.000475 are reported in this work.

3.1 Introduction

Laser radiation induced permanent refractive index (RI) change has been widely studied to tailor optical properties of transparent dielectric materials and waveguides [63-65]. Modification of dielectric properties in glass offers direct fabrication of three-

dimensional photonics devices [66, 67]. Approximation of the RI to be inscribed in an optical fiber is critical for design and fabrication of in-fiber photonic devices. Measurement of the RI also offers useful quality control in the fabrication of optical components. Therefore, development of efficient and cost-effective methods for quantifying the amount of RI change in optical fiber is crucial to the design of fiber-optic sensors and communication systems [68, 69].

Several approaches have been demonstrated to determine refractive index profile (RIP) in an optical fiber. In-fiber RI change can be measured using the refracted near-field (RNF) method with considerable index resolution; however, this technique requires fiber cleaving and subsequent polishing of its cleaved face [70]. The RNF method is not suitable to map the RIP along the propagation axis of an optical fiber. The multi-wavelength interferometry technique offers direct measurement of the RIP in an optical fiber, employing Fourier-transform spectroscopy [71]. The differential interference contrast (DIC) approach estimates the RIP using image contrast from the phase variation in optical fiber [72]. Three-dimensional measurement of RIP in the optical fiber can be achieved using computerized tomography (CT) [73]. The measurement of RI using the above techniques is costly and involves a complex reconstruction process. By employing fiber Bragg grating (FBG) based Fabry-Perot interferometers, the measurement of RI change in standard single mode fiber (SMF), written by both ultraviolet [74] and infrared laser [75], has been reported. Construction of a grating-based Fabry-Perot interferometer can be challenging and expensive as it requires two identical FBGs to be inscribed in an optical fiber at a certain distance apart.

In this study, we propose, for the first time, the use of a fiber-optic Mach-Zehnder

interferometer (MZI) device to measure the effective refractive index change in the core of a standard SMF. Fiber-optic MZI device is well studied, easy to fabricate, and suitable for diverse sensing applications [49, 53, 58, 76]. This work investigates the potential of this interferometer to cost-effectively measure the effective RI change in the core of an optical fiber.

3.2 Sensor Operating Principle

A typical MZI sensor has both reference and sensing arms. A beam splitter (ideally with 50/50 splitting ratio) is used to split a beam of light into two, which are subsequently recombined by a coupler. The recombined beams interfere with each other and create an interference fringe depending on the optical path difference (OPD) between the two arms. To detect or measure a physical quantity, the reference arm of the MZI is isolated whereas the sensing arm is exposed to the measurand. The measurand alters the light propagation in the sensing arm, thus changing the existing OPD between the two arms. The variation in the OPD results in a spectral shift of the interference pattern. An MZI can be constructed in an optical fiber by splitting the core mode into core and cladding modes and then recombining them into a core mode. When the refractive index of the core of an in-fiber MZI is altered over a particular length, it changes the effective refractive index of the core mode. Therefore, the core light undergoes a phase change that leads to a change in the OPD between the core and cladding modes. The variation in the OPD induces a shift in the transmission spectrum, and it offers a simple way to measure the effective refractive index change in the core of an optical fiber.

Figure 3.1(a) shows the schematic of an MZI configuration used in this study. Splicing

an SMF stub between two SMFs with a slight lateral offset enables splitting and recombining a light beam at the first and second splicing points, respectively.

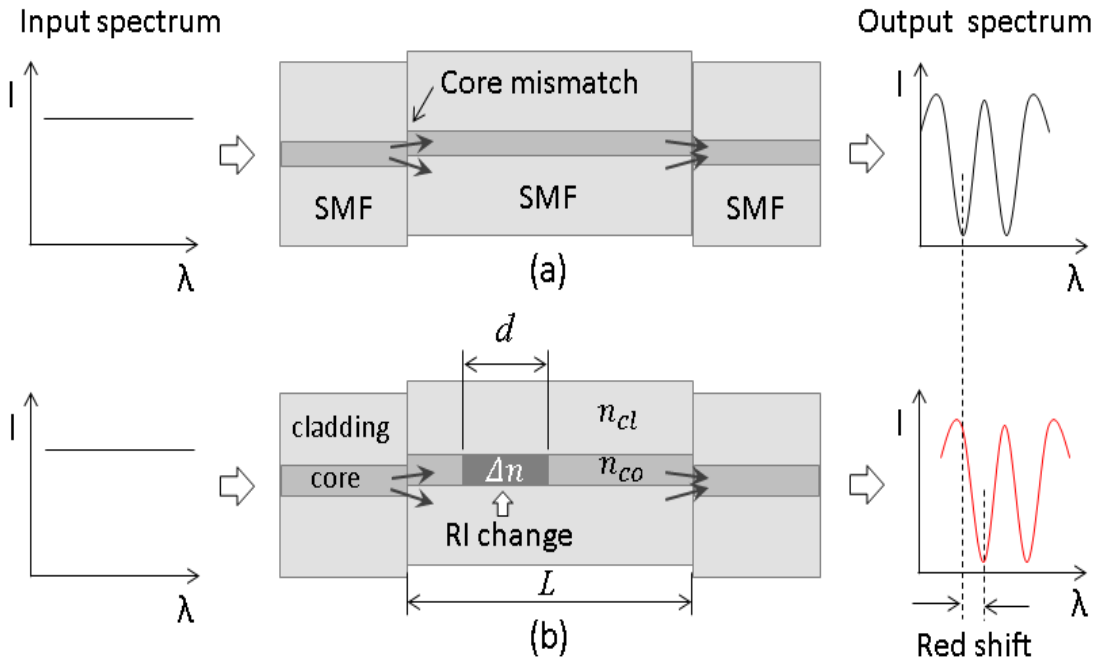

Figure 3.1 Schematic of the MZI operating principle (a), and spectral shift due to core index modification in the MZI (L: length of the interferometer, d: length of core scanned with laser radiation) device (b).

The optical path difference between the core and cladding mode beams in Figure 3.1 (a) constructs the transmission spectrum which can be expressed as [77]:

$$I(\lambda) = I_{core} + I_{clad} + 2\sqrt{I_{core} I_{clad}} \cos\varphi \qquad \textbf{(Eq. 3.1)}$$

where I_{core} and I_{clad} are the intensity of light in the core and cladding modes, respectively. $\varphi = 2\pi\Delta n_{eff} L/\lambda$ is the phase difference between core and cladding modes that produces the interference fringe in the transmission, $\Delta n_{eff} = n_{co} - n_{cl}$ is the effective refractive index between core and cladding modes, L is the length of the MZI, and λ is the wavelength of light. For $\varphi = (2m+1)\pi$ in (1), the mth order attenuation peak is given by [77]:

$$\lambda_m = 2L(n_{co} - n_{cl}) / (2m+1) \quad \textbf{(Eq. 3.2)}$$

When the effective RI of the core of an MZI is changed by Δn over a length of *d* as shown in Figure 3.1 (b), the overall effective refractive index of the core mode is changed to n'_{co}. Therefore, the attenuation peak shows red shift in the transmission spectrum as shown in Figure 3.1. The wavelength of the new attenuation peak can be written as:

$$\lambda'_m = 2L(n'_{co} - n_{cl}) / (2m+1) \quad \textbf{(Eq. 3.3)}$$

The induced spectral shift results due to the alteration of core refractive index and it can be approximated using Eq. (3.3). This technique provides a simple yet effective way to measure the amount of index modification in an optical fiber.

3.3 Sensor Structure and Characteristics

As shown in Figure 3.2 (a), the MZI structure was constructed by fusion splicing of Corning SMF-28 ULL optical fibers. A small stub of an SMF was spliced between lead-in and a lead-out SMFs with a slight core misalignment. The Fujikura (FSM-40PM) splicer set at an arc power of 20 bit and an arc exposure time of 2000 millisecond was used for the splicing operation. The sensor assembly was coupled to a light source and an optical spectrum analyzer to monitor the transmission spectrum. During splicing, the core offsets at the splicing points were manually adjusted to achieve a considerably strong transmission interference fringe. As shown in Figure 3.2 (b), for the MZI length of 17 mm, the fringe pattern with an average fringe spacing of ~28 nm was observed.

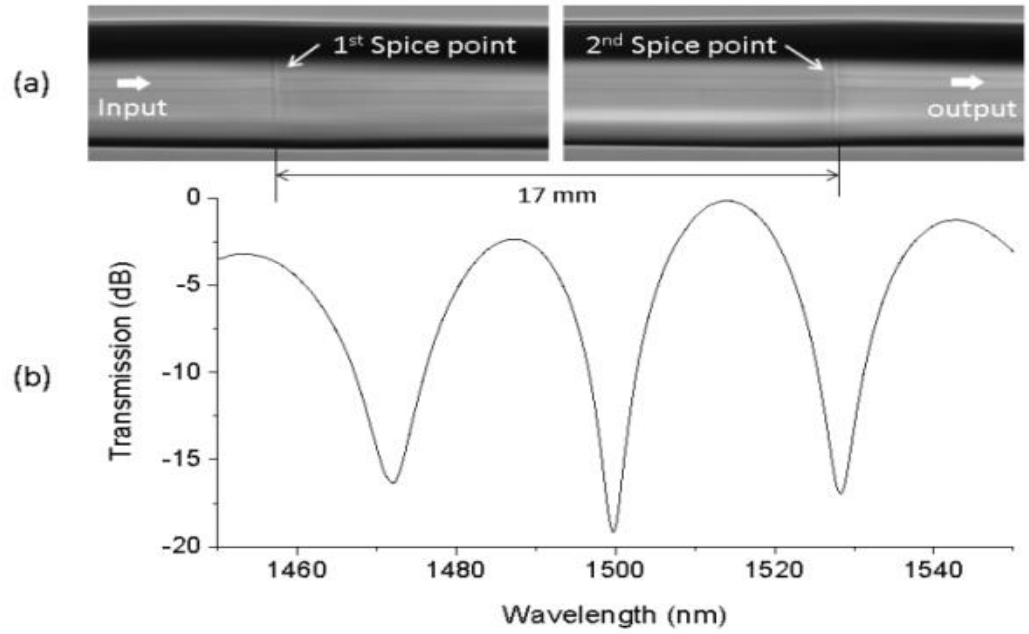

Figure 3.2 The MZI in core-offset configuration. Microscope image of a 17 mm stub of an SMF fusion spliced (slightly misaligned) between lead-in and a lead-out SMFs (a), and the fringe pattern of the interferometer (b).

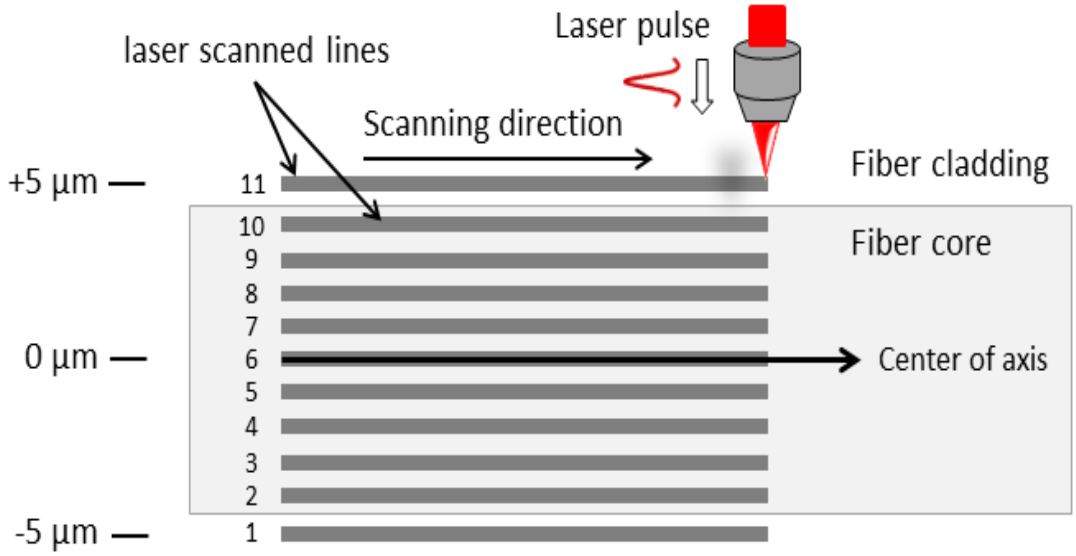

Figure 3.3 Schematic of laser-induced index modification pattern in the optical fiber to examine the spectral response of the MZI sensor.

The spectral response of the transmission mode interferometer was studied by gradually altering the effective RI of the core over a certain fiber length and examining the subsequent fringe shift, as shown in Figure 3.3. SMF-28 ULL fiber used in this

experiment has a mode-field diameter of 10.5± 0.5 μm at 1550 nm and a core diameter of 8.2 μm. A femtosecond laser (*Spectra-Physics Ti: Sapphire* laser with center wavelength: 800 nm, pulse width: 120 fs, and pulse repetition rate: 1 kHz) was used to write an inhomogeneous RI change into the core. Fernandes et al. [65] have detail studies on writing inhomogeneous RI in optical fibers using the ultrafast laser radiation. An iris diaphragm was used to restrict the beam diameter to 2 mm (original beam diameter: 6 mm). The laser pulses (pulse energy: 14.40 μJ) were focused with a microscope objective lens (NA: 0.75, 40X) to elevate average power density at the focal point and write higher RI. The millimeter-long lines within the core and core-cladding interface of the MZI were scanned using a point-by-point inscription method at the speed of 0.05 mm/s. The inset of Figure 3.4 shows the characteristic fringe shifts observed when a 1 mm long fiber core was scanned with a period of 1 μm as depicted in Figure 3.3. The index modification within the fiber core yields significant and linear spectral shifts as shown in Figure 3.4. The irradiance of mode-field fades away at the core-cladding interface. Therefore, a minor spectral shift was observed when the RI was written in the core near the core-cladding interface, which is also in good agreement with the *optiwave* simulation data. Fiber cladding cross-section is much larger compared to the core and as shown in Figure 3.4, index change in the cladding near core-cladding interface does not cause any significant spectral shift. Therefore, a small index change in the cladding was ignored.

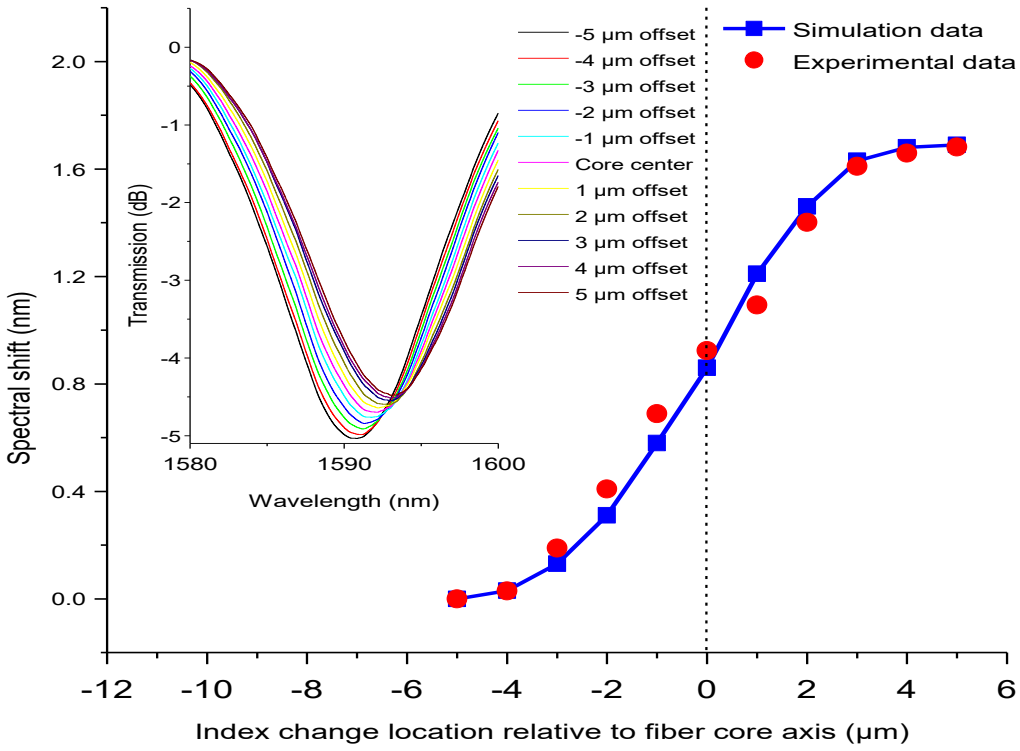

Figure 3.4 The spectral shifts observed when the fiber core within the MZI was scanned (from one core-cladding interface to another as shown in Figure 3.3) along its propagation axis over a length of 1 mm.

3.4 Measurement of In-fiber RI Changes

In order to study the influence of laser pulse energy on the amount of effective core index modification, several identical small sections (length: d) of the core within the MZI were scanned with different pulse energies as illustrated in Figure 3.5. A 17 mm long core-offset MZI was used in this experiment. The fiber core was scanned in the transverse direction, relative to its propagation axis, with a period of 1 μm at the speed of 0.05 mm/s. The pulse energy was gradually increased for each scan. Figure 3.6 depicts the dependency of the spectral shift of the interferometer to pulse energy. For d= 200 μm, greater red shifts were recorded for an RI written with higher pulse energies. The amount of red shift obtained in this study is used in the following section to estimate the in-fiber effective core RI change.

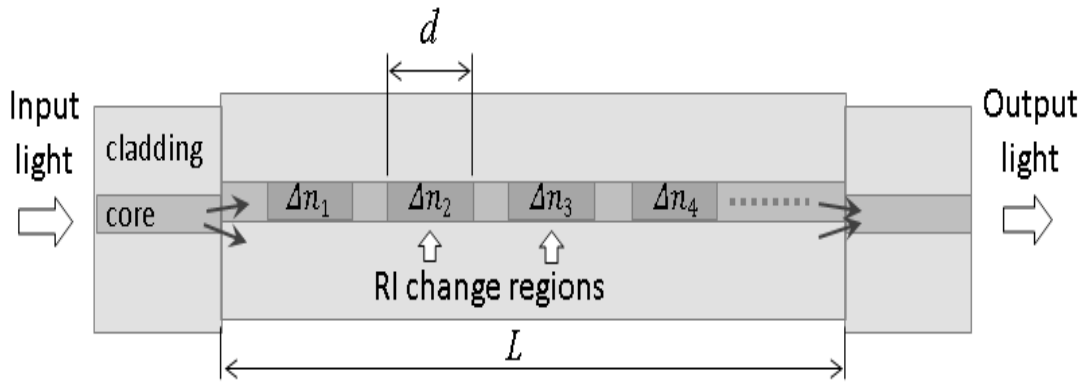

Figure 3.5 Experimental schematic showing writing of higher RI progressively over a core length of 'd'.

When a refractive index is inscribed over the core length of *'d'* as shown in Figure 3.1(b) and Figure 3.5, it changes the overall effective core mode index for the entire length *L* of the interferometer. The mode effective refractive index of the core-arm of MZI device is then given by:

$$n'_{co} = \frac{(n_{co} + \Delta n)d + n_{co}(L-d)}{L} \qquad \textbf{(Eq. 3.4)}$$

Dividing Eq. (3.3) by Eq. (3.2) and then substituting for n'_{co} we get:

$$\frac{\lambda'_m}{\lambda_m} = \frac{1}{n_{co} - n_{cl}}\left(n'_{co} - n_{cl}\right)$$

$$= \frac{1}{n_{co} - n_{cl}}\left[\frac{(n_{co} + \Delta n)d + n_{co}(L-d)}{L} - n_{cl}\right]$$

$$= \frac{\Delta n d}{(n_{co} - n_{cl})L} + 1$$

Or, $\lambda'_m = \frac{\Delta n d \lambda_m}{\left(n_{co} - n_{cl}\right)L} + \lambda_m$

Or, $\lambda'_m - \lambda_m = \Delta\lambda = \frac{\Delta n d \lambda_m}{L\left(n_{co} - n_{cl}\right)}$

$$Hence,\ \Delta n = \left(n_{co} - n_{cl}\right)\frac{\Delta\lambda}{\lambda_m}.\frac{L}{d} \qquad \textbf{(Eq. 3.5)}$$

where, $\Delta\lambda$ is the red shift of the interference fringe observed for the core mode effective index change of Δn over the length of d. The correspondence between the core mode effective index and the actual refractive index change depends on the overlap between the mode profile and the spatial distribution of the refractive index change. As shown in Figure 3.4, the insignificant spectral shift was observed when the RI change occurred in the cladding of the fiber. Therefore, considering a reasonable overlap between the core mode profile and the spatial distribution of the core refractive index change, Eq. (3.5) provides a simple approach to measure the effective RI change in an optical fiber.

The in-line fiber-optic MZI was rigidly fixed on the 3-axis stage prior to the core index modification to ensure that the tension on the fiber remains unchanged during the experiment. As shown in Figure 3.5, the d= 200 μm core segments, at different axial locations in the interferometer, were laser scanned (scanning period: 1μm, speed: 0.05 mm/s) with gradually increasing pulse energies. The corresponding spectral shifts were observed as shown in Figure 3.6. The amount of spectral shift can be inserted into Eq. (3.5) to estimate the amount of effective RI changes that was inscribed in the fiber core. Figure 3.7 demonstrates the effective core RI measurement outcomes as a function of pulse energy. The results were obtained for L=17 mm, d= 200 μm, λ_m=1474.37 nm, n_{co}-n_{cl}= 0.0053 (n_{co}= 1.4620, n_{cl}= 1.4567). The amount of effective core RI change is directly proportional to the spectral shift as n_{co}, n_{cl}, λ_m, L, and d in Eq. (3.5) are constants. The effective RI changes as high as 0.01356 and as low as 0.000475 in the core of an MZI

are reported in this work for average pulse energies of 13.532 µJ and 12.908 µJ, respectively. Tightly focused ultrafast pulses were used in this study to inscribe filamentary voids at the focal point. The length of the filamentary voids increases with the rise in peak power of the radiated pulses. An increase in the average pulse energy leads to an increase in the peak pulse power which, in turn, augments the length of the filamentary voids. Therefore, a higher RI is likely to be written over a larger core cross section as the pulse energy is gradually increased. This might explain the increase in the effective RI change for an increase in pulse energy.

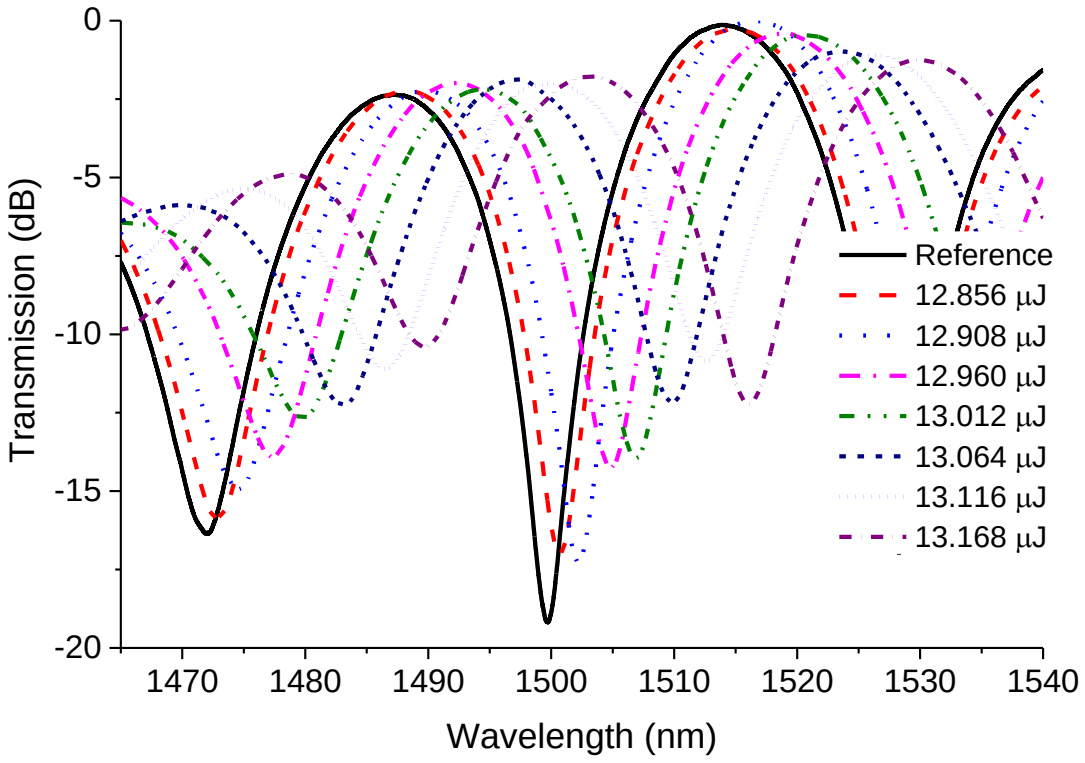

Figure 3.6 The gradual increase in red shift of the MZI's transmission spectrum, when a 200 µm length of the core was scanned with pulses. The pulse energy was gradually increased for each scan.

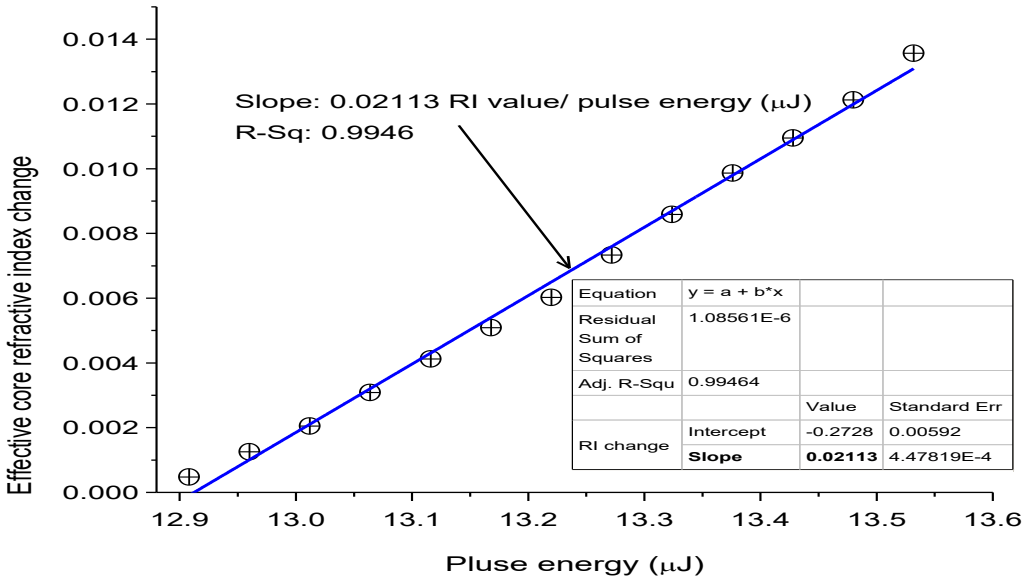

Figure 3.7 The linear dependency between effective core refractive index change and input pulse energy.

3.5 Conclusion

In this study, the use of a fiber-optic MZI is proposed to measure in-fiber RI changes. The core and the cladding of the SMF are respectively used as the sensing and reference arms of the MZI. The fringe shift of the MZI, caused by the core index alteration, is used for the RI measurement. The measurement of RI change, as high as 0.01356 and as low as 0.000475, is demonstrated in this work. The technique offers a simple yet effective approach for quantifying the in-fiber effective RI change. This work has the potential to provide a cost effective approach for estimating the laser induced RI change in optical fibers, which is vital for the design and fabrication of in-fiber photonic devices.

Chapter 4 Miniaturized Tapered Photonic Crystal Fiber Mach-Zehnder Interferometer for Enhanced Refractive Index Sensing

This paper was published in Journal of IEEE Sensors Journal in 2016.

Farid Ahmed, Vahid Ahsani, Luis Melo, Peter Wild, and Martin B. G. Jun. "Miniaturized Tapered Photonic Crystal Fiber Mach-Zehnder Interferometer for Enhanced Refractive Index Sensing", IEEE SENSORS JOURNAL, VOL. 16, NO. 24, DECEMBER 15, 2016

Abstract

Miniaturized Mach-Zehnder interferometer (MZI) is constructed using sharply tapered photonic crystal fiber for highly sensitive ambient refractive index (RI) measurement. The sensor is fabricated by fusion splicing a small stub of photonic crystal fiber (PCF) between standard single mode fibers (SMFs) with fully collapsed air holes of the PCF in splicing region. Influence of sharp tapering of the PCF is then studied using two different hydrogen flame diameters of 1 and 3.5 mm at the tip. Tiny flame geometry enables sharp tapering of the PCF for a short fiber length and provides higher RI sensitivity. It appears that sharp tapering has a greater impact on RI sensitivity enhancement compared to decrease in taper waist diameter. The MZI with the taper waist diameter of 65 μm and the length of 3.8 mm offers RI sensitivity of 334.03 nm/RIU, 673.91 nm/RIU, and 1426.70 nm/RIU within the RI range of 1.3327 to 1.3634, 1.3634 to 1.3917, and 1.3917 to 1.4204, respectively.

4.1 Introduction

The interference of light in optical fibers has been used in precision measurement

systems and sensors. The unique properties such as miniature size, light weight, immunity to electromagnetic wave, and ability for high resolution detection of fiber-optic interferometric sensors have made them superior candidates over conventional sensors for environmental monitoring applications. In particular, fiber-optic Mach-Zehnder interferometers offer good sensitivity to ambient refractive index measurement. A typical MZI has a reference and a sensing ain trm. An incident light is split into two arms using a beam splitter and then recombined by a second splitter. The recombined lights at the second splitter produce an interference fringe based on the optical path difference (OPD) between the two arms. For MZI based ambient RI sensing, the reference arm is kept isolated while the sensing arm is exposed to solutions to be detected. The signal deviation in the sensing arm induced by ambient RI changes the OPD of the MZI can be quantified by examining the variation in the interference pattern.

Optical fibers can be configured to allow splitting and recombining of light in order to control their optical paths. Creating optical path difference between two modes in an optical fiber and eventually recombining them into a single mode, it is possible to construct sensors in optical fibers that are extremely compact and economic. The fiber-optic MZIs are simple yet effective tools for measurement of ambient refractive index.

The long period gratings (LPGs) are the widely used RI sensors, where the shift in transmission spectrum generated by intermodal coupling between forward-propagating core and cladding modes is used for sensing applications [9, 10, 13]. To further enhance RI sensitivity, MZI has been constructed using a pair of long period gratings [78]. However, the gratings are often expensive and work only in a limited band(s) of wavelengths due to phase matching phenomenon of fiber gratings. Considerable research

work has been conducted to achieve alternative MZI configurations including core mismatch, use of multimode fiber segments or small core SMF in standard SMF, air-hole collapsing of PCF and fiber tapering [14]. Sensors based on PCF are attracting considerable attention because photonic crystal fibers show unique optical properties due to their periodic microstructure along fiber length [79]. The modal and light guidance properties of PCFs are appealing for ambient refractive index sensing. The first MZI using PCF was demonstrated by MacPherson et al. in 2001 [80]. Since then, PCF based fiber-optic MZI sensors in diverse structural configurations have been used in many sensing applications. MZI sensor in SMF-PCF-SMF configuration with sensing length of 3.5 cm to 5 cm has been demonstrated for RI sensor [81]. Li et al. have proposed PCF based MZI sensor with taper waist diameter down to 30 μm and sensing length of ~2.4 cm to achieve RI sensitivity of 1600 nm/RIU [82]. Too much reduction in taper waist may reduce rigidity of the sensor and in point sensing applications sensor with shorter length is desirable. To keep the sensor length considerably small, acid etching of the PCF also has been reported [83, 84]. Chemical etching using hydrofluoric acid is probably not the best method for many laboratory setups. So, alternative approaches are required to achieve miniature MZI that has considerable sensitivity for ambient RI sensing.

In this work, we present sharply tapered miniature PCF based MZI sensors that show high ambient RI sensitivity. The sensors are built by splicing small stubs of PCF between SMFs. The PCF is then tapered using a custom made tapering machine. Figure 4.1 illustrates the two-step process involved in sensor fabrication. As shown in Figure 4.1(a), the basic MZI structure is constructed by splicing a small stub of PCF between standard SMFs. In the second step, the PCF is tapered while the SMFs on both sides remain

unchanged. During splicing, a small segment of PCF collapse that diffracts the fundamental core mode. As pointed out in Figure 4.1 (b), at first interface (SMF and PCF), the incident light spreads into both core and cladding of PCF and then recombine at the second interface (PCF and SMF). The core mode is confined in the core while the propagation characteristic of the cladding modes depends on the RI difference at cladding-ambient interface. Smaller diameter of the PCF allows the cladding modes to extend much closer to the ambient solution; hence, the sensor shows high sensitivity to any change of RI in the ambient environment.

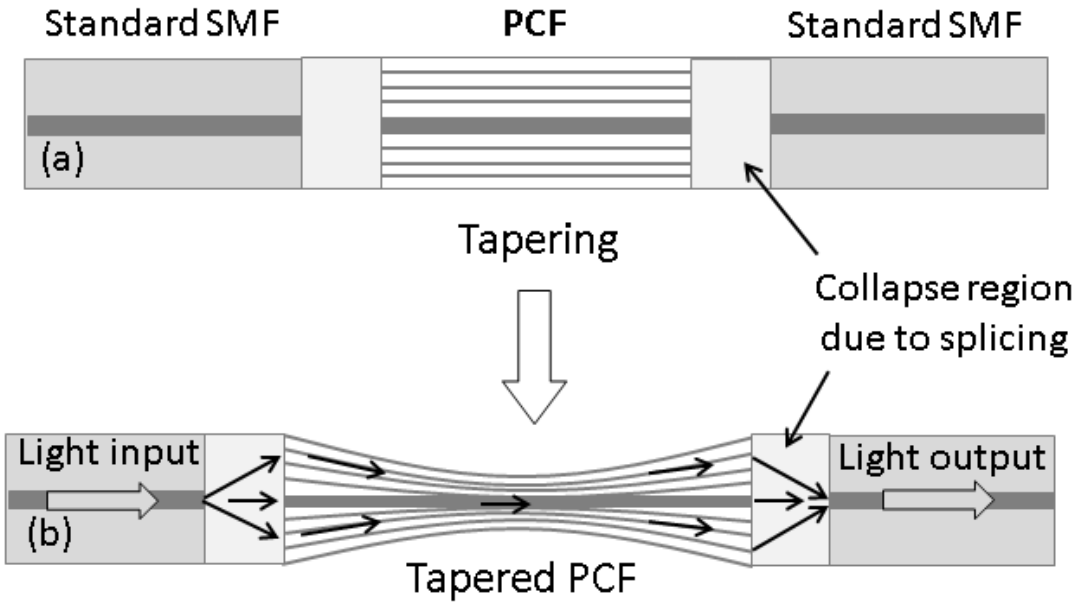

Figure 4.1 Schematic of the PCF based MZI sensor (a), and tapering of the PCF to enhance ambient refractive index sensitivity (b).

4.2 Sensor Fabrication

Figure 4.2 shows 3D model of the tapering machine used in this experiment. The fiber holders were mounted on servomotor driven linear stages that run with the resolution of 1µm/pulse. The stages were attached on an adjustable linear stage that offers convenient fixturing of the fiber along X-axis. Hydrogen gas at pressures of 5 PSI and 20 PSI was

feed into the fixed orifice and converging/diverging nozzles, respectively to produce the flames. A fixed orifice nozzle with orifice diameter of 250 µm and a converging/diverging nozzle (inner and outer orifice diameters are 50 µm and 150 µm, respectively) were used to study the tapering performance. A ultra-violet camera was used to monitor the overall flame geometry. As shown in Figure 4.3, two flow meters were used to confine flames of fixed orifice nozzle and converging/diverging nozzle to the diameters of 3.5 mm and 1 mm, respectively. The nozzles were mounted on the Y-Z micrometer stage that facilitates easy flame adjustment relative to the optical fiber. A K-type thermocouple was used to measure flame temperature. The temperature of the flame where fiber passes through was measured ~ 1100 ˚C. The whole tapering operation is automated using LabVIEW programing environment. A CCD camera was used to monitor in-situ tapering operation.

A short length of single mode PCF was first fusion spliced between a lead-in and a lead-out SMF-28 fiber. The holey structure of the PCF has much lower softening point than that of SMFs, and thus at each splicing point the air holes of the PCF entirely collapse over a short length. In a typical splicing machine, the intensity and arc exposure duration of the fusion process can be tuned. This allows controlling the collapse length of the PCF at each splice point.

The Fujikura (FSM 40PM) fusion splicer was used to splice standard SMF to PCF with an arc power of 10 bit exposed for 1500 millisecond. An average transmission loss of ~ 5 dB was observed during the splicing operation. Figure 4.4 (a) shows the splicing of SMF with PCF where a small segment of the PCF (156 µm) collapses due to the applied arc heat. The collapse region of the PCF splits the core mode into core and

cladding modes at first splice point and then recombines them at the next splice point to construct MZI configuration. Both the standard SMF and PCF are stripped off from polymer coating before fusion splicing. In this case, the surrounding air acts as a low index cladding and confines the higher order modes within the PCF.

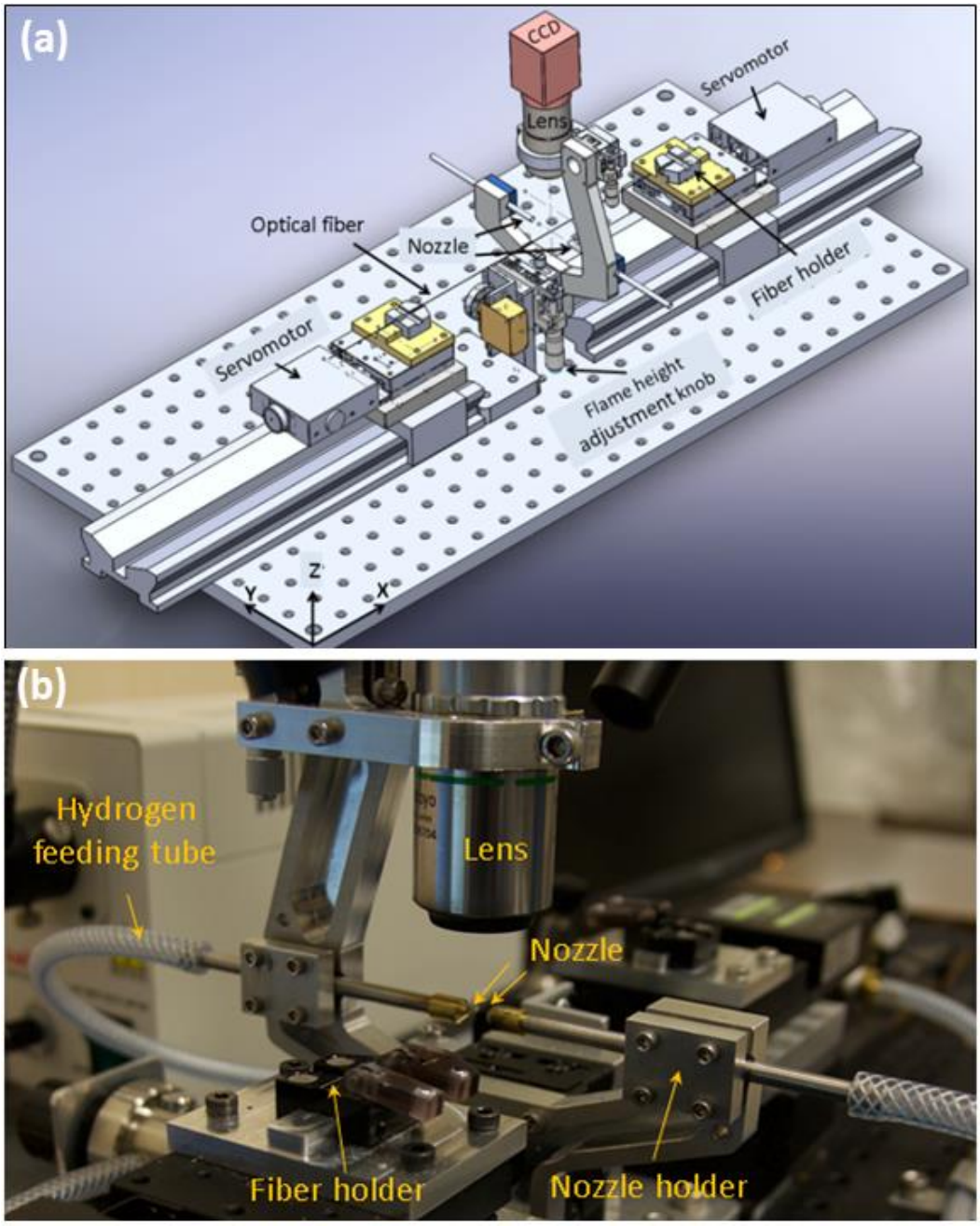

Figure 4.2 Isometric view of the device used for tapering photonic crystal fiber (a) and the magnified image of the nozzle setup (b).

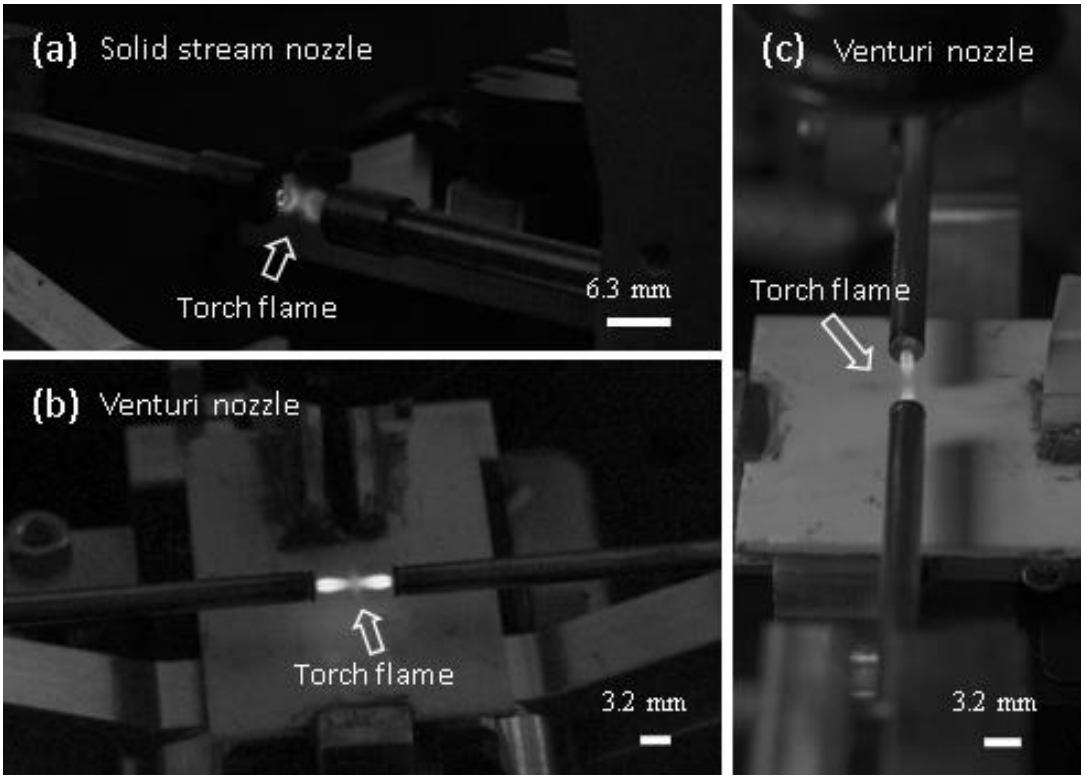

Figure 4.3 The flame geometrics achieved using particular torch nozzle designs. The nozzle with a constant orifice diameter of 250 µm provides a flame tip diameter of ~3.5 mm (a). The converging/diverging nozzle with an inner orifice diameter of 50 µm and an outer orifice diameter of 150 µm provides a flame diameter of ~ 1 mm (b and c).

In presence of the fixed orifice nozzle flame (Figure 4.3 (a)), two motorized stages pulled the PCF (initial length: 5 mm) over a length of 3 mm at a constant speed of 25 µm/s. This provides the taper angle of 0.95°, waist diameter of 50 µm, and sensor length of 8 mm as shown in Figure 4.4 (b). The smaller flame diameter of the converging/diverging nozzle (Figure 4.3 (b & c)) produced taper waist diameters of 70 µm and 65 µm when the fiber was pulled over a length of 1.5 mm with the speed of 35 µm/s and 25 µm/s, respectively. Sensor lengths of the tapered PCF samples shown in Figure 4.4 (c) and 4.4 (d) are 4 mm and 3.88 mm, respectively. The taper angles in Figure 4.4 (c) and Figure 4.4 (d) are 2° and 2.4°, respectively. Reduced fiber diameter and sharp tapering enable stronger mode interaction with the ambient solutions to enhance RI

sensitivity of the sensor. The taper diameter can be further reduced to obtain a greater sensitivity. The double nozzle flame configuration retains fiber symmetry during the tapering operation. Figure 4.5 shows the cross sections of the PCF at taper waist before and after tapering. No significant fiber deformation was observed after tapering as shown in Figure 4.5 (right). The transmission loss after the tapering operation was ~0.5 dB.

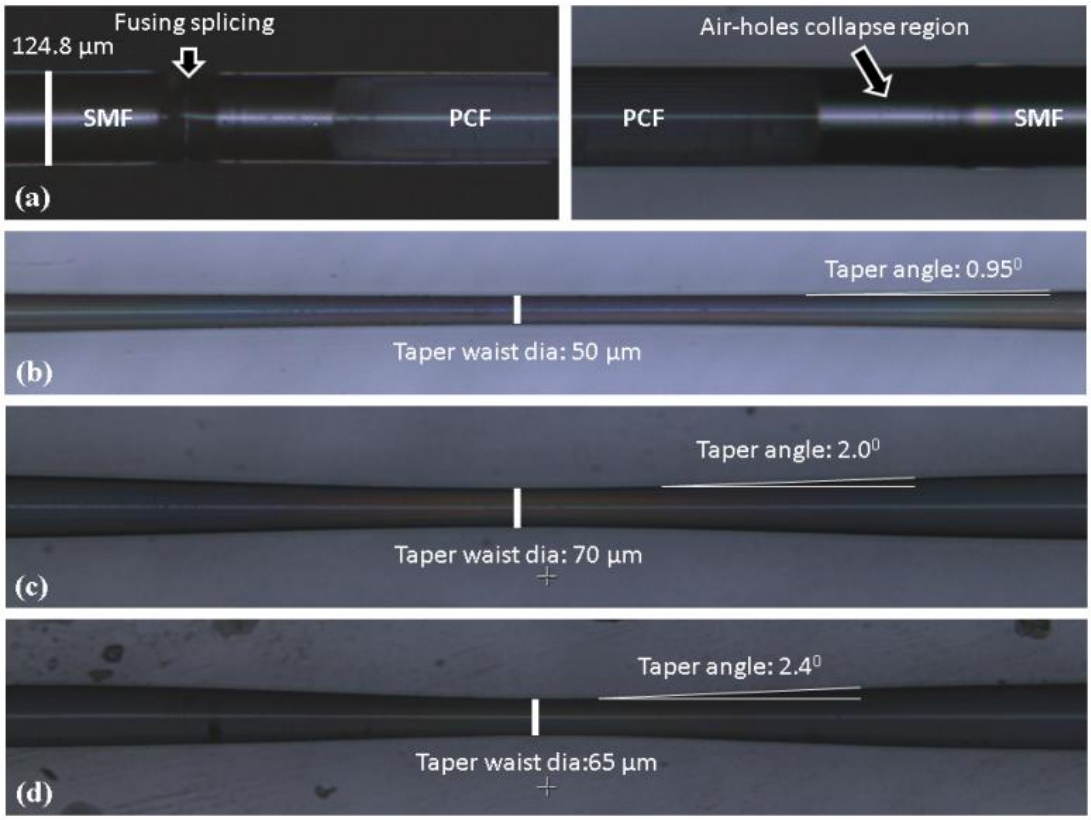

Figure 4.4 Microscope images of the fusion splicing of PCF with standard SMF and the taper morphologies obtained using different tapering conditions. The air-holes of the PCF collapse over a length of 156 µm at both splice points (a). The taper waist diameter of 50 µm with a taper angle of 0.950˚ is achieved using fixed orifice nozzle. Using the converging/diverging nozzle, the taper diameter of 70 µm with taper angle of 2.0˚ and the taper diameter of 70 µm with taper angle of 2.40˚ are achieved using tapering speed of 35 µm/s and 25 µm/s, respectively.

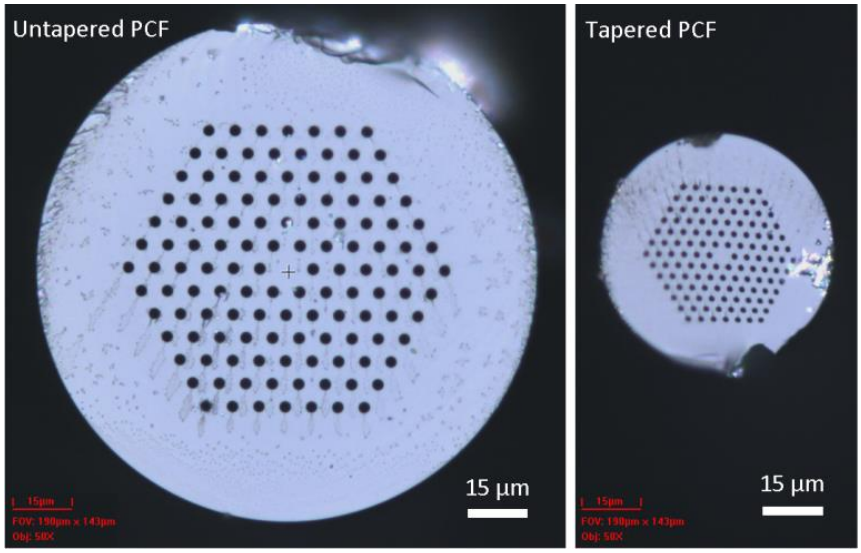

Figure 4.5 Cross sections of the PCF showing before and after tapering of the fiber using fixed orifice nozzle flame. The cross section of the tapered fiber is taken at the waist region.

4.3 Spectral Response

The air-holes collapse length of the PCF at both splice points tailors the transmission spectrum of this interferometric device. Collapse length determines the amount of beam splitting at first splicing region. As shown in Figure 4.4 (a), the collapse length was found to be 156 µm when the splicing was done with an arc power of 10 bit and exposure time of 1500 millisecond. Let's consider the evolution of propagating beam shown in Figure 4.1 (b) as it travels from the lead-in SMF, through the PCF and finally to the lead-out SMF. When the fundamental SMF mode reaches the collapsed region of PCF it starts to diffract, and thus the mode broadens. For a beam centered at wavelength λ, with the initial spot size w_0 (at the first SMF-PCF interface) broadens to a new size of w when it propagates a length l_1 of the collapse region and is given by [85]:

$$w = w_0 \sqrt{1 + \left(\frac{\lambda l_1}{\pi n_f w_0^2}\right)^2} \qquad \textbf{(Eq. 4.1)}$$

where n_f is the refractive index of the collapse region of PCF. For the center wavelength λ = 1.542 µm, collapse length of PCF l_1 = 156 µm, index of collapse region n_f = 1.444 and initial spot size w_0 = 5 µm, the new spot size at the end of collapse region of PCF will be w = 11.72 µm. Therefore, at the end of collapse region, the PCF will be excited with a Gaussian beam of diameter 2w = 23.45 µm which is much larger than its core size. The combined effect of mode field mismatch and the modal characteristics of the PCF [86] excite certain core and cladding modes in the PCF that have different propagation constants [87]. Both modes propagate along the PCF and enter the second collapse region of the PCF. The collapse region causes further diffraction and finally the core and cladding modes recombine due to the filtering of the subsequent SMF. The core and cladding mode interfere and provide a transmission spectrum given by [88]:

$$I = I_{co} + I_{cl} + 2\sqrt{I_{co}I_{cl}}cos(\delta + \varphi_0) \quad \textbf{(Eq. 4.2)}$$

$$\delta = (2\pi/\lambda)\int_L^{I_{co}-I_{cl}} dz \quad \textbf{(Eq. 4.3)}$$

where I is the intensity of the interference signal, I_{co} and I_{cl} are the intensities of the core and cladding modes, δ is the phase difference of the two modes, n_{co} and n_{cl} are the effective indices of the core and cladding modes. L and λ are the length of the PCF and operating wavelength, respectively.

Typically, the MZI sensors are very sensitive to fiber bending, so the sensor was firmly fixed on a fiber holder. Then the fiber was coupled with a broad band light source (AFC BBS-1550), and a spectrum analyzer (PHOTONETICS Walics) to analyze the optical characteristics of the tapered PCF MZI. Figure 4.6 shows the transmission spectra

of the interferometer. The length and the waist diameter of the PCF were 8 mm and 50 µm, respectively. The cladding mode becomes lossy as the taper waist diameter gradually decreases, because the transition region of the taper PCF is nonadiabatic [82].

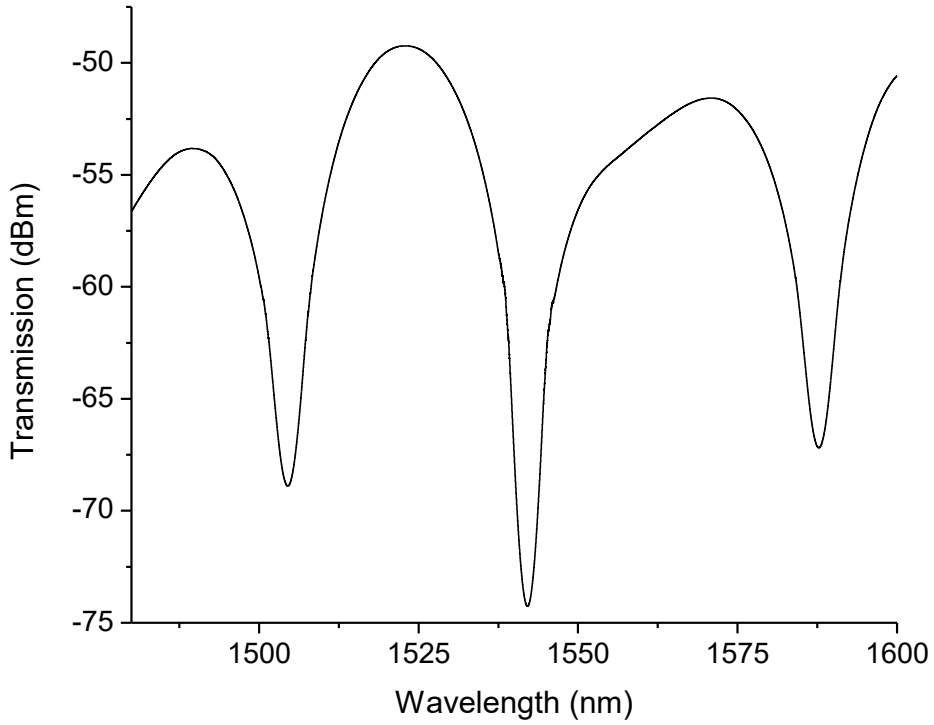

Figure 4.6 Transmission spectrum of the in-fiber MZI in SMF-Tapered PCF-SMF configuration.

The MZI constructed using air-holes collapse typically displays sinusoidal interference spectra over a broad wavelength range. The fringe spacing (Δλ) of the MZI configuration is given by [89]:

$$\Delta\lambda = \lambda^2/(\Delta n_{eff} L) \qquad \textbf{(Eq. 4.4)}$$

where Δn_{eff} is the difference of effective refractive indices between the modes contributing in the interference, and L is the sensor length. Therefore, for a given Δn_{eff}, the fringe spacing of the MZI sensor can be controlled using appropriate length of the PCF between the SMFs. Figure 4.7 shows length dependent fringe spacing of the MZI

for both untapered and tapered PCF. The fringe period of the untapered PCF interferometer gradually decreases as the length of the sensor increases. However, the fringe period dramatically decreases in tapered PCF interferometer with increase in sensor length as shown in Figure 4.7. A drastic increase in Δn_{eff} with the reduction of fiber diameter may explain this phenomenon.

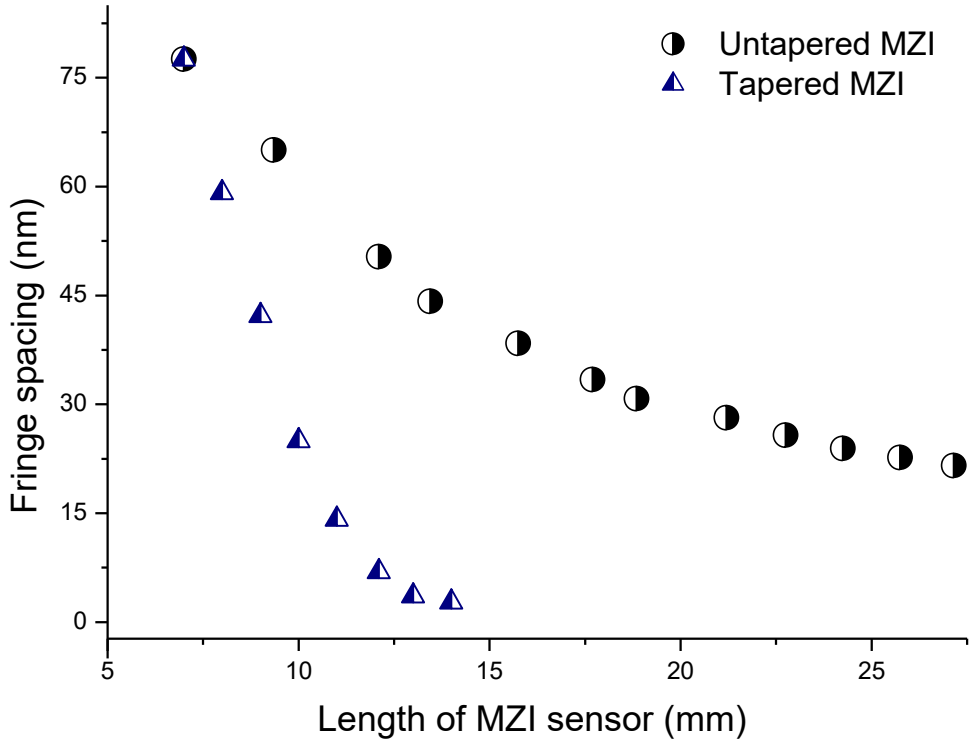

Figure 4.7 Transmission mode fringe spacing of the PCF MZI as a function of the length of PCF.

4.4 Refractive Index Sensing

The refractive index sensitivity of the MZI is defined as the wavelength (λ_i) shift divided by ambient refractive index (n_a) change [83]:

$$S = \frac{d\lambda_i}{dn_a} = \frac{\lambda_i}{n_{cl} - n_{co}} \frac{\partial (n_{cl} - n_{co})}{\partial n_a} \qquad \textbf{(Eq. 4.5)}$$

The effective refractive indices of the core and cladding modes depend on the local

diameter of the tapered PCF. When the fiber diameter is large, n_{co} is constant because the core mode is isolated from the ambient index. However, for tapered PCF, the ambient index (n_a) alters the index of the cladding mode due to the interaction between the ambient solution (n_a) and evanescent field of the cladding mode. Figure 4.7 shows that effective indices of the core and cladding modes depend on the fiber diameter. A decrease in fiber diameter increases the difference of effective refractive indices between core and cladding modes. This explains why fringe spacing dramatically decreases with increase in fiber length in the tapped PCF MZI. An increase in ambient index has greater impact on sensitivity enhancement according to equation (4.5).

To compare the ambient RI sensitivities at different PCF diameters, Qiu et al. have introduced enhanced ratio which is the ratio of the sensitivities for fiber diameter < 125 μm (tapered fiber) and untapered fiber [84]. Both fiber diameter and excited cladding modes modify the enhanced ratio. For a particular value of ambient RI, the enhanced ratios of several cladding modes were examined. The sensitivities of the cladding modes were found to show similar trend and rapidly increase with decreasing diameter of the PCF. For the PCF diameter of 80 μm, the RI sensitivity has been reported to increase almost 100 times.

Both the untapered and tapered PCF interferometric sensors were characterized with different concentration of glycerin solutions at room temperature. To achieve characterization data, the devices were immersed in glycerin solutions of variable concentration. After each test, the sensor was thoroughly cleaned up before immersing it in subsequent higher concentrated glycerin solution. Figure 4.8 shows the wavelength

shifts due to the change of surrounding refractive index between the values of 1.3327 to 1.4204. As the surrounding RI increases, the dip wavelength of the transmission wave experiences a red-shift. The tapered PCF based MZI clearly shows higher sensitivity compared to untapered PCF interferometer. It is evident in Figure 4.8 that sharper tapering over a short length of PCF offers greater sensitivity even if the taper waist diameter is relatively larger. Therefore, higher RI sensitivity can be achieved without losing considerable rigidity of the sensor structure.

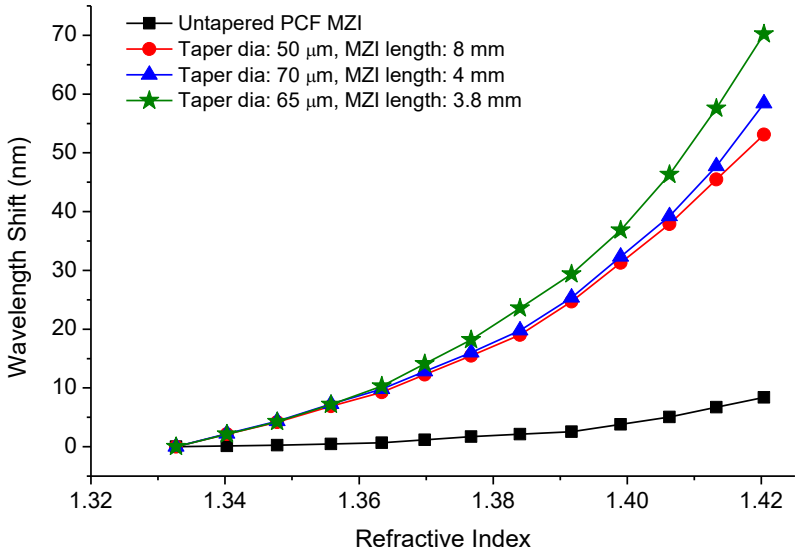

Figure 4.8 The overall refractive index sensitivity plots for both untapered and tapered PCF based MZI sensor.

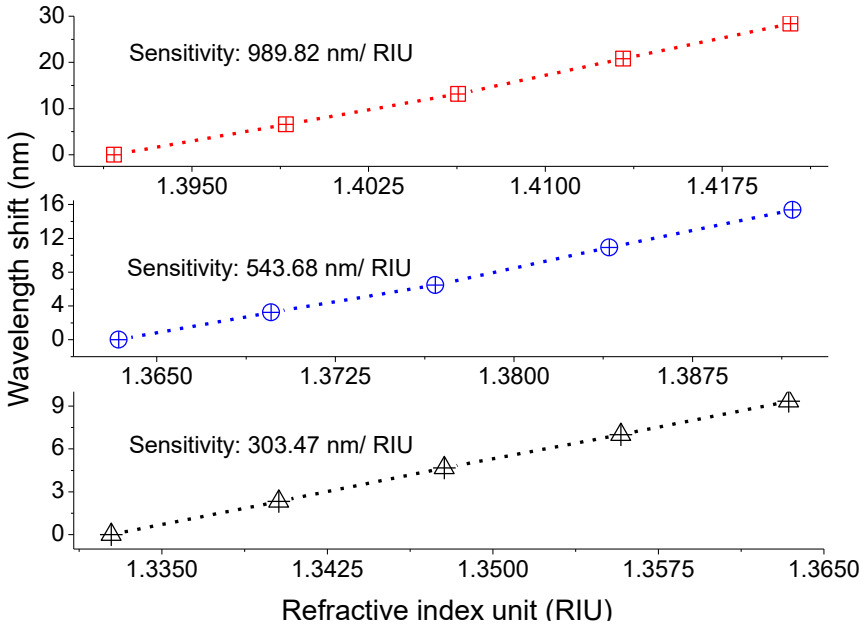

Figure 4.9 Elaborated refractive index sensitivity analysis of the MZI sensor (taper waist diameter: 50 µm, sensor length: 8 mm) for different index ranges of the solutions. The interferometer shows highest sensitivity of ~990 nm/RIU for RI range of 1.3917 to 1.4204

The performance of the tapered PCF MZI is evaluated by its sensitivity which is defined as the amount of resonance wavelength shift divided by the change in refractive index of the solution that causes the spectral shift. To compare the RI sensitivities between the sensors (one with taper waist diameter of 50 µm and sensing length of 8 mm, the other with taper waist diameter of 65 µm and sensing length of 3.88 mm) their RI responses shown in Figure 4.8 are divided into subplots in Figure 4.9 and Figure 4.10. The subplots show individual RI sensitivity of each interferometer for the ambient RI range of 1.3327 to 1.3634, 1.3634 to 1.3917, and 1.3917 to 1.4204. The subplots in Figure 4.9 show RI sensitivity of 303.47 nm/RIU, 543.68 nm/RIU, and 989.82 nm/RIU within the RI range of 1.3327 to 1.3634, 1.3634 to 1.3917, and 1.3917 to 1.4204, respectively. The subplots in Figure 4.10 show RI sensitivity of 334.03 nm/RIU, 673.91 nm/RIU, and 1426.70 nm/RIU within the RI range of 1.3327 to 1.3634, 1.3634 to 1.3917, and 1.3917

to 1.4204, respectively. Clearly, a sharper tapering over a shorter length of the fiber presents considerably higher RI sensitivity for given taper waist diameter.

4.5 Conclusion

We propose highly sensitive miniature RI sensor based on sharply tapered PCF MZI. The interferometer is constructed by fusion splicing of a small stub of PCF between SMFs and subsequent tapering of the PCF. The MZI sensor with taper waist diameter of 50 µm and length of 8 mm shows the maximum RI sensitivity of ~ 990 nm/RIU, while the senor with taper waist diameter of 65 µm and length of 3.88 mm shows the maximum RI sensitivity of ~ 1427 nm/RIU. Therefore, the RI sensitivity of tapered PCF interferometers can be greatly enhanced by means of sharp tapering for a particular taper waist diameter. Similar PCF MZI sensor shows temperature sensitivity of ~8 pm/ $^{\circ}$C [82] which is insignificant compare to its RI sensitivity. Low temperature sensitivity makes it an effective RI sensor.

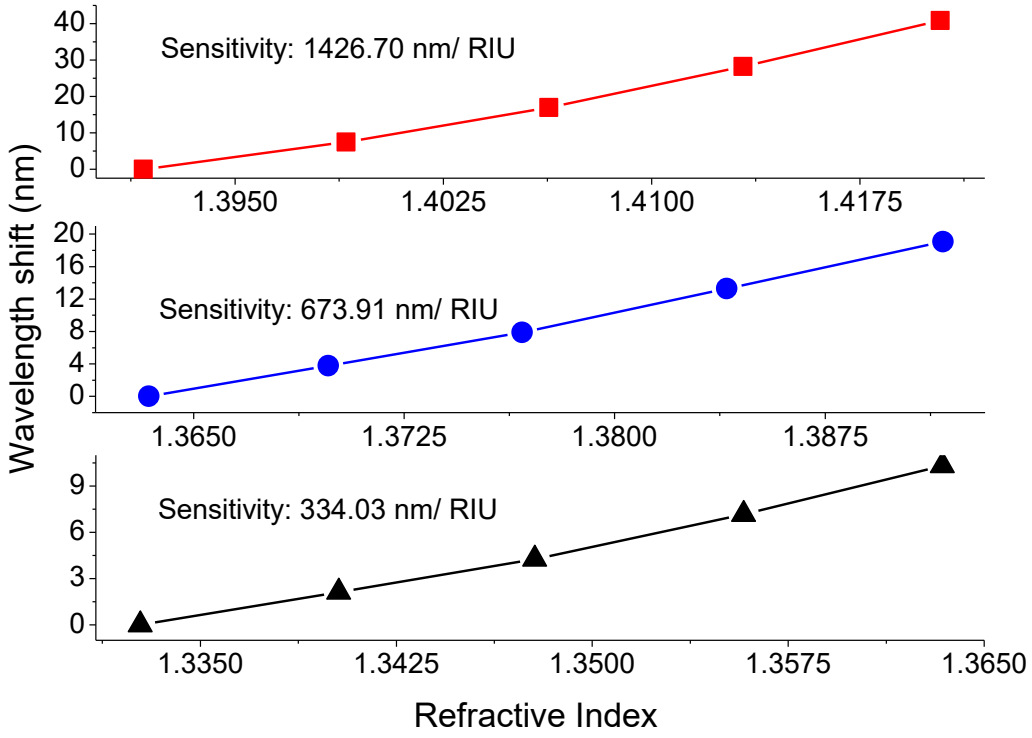

Figure 4.10 Elaborated refractive index sensitivity analysis of the MZI sensor (taper waist diameter: 65 µm, sensor length: 3.88 mm) for different index ranges of the solutions. The interferometer shows highest sensitivity of ~1427 nm/RIU for RI range of 1.3917 to 1.4204.

Chapter 5 Tapered Fiber-Optic Mach-Zehnder Interferometer for Ultra-High Sensitivity Measurement of Refractive Index

This paper was published in Journal of MDPI Sensors in 2019.

Vahid Ahsani, Farid Ahmed, Martin B. G. Jun, and Colin Bradley. "Tapered Fiber-Optic Mach-Zehnder Interferometer for Ultra-High Sensitivity Measurement of Refractive Index", Sensors 2019, 19, 1652; doi:10.3390/s19071652

Abstract

A Mach-Zehnder interferometer (MZI) based fiber-optic refractive index (RI) sensor is constructed by uniformly tapering standard single mode fiber (SMF) for RI measurement. A custom flame-based tapering machine is used to fabricate microfiber MZI sensors directly from SMFs. The fabricated MZI device does not require any splicing of fibers and it shows an excellent RI sensitivity. The sensor with a cladding diameter of 35.5 μm and a length of 20 mm exhibits the RI sensitivity of 415 nm/RIU for RI range of 1.332 to 1.384, 1103 nm/RIU for RI range of 1.384 to 1.4204 and 4234 nm/RIU for RI range of 1.4204 to 1.4408, respectively. The sensor reveals a temperature sensitivity of 0.0097 nm/°C, which is relatively low in comparison to its ultra-high RI sensitivity. The proposed inexpensive and highly sensitive optical fiber RI sensors have numerous applications in chemical and biochemical sensing fields.

5.1 Introduction

Fiber-optic refractive index (RI) sensors have attracted considerable attention for chemical and biochemical monitoring applications over the past few years [3, 4] because of their useful characteristics, such as: small size, high-resolution detection, excellent

aging characteristics, ability to operate in chemically hazardous environments, and immunity to electromagnetic noise. Many researchers have tried to enhance the effectiveness of optical fiber RI sensors by improving sensitivity [90], enhancing resolution [91], simplifying fabrication techniques [92], dropping cost [93], increasing the robustness of sensor structure [94], and reducing insertion loss [95].

Gratings and interferometers are the two main configurations studied for fiber-optic RI sensing [5]. Although the long period gratings (LPGs) are one of the broadly used RI sensors [9-13], writing gratings are usually expensive and function only in narrow wavelength bands due to fiber gratings phase matching phenomenon. In-fiber interferometers such as Fabry-Perot interferometer (FPI), Michelson interferometer (MI), and Mach-Zehnder interferometer (MZI) have been introduced as alternative and viable approaches for RI sensing [14]. Also, the combination of interferometers and gratings has been reported in the literature; for instance, MZI has been constructed based on a pair of LPGs to increase RI sensitivity further [14, 15].

Fiber-optic MZI sensors have been used in diverse monitoring applications including ambient RI [77, 96], temperature [97], pressure [98], torsion [99], and structural health [100] measurements. Recently, fiber MZI based RI sensing has gained considerable attention due to its enhanced sensitivity and fabrication simplicity. Alternative configurations for MZI sensors can be achieved utilizing various fiber types (such as multimode [14, 93, 101], microfiber [45], or photonic crystal fiber (PCF) [14, 47, 102]) or fabrication techniques (such as surface plasmon resonance (SPR) [91, 103, 104], core mismatch [14, 105, 106], and tapering [14, 107]). For example, concatenation of core-offset section and SMF abrupt taper is suggested to form an MZI [108]. This sensor

revealed a relatively low RI sensitivity of 28.2 nm/RIU for a sensor length of 30 mm and its fabrication involved complex steps. In 2015, Zhao et al. [109] reported a 30 mm long all-fiber MZI-based RI sensor by splicing an SMF stub between two SMFs with small core offset at two splicing points. The fabricated sensor showed the RI sensitivity of 78.7 nm/RIU in the range of 1.333 to 1.374 [109]. Although the fabrication process was simple and cost-effective, the reported RI sensitivity was relatively low. Another MZI sensor for RI measurement based on sandwiching and core-mismatched splicing of an SMF between two short sections of thin-core fibers was proposed by Rong et al. [105]. The maximum RI sensitivity of 159 nm/RIU for water-based solutions with an RI close to 1.33 was reported. In 2015, a PCF taper-based MZI for sensing changes in refractive index was presented with an RI sensitivity of 51.902 nm/RIU by Wu et al. [107]. The MZI sensor was fabricated by splicing a stub of PCF between two SMFs followed by PCF tapering. Such MZI configurations may not be feasible for many monitoring applications due to their weak mechanical strength and the use of expensive fiber. An inexpensive and simple to fabricate RI sensor with RI sensitivity of 158.4 nm/RIU based on two cascaded SMF tapers was demonstrated by Wang et al. in 2016 [110]. The fabrication of an MZI sensor for RI measurement from a long tapered single mode fiber was proposed by Yadav et al. [111]. The protein sensing device exhibited an RI sensitivity of about 1500 nm/RIU in the limited RI range of 1.3325 to 1.3377.

In this work, we present an ultra-high sensitivity, easy to fabricate, inexpensive, and mechanically robust in-line MZI based RI sensor constructed by tapering an SMF. A customized flame-based tapering machine was used to achieve sharp taper transitions and a uniform long taper waist in an SMF to create the MZI structure. For a specific taper

waist length, the dependence of the sensor's RI sensitivity on taper waist diameter (TWD) was investigated. In the RI range of 1.333 to 1.38, the RI sensitivities of 203 nm/RIU, 230 nm/RIU, 250 nm/RIU, 292 nm/RIU, and 415 nm/RIU were achieved for sensors with TWDs of 62 µm, 51.5 µm, 49 µm, 40 µm, and 35.5, respectively. A maximum RI sensitivity of 4234 nm/RIU was attained in the RI range of 1.4204 to 1.4408 for TWD 35.5 µm and taper waist length of 19.8 mm.

5.2 Principle of Sensor Operation

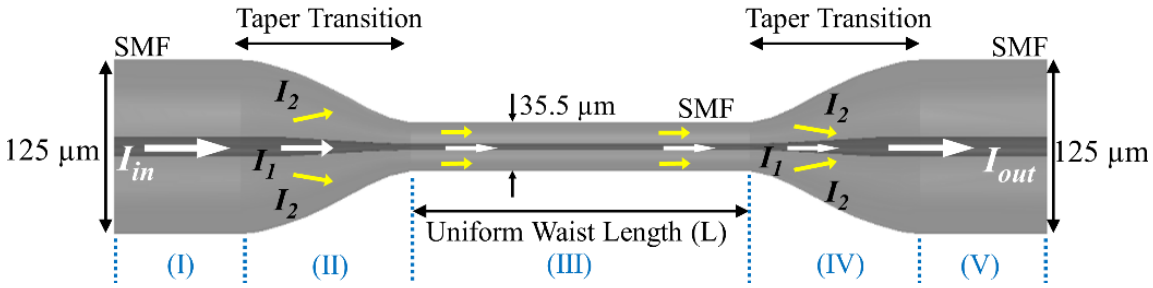

Figure 5.1 Schematic diagram of the internal structure of a microfiber MZI that was fabricated employing the long uniform tapering technique.

Nearly adiabatic tapering (both in down-taper and up-taper region) of SMF was used to achieve the MZI configuration. Such down-taper region is shown excite at least a few leaky modes which then recombine with the core more at the up-taper region to produce an interference pattern [112]. Figure 5.1 illustrates the schematic of the long uniform tapered based Mach-Zehnder interferometer, which was constructed using an SMF. In the schematic, when light travels from the region (I) to (II), higher order modes are excited which travel along with the fundamental mode through the tapered region (III). Because of the significant difference between glass and air indices, the fundamental and higher order modes couple back together in the region (IV) to form an interferometric pattern. The resultant interference spectrum is described by the following formula [113]:

$$I_{out} = I_1 + I_2 + 2\sqrt{I_1 I_2}\cos(\Delta\varphi) \quad \textbf{(Eq. 5.1)}$$

where I_{out}, I_1, and I_2 are the intensities of the interference signal, core, and cladding modes, respectively. $\Delta\varphi$ is the phase difference between the core and cladding modes that can be described by the following equation:

$$\Delta\varphi = \frac{2\pi}{\lambda}(\Delta n_{eff})L \quad \textbf{(Eq. 5.2)}$$

where λ is the light source central wavelength and L is the fiber uniform waist length. Δn_{eff} is the variance between the effective RI of the core and cladding modes:

$$\Delta n_{eff} = n_{eff}^{core} - n_{eff}^{cladding} \quad \textbf{(Eq. 5.3)}$$

where n_{eff}^{core} and $n_{eff}^{cladding}$ are the effective refractive indices of the core and cladding modes of the SMF, respectively. From Eq. (5.1) and (5.2), it can be found that the maximum transmission can happen when $\Delta\varphi = 2\pi(\Delta n_{eff})L/\lambda = 2m\pi$ (m is an integer). Therefore, the transmission signal shows peaks at the following wavelengths:

$$\lambda_m = (\Delta n_{eff})L/m \quad \textbf{(Eq. 5.4)}$$

$n_{eff}^{cladding}$ and Δn_{eff} will change if the RI of the solution being measured is differed. $\Delta\lambda_m$ describes the m order shift of the interference spectrum and is given by:

$$\Delta\lambda_m = \frac{(\Delta n_{eff} + \Delta n)L}{m} - \frac{\Delta n_{eff} L}{m} = \frac{\Delta n L}{m} \quad \textbf{(Eq. 5.5)}$$

where Δn is the change in the RI of the measurand solution. Thus, from Eq. (5.3), it can be seen that the variation of the transmission signal is a function of Δn when the

length of the sensor (*L)* is constant.

5.3 Sensor Fabrication

Figure 5.2 (a) displays the Computer Aided Design (CAD) assembly model of the customized flame-based tapering machine designed for the sensor fabrication. The enlarged image in Figure 5.2 (b) shows the shutter mechanism integrated into the system to provide a controlled heat deposition into the fiber that in turn offers an accurate geometry of the tapered profile. A pair of converging/diverging nozzles as shown in Figure 5.3 was used to generate a heated volume that had a length of about 0.8 mm along the direction of the fiber axis. hydrogen (99.99 % pure) at a pressure of 20 psi was fed into the nozzles to avoid pollution on the tapered fiber. The flame temperature was controlled to remain above the fiber's softening point whilst keeping it below the glass's melting point. For standard single mode fiber (SMF) the required temperature of 900 °C was maintained. After stripping and perfectly wiping the mid-section of an SMF with acetone, the fiber was clamped on two linear motorized stages. Travel distance, the speed of each stage, and delay time to open or close the shutter were set in the tapering control software independently. The tapering parameters were tuned and optimized to obtain several tapered waist diameters as shown in Table 5.1.

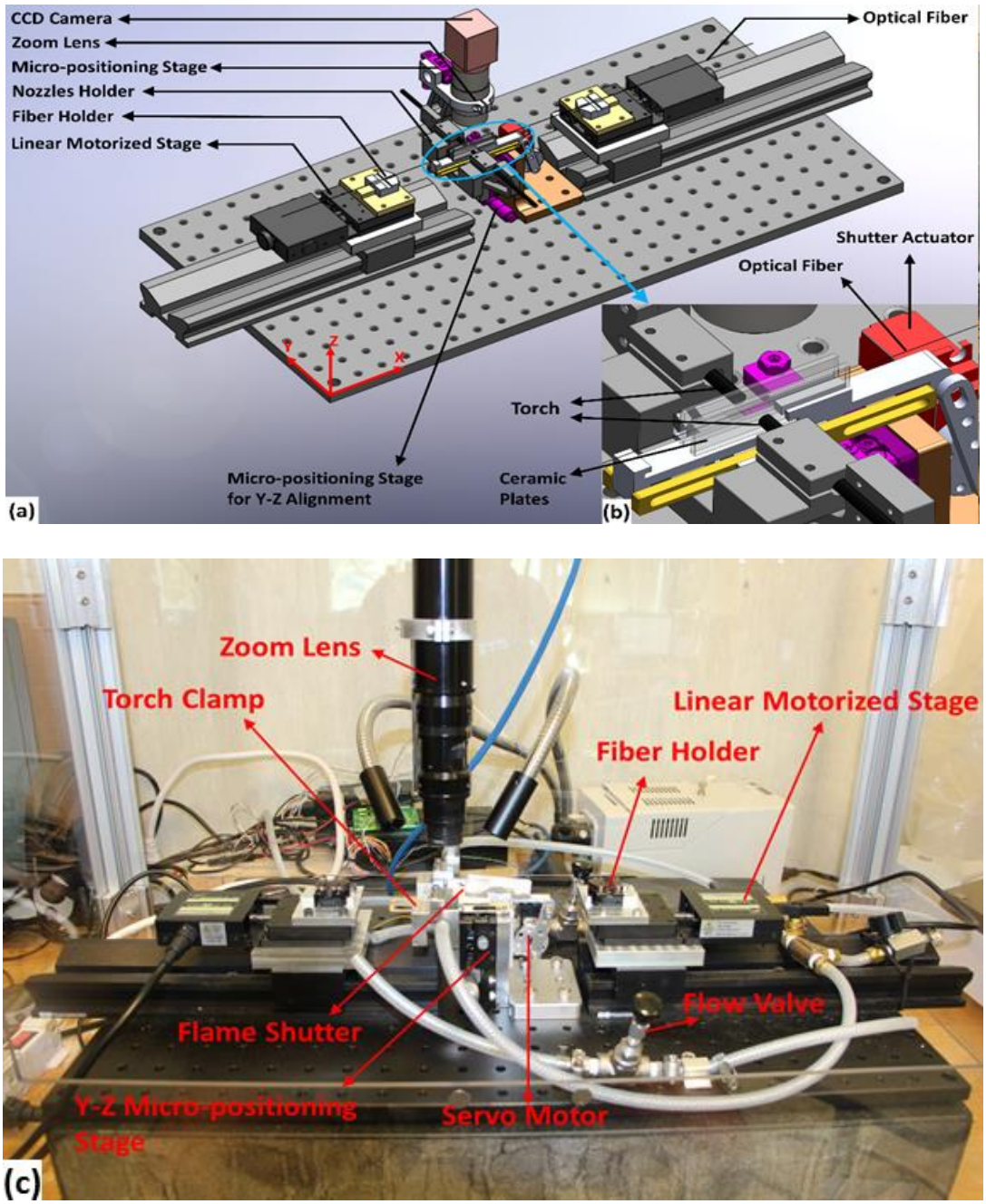

Figure 5.2 (a) Assembly model of the custom flame-based tapering machine and, (b) design of the sliding shutter mechanism to control heat delivery to the fiber, and (c) assembled custom flame- based tapering machine.

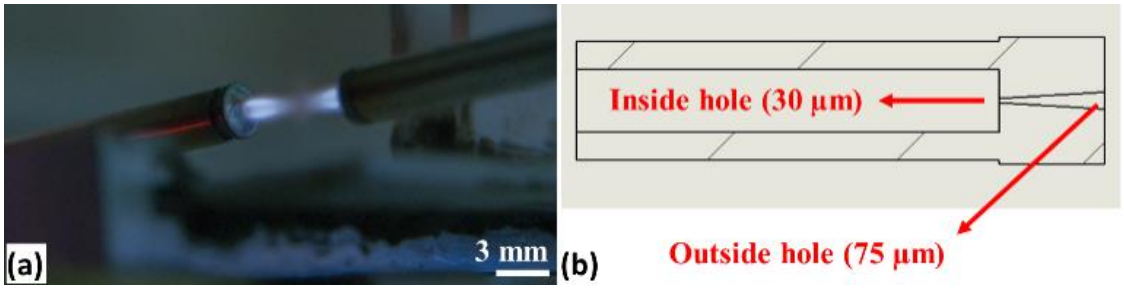

Figure 5.3 (a) Size of hydrogen flame used for long uniform tapering and, (b) the cross-section of the fabricated converging/diverging micro nozzle.

Table 5.1 The manufacturing process parameters controlled to fabricate the sensors with a range of sensitivities.

Pushing Speed (µm/s)	Pushing Distance (mm)	Pulling Speed (µm/s)	Pulling Distance (mm)	Shutter Open Delay (ms)	Shutter Close Delay (ms)	TWD (µm)
25	5	100	20	2000	0	62
25	3.5	140	19.6	2000	500	51.5
30	3	195	19.5	2000	500	49
25	2.2	225	19.6	2000	500	40
25	1.8	275	19.8	2000	500	35.5

The difference in the pulling and pushing speeds causes the fiber material to move in front of the flame and thus creates a long uniform taper profile. The generated sharp tapering angle split the core light into core and cladding light at the first transition region while the second transition re-combined these two beams of light into a core light. Therefore, because of the optical path difference (OPD) between core and cladding arms, an interference fringe was generated. Although the core mode is restricted in the core, the transmission properties of the cladding modes can change as a result of the RI variation at the cladding-ambient interface. Smaller fiber diameter enables the cladding modes to reach closer to the measurand solution. Therefore, this enabled sensors with an improved RI sensitivity to be fabricated. Figure 5.4 shows the left and right taper transition profiles and the uniform taper waist of 35.5 µm in the middle.

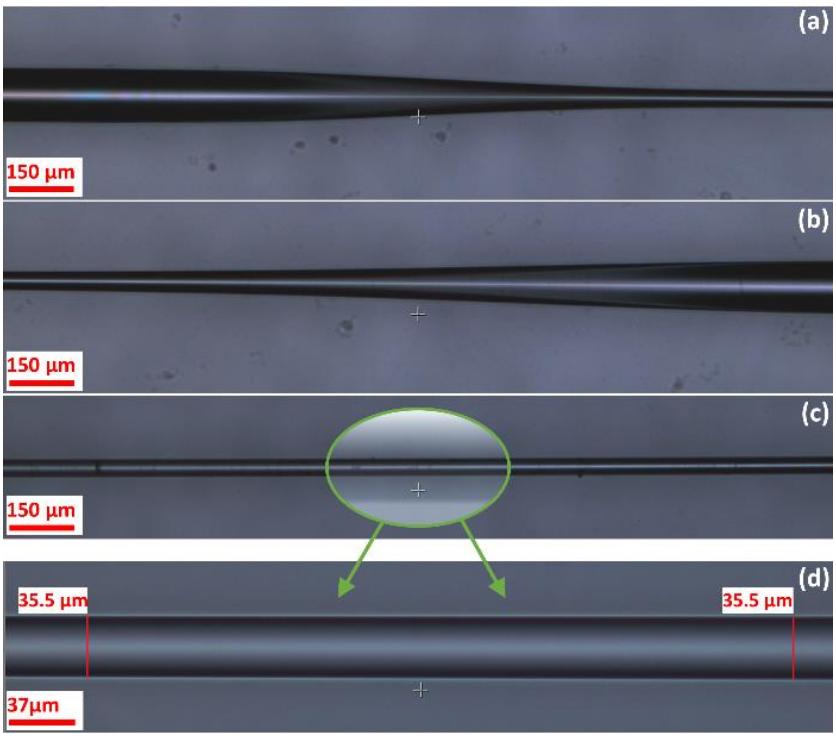

Figure 5.4 (a and b) SMF taper transition, (c) long uniform taper waist, (d) magnified image of the uniform taper waist.

5.4 Results and Discussion

Due to the high sensitivity of MZI sensors to fiber twisting, the sensor was thoroughly secured on two fiber clamps in the RI characterization setup. Subsequently, the fiber was connected to a broadband light source (AMONICS ASLD-CWDM-5-B-FA, Spectrum range: 1250- 1650 nm) and a spectrum analyzer (PHOTONETICS Walics, Resolution: 0.02 nm, Spectrum range: 1450- 1650 nm), to study the optical characteristics of the tapered microfiber MZI. The schematic of the RI characterization setup is illustrated in Figure 5.5. The response of interference fringes due to ambient RI change was examined for the MZIs with fiber TWDs of 62 µm, 51.5 µm, 49 µm, 40 µm, and 35.5 µm. These sensors were characterized with glycerin solutions of various concentrations at a room

temperature of 22 °C. They were submerged in glycerin solutions of different RI ranging from 1.332 to 1.440 to achieve characterization data. After each step, sensors were thoroughly cleaned with acetone, before immersing them in an increasingly greater concentration of glycerin solution. Figure 5.6 illustrates the ambient RI dependent spectral response of the MZI sensor with the TWD of 35.5 µm. The interference between broadband core mode and narrowband cladding mode may give rise to the asymmetric spectrum as explained by Fano interference phenomenon [114]. The MZI structure that generates such transmission interference is also very sensitive to an external perturbation such as ambient RI change. This might explain why this sensor is ultra-sensitive to RI.

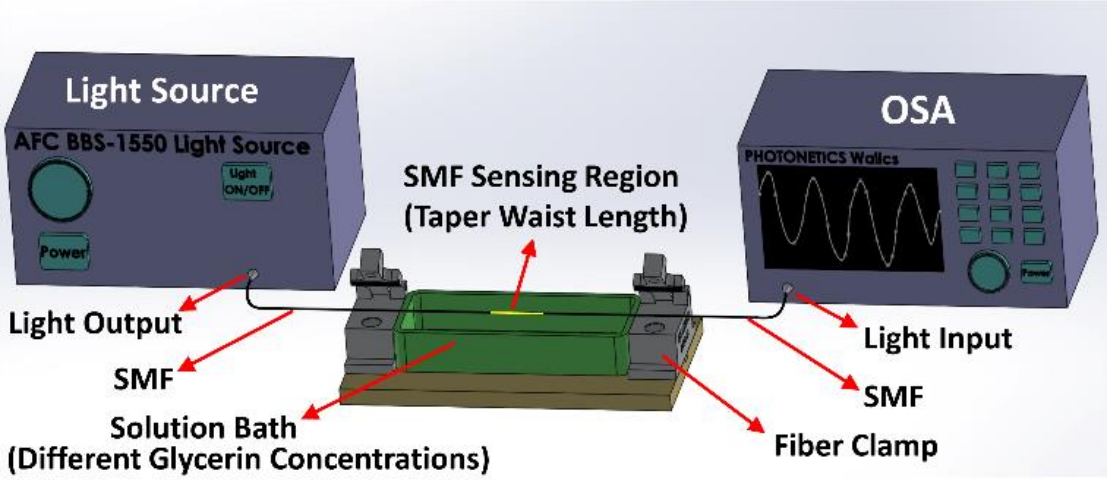

Figure 5.5 Schematic diagram of experimental setup for refractive index characterization, OSA (Optical Spectrum Analyzer).

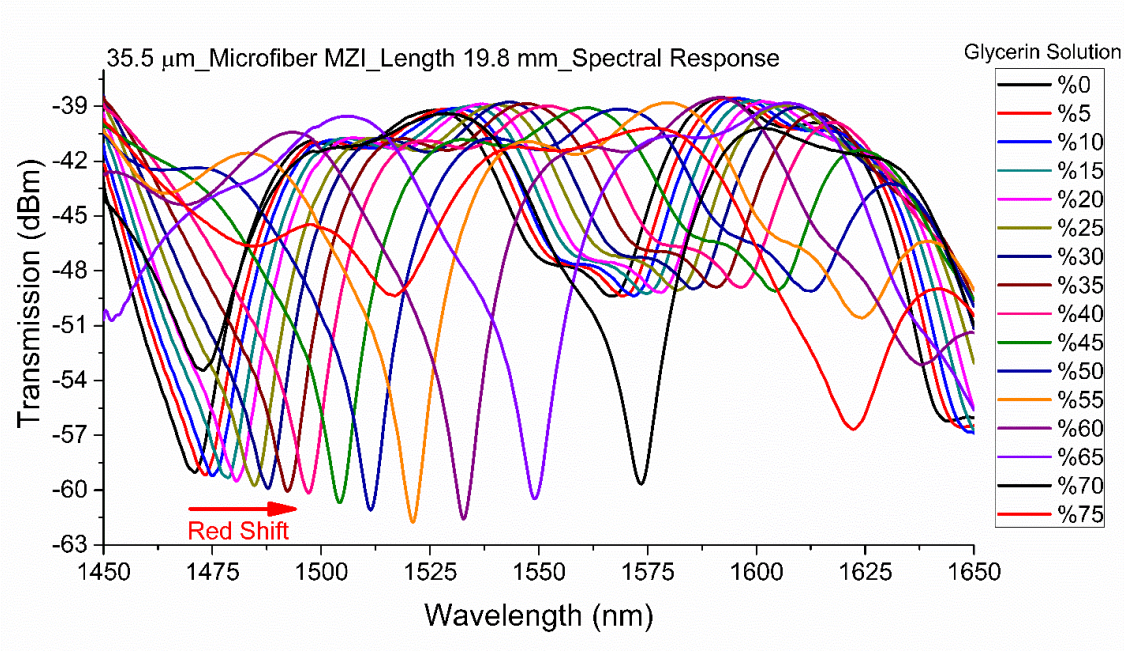

Figure 5.6 Spectral response of the MZI sensor with a 35.5 µm TWD to various concentrations of glycerin solution.

Figure 5.7 displays the RI dependent wavelength shifts of three tapered MZIs with different TWDs. The plot also includes the absolute value of wavelength shifts due to ambient RI change of the RI sensor fabricated by splicing a microfiber (diameter: 40 µm) between a lead-in and lead-out SMFs. As the surrounding RI increases, a red-shift was observed in the MZI interference fringe. The performance of the microfiber MZIs were evaluated by their sensitivities which were interpreted as the ratio of resonance wavelength shift to the variation in solution refractive index. The microfiber MZI with smallest TWD (35.5 µm) was chosen and its elaborated sensitivity graphs plotted in Figure 5.8, which shows more details of RI sensitivity analysis. Three subplots were generated from Figure 5.6 for index ranges of 1.3327 to 1.3840, 1.3840 to 1.4204 and 1.4204 to 1.4408 (Figure 5.8).

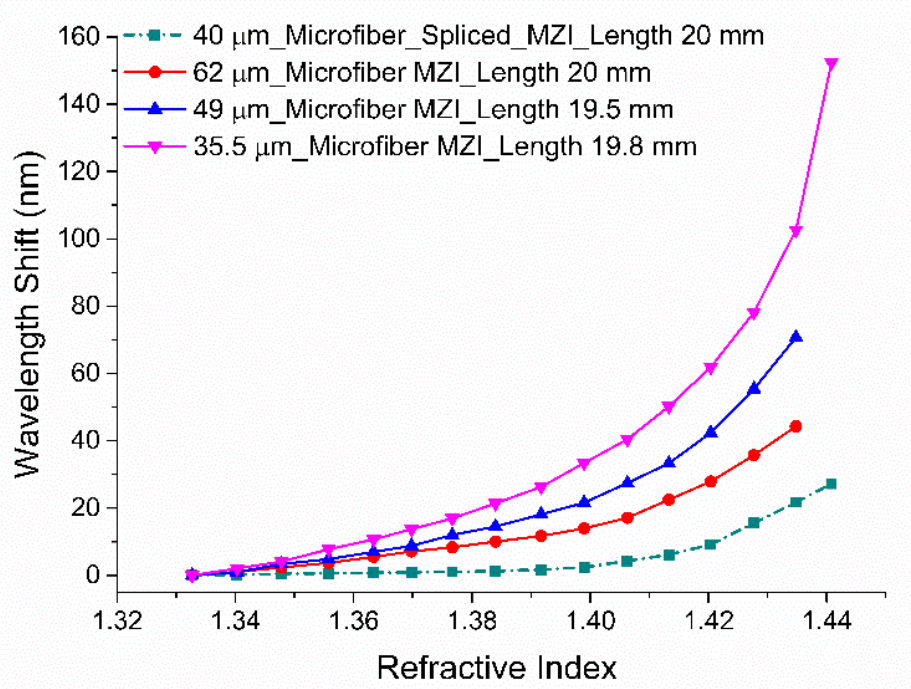

Figure 5.7 The spectral shift of the microfiber MZIs, with various waist diameters, due to changes in RI.

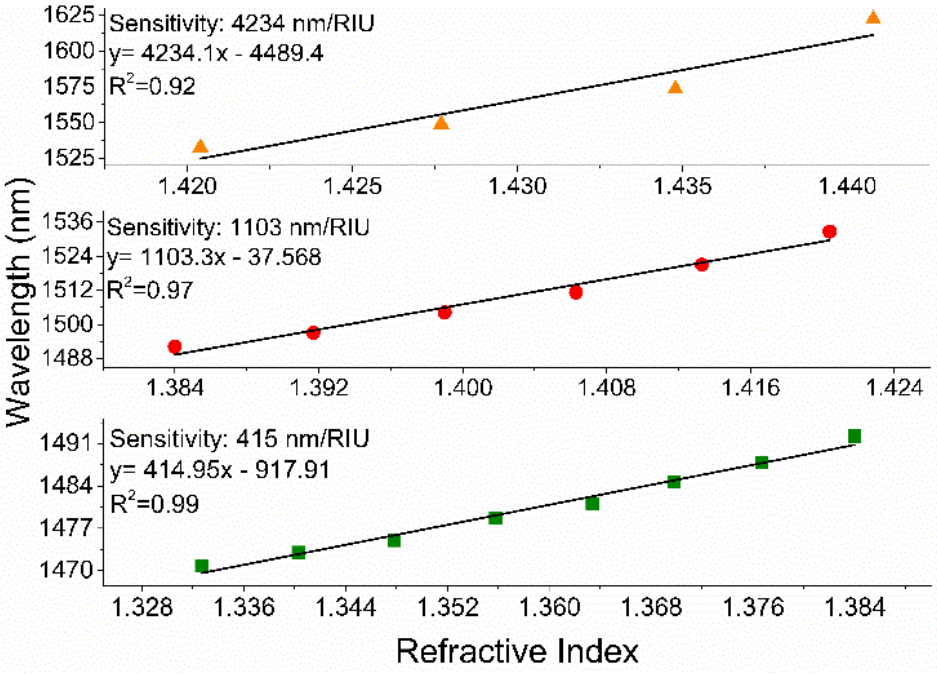

Figure 5.8 Linearization of the MZI sensor's wavelength shift necessary to characterize sensitivity in three RI ranges. The characterized sensor has a TWD of 35.5 µm and taper waist length of 19.8 mm. The maximum RI sensitivity of ~ 4234 nm/RIU in the RI range of 1.4204 to 1.4408 was achieved.

The effect of temperature cross-sensitivity needs to be considered in ambient RI measurement as the RI of most solutions changes with temperature variation. To determine the temperature response of the sensor configuration, an MZI sensor with a TWD of 35.5 µm and a length of 19.8 mm was placed in an oven for temperature characterization. The oven temperature gradually elevated from 25 °C to 65 °C in 5 °C increments. The correlation between the wavelength shift and the sensor's temperature is shown in Figure 5.9. The temperature sensitivity of the MZI sensor is 0.0097 nm/°C. As a result, the RI measurement error, because of temperature effect, is approximately 2.33×10^{-5} RIU/°C and, therefore, negligible.

Figure 5.10 illustrates the effect of decreasing TWD (while keeping the taper waist length approximately constant) on RI sensitivity of the fabricated MZIs in various RI ranges. As the TWD decreases, the RI sensitivity of the fabricated MZIs increases nonlinearly. Microfiber MZIs with fiber diameters of 35.5 µm, 40 µm, 49 µm, 51.5 µm, and 62 µm were characterized for RI range from 1.3327 to 1.4348.

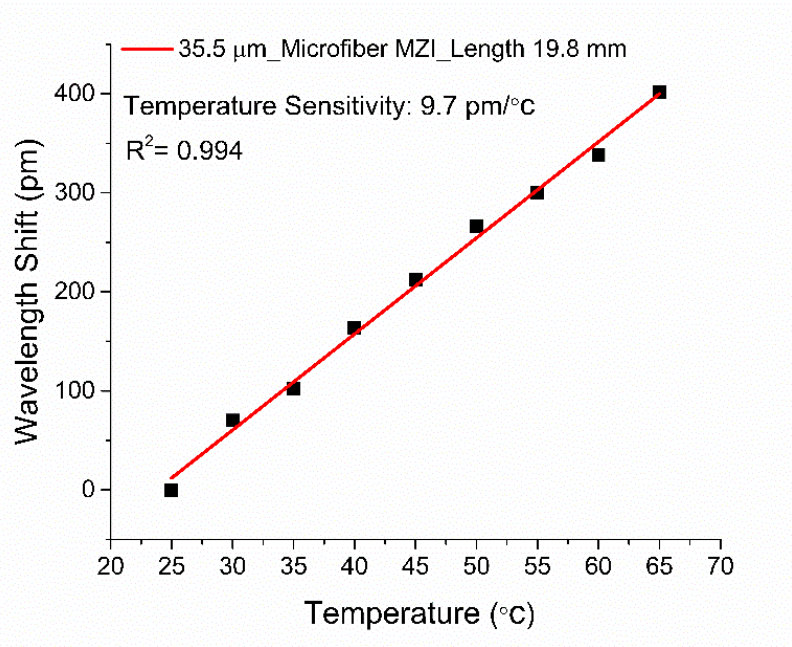

Figure 5.9 Temperature characterization of the microfiber MZI RI sensor with a TWD of 35.5 µm.

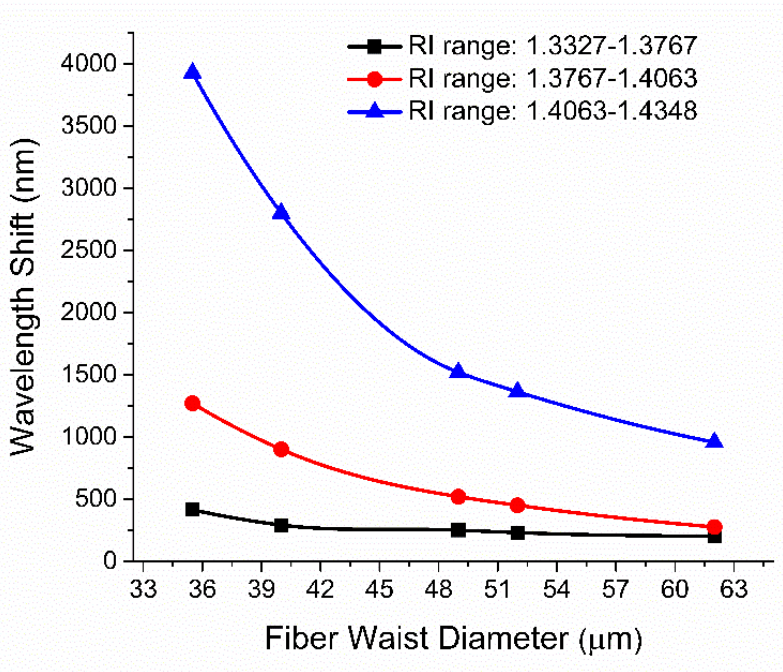

Figure 5.10 The relation between spectral wavelength shift and fiber waist diameter for various microfiber MZIs with different TWDS.

The results of the RI sensitivity analysis for microfiber MZIs with TWDs of 62 µm, 49 µm, and 35.5 µm, over six different refractive index ranges are summarized in Table

5.2.

Table 5.2 The RI sensitivity of three microfiber MZIs with various TWDs and constant taper lengths are shown for different RI ranges.

RI Range / TWD	1.3327 to 1.3767	1.3767 to 1.4063	1.4063 to 1.4348	1.3327 to 1.3840	1.3840 to 1.4204	1.4204 to 1.4408
Microfiber MZI (62 μm)	203 nm/RIU	290 nm/RIU	957 nm/RIU	NA	NA	NA
Microfiber MZI (49 μm)	277 nm/RIU	550 nm/RIU	1520 nm/RIU	NA	NA	NA
Microfiber MZI (35.5 μm)	NA	NA	NA	415 nm/RIU	1103 nm/RIU	4234 nm/RIU

5.5 Conclusion

An easy and cost-effective fabrication of a fiber-optic MZI for ultra-high sensitivity RI measurement is proposed in this study. The MZI is constructed by tapering a standard SMF-28 fiber. Several MZIs, with constant taper length but different uniform TWDs, were fabricated to investigate the sensor's structural influence on RI measurement. The MZIs with uniform TWDs of 62 μm, 49 μm, and 35.5 μm show the maximum sensitivities of 956 nm/RIU, 1520 nm/RIU, and 4234 nm/RIU, respectively. The MZI device shows a temperature sensitivity of 0.0097 nm/°C which is insignificant relative to its RI sensitivity. Since the fabrication of this sensor does not require any splicing, it is likely to have insignificant insertion losses and stronger mechanical properties compared to spliced microfiber MZI. Also, the high sensitivity characteristic of Mach-Zehnder interferometers makes them suitable for chemical, biochemical, and biological sensing in an aqueous environment.

Chapter 6 Conclusion, and Future Work

6.1 Conclusion

The research work presented in this dissertation comprises four peer-reviewed and published journal papers and one peer-reviewed conference paper. It provides a description of the research process that developed the design and fabrication of fiber-optic sensors for measuring ambient refractive index changes within different RI ranges. The main objective of the research was to find alternative sensor configuration and fabrication techniques to construct optical fiber sensors, in particular MZIs, for RI measurement with high RI sensitivity, while keeping manufacturing cost and complexity low.

Chapter 2 presented research on fabricating a sensor device that measures temperature and refractive index simultaneously. This work addressed the technical challenge of measuring ambient refractive index change of solutions while the ambient temperature varies. Fabrication of Mach-Zehnder interferometer using a short stub of single mode microfiber sandwiched between two standard single mode fibers was proposed. Fiber Bragg grating was then inscribed on the microfiber, using a pulse laser and the point-by-point inscription method. The device's compact sensor package was characterized as an RI sensor with various concentrations of glycerin solutions in the RI range of 1.33 to 1.44. Testing of the sensor included a temperature characterization, to determine its temperature sensitivity. As anticipated, the FBG's signal was not sensitive to ambient RI changes, while the MZI signal was sensitive to both ambient RI changes and temperature changes. Therefore, a systematic approach was suggested to properly use the sensor device as a temperature compensated RI sensor. The sensor package itself can also be

used to measure temperature and RI changes simultaneously.

The work presented in chapter 3 builds upon the research explained in chapter 2. During the fabrication of Fiber Bragg Gratings on microfiber using a pulse laser, the question arose as to whether or not one can measure the amount of in-fiber refractive index change that occurs while the gratings are inscribed. This led to a study on designing and fabricating a cost-effective device to measure the amount of pulse energy that causes the in-fiber refractive index to change. Therefore, the novel idea of using an easy to fabricate MZI sensor that indirectly measures the amount of refractive index modulation caused by the femtosecond laser on the core of standard single mode fiber was pursued. That MZI device was fabricated using a small stub of SMF, which was spliced between lead-in and a lead-out SMFs with a slight core misalignment. The core and cladding of the single mode fiber were used as sensing and reference arms, respectively. The in-line fiber-optic MZI was firmly positioned on a 3-axis stage prior to the core index modification, to ensure that the tension on the fiber remained unaffected during the experiment. The fringe shift of the MZI, caused by the core index modification due to laser pulses, was used to indicate RI measurements. The measurement of RI change, as high as 0.01356 and as low as 0.000475, was demonstrated. These fabrication techniques provide a simple yet effective method for quantifying in-fiber effective RI changes. This research has the potential to provide a cost effective approach for estimating laser-induced RI changes in optical fibers, which is indispensable for the design and fabrication of in-fiber photonic devices.

Chapter 4 outlined the design and manufacturing of a custom flame-based tapering machine to be used in fiber-optic sensor fabrication. The machine was designed to cover

a wide range of tapering techniques. Photonic Crystal Fiber (PCF) was used as an RI sensing device. Various sensors with different lengths of PCF were constructed. For each sensor, PCF with a specific length was spliced between two standard single mode fibers in fabricating Mach-Zehnder Interferometers. The fabricated MZIs were then tapered, with different tapering conditions, down to various fiber diameters. This approach was applied to experimentally observe the performance of the tapered sensors during and after the tapering process. Cross sections of the fabricated tapered PCF-MZIs were observed under an optical microscope, to ensure that the array of air holes along the PCF were preserved during and after the tapering process. The manufactured sensors were characterized with an array of glycerin solutions with different concentrations, ranging from 0% to 80% in 5% increments and from RI of 1.33 to 1.42, respectively. The MZI sensor with a taper waist diameter of 50 µm and a length of 8 mm recorded the maximum RI sensitivity of ~ 990 nm/RIU in the RI range of 1.3917 to 1.4204, while the senor with taper a waist diameter of 65 µm and a length of 3.88 mm revealed the maximum RI sensitivity of ~ 1427 nm/RIU over the same RI range. It was reported that the RI sensitivity of tapered PCF interferometers can be greatly enhanced by means of sharp tapering for a particular taper waist diameter. Because similar PCF MZI sensors have shown the low temperature sensitivity of ~ 8 pm/ ^{0}C, it can be concluded that the fabricated sensor can be reliably used as an effective, highly sensitive RI sensor in various chemical and bio-chemical applications.

The work presented in chapter 5 continued the research shown in chapter 4. The custom and unique tapering machine designed and developed through the present research was utilized to fabricate an easily produced and cost-effective fiber-optic MZI

for ultra-high sensitivity RI measurement. The proposed MZI sensor was constructed using only one piece of single mode fiber, sharply and uniformly tapered. The machine was controlled so that it could perform nearly adiabatic tapering (both in down-taper and up-taper regions) of an SMF, to achieve the desired MZI configuration. The integration of the converging/diverging nozzles to generate a heated volume, which had a length of about 0.8 mm along the direction of the fiber axis, and the accurate ceramic shutter mechanism into the system provide a controlled heat deposition into the fiber that in turn offers an accurate geometry of the tapered profile. Equivalent levels of accuracy are usually only provided by commercial laser-based or arc-based tapering machines. The effect of different taper waist diameters (TWD) on the ambient RI sensitivity of various SMF MZIs with a fixed length of about 20 mm were investigated. The fabricated SMF MZI sensors with TWDs of 62 µm, 51.5 µm, 49 µm, 40 µm, and 35.5 µm were characterized for RI sensing with glycerin solutions of various concentrations at a room temperature of 22 °C. The MZIs with uniform TWDs of 62 µm, 49 µm, and 35.5 µm showed maximum sensitivities of 956 nm/RIU, 1520 nm/RIU, and 4234 nm/RIU, respectively. The MZI device shows a temperature sensitivity of 0.0097 nm/°C, which is negligible in comparison to its RI sensitivity. Considering the fabrication of this sensor, which does not require any splicing, it is likely to have only insignificant insertion losses and stronger mechanical properties when compared to spliced microfiber MZIs. Further, the ultra-high RI sensitivity of the proposed Mach-Zehnder Interferometer makes it suitable for chemical, biochemical, and biological sensing in aqueous environments.

6.2 Future Work

Future research work that could extend and complement results presented in this dissertation may include the following topics:

- Other fiber-optic types, such as Multimode Fibers, can be used to fabricate Mach-Zehnder Interferometers while integrating tapering processes with sharp tapering angles.
- Simulation of the tapering process presented in this dissertation to better understand the effect of each parameter that is involved.
- Modeling the effect of tapering angle on the mode field mismatch and the modal characteristic of the tapered fiber with sharp tapering angle could uncover the most effective tapering angle. Consequently, the full with at half maximum (FWHM) of the transmission valley of an MZI determines the resolution of sensing as the resolution is inversely proportional to FWHM.
- Investigating the effect of tapering hollow-core photonic crystal fiber (HC-PCF) for fiber-optic MZI fabrication. In particular, observing the potential geometry deformation of the hollow core.
- Studying the fabrication challenges of the tapered MZI sensor with Bragg grating for fabrication of a temperature compensated and highly sensitive refractive index sensor.
- Investigating the idea of using ceramic rings instead of nozzles and flames to heat up the optical fiber. This can provide a more uniform heat deposition into the optical fiber, thus more uniform taper profiles could be achieved.

Bibliography

[1] K. T. V. Grattan and T. Sun, "Fiber optic sensor technology: an overview," *Sensors and Actuators A: Physical,* vol. 82, no. 1–3, pp. 40-61, 5/15/ 2000.

[2] P. Wang, H. Zhao, X. Wang, G. Farrell, and G. Brambilla, "A Review of Multimode Interference in Tapered Optical Fibers and Related Applications," *Sensors (Basel),* vol. 18, no. 3, Mar 14 2018.

[3] X.-d. Wang and O. S. Wolfbeis, "Fiber-Optic Chemical Sensors and Biosensors (2013–2015)," *Analytical Chemistry,* vol. 88, no. 1, pp. 203-227, 2016/01/05 2016.

[4] D. Wu *et al.*, "Refractive index sensing based on Mach–Zehnder interferometer formed by three cascaded single-mode fiber tapers," *Applied Optics,* vol. 50, no. 11, pp. 1548-1553, 2011/04/10 2011.

[5] Y. Xu, P. Lu, L. Chen, and X. Bao, "Recent Developments in Micro-Structured Fiber Optic Sensors," *Fibers,* vol. 5, no. 1, p. 3, 2017.

[6] V. Bhatia and A. M. Vengsarkar, "Optical fiber long-period grating sensors," *Optics Letters,* vol. 21, no. 9, pp. 692-694, 1996/05/01 1996.

[7] A. D. Kersey *et al.*, "Fiber grating sensors," *Journal of Lightwave Technology,* vol. 15, no. 8, pp. 1442-1463, 1997.

[8] A. Othonos, "Fiber Bragg gratings," *Review of Scientific Instruments,* vol. 68, no. 12, pp. 4309-4341, 1997.

[9] J. Joo-Nyung, K. Se Yoon, K. Sun-Wook, and K. Min-Sung, "Temperature insensitive long-period fibre gratings," *Electronics Letters,* vol. 35, no. 24, pp. 2134-2136, 1999.

[10] B. Li, L. Jiang, S. Wang, H.-L. Tsai, and H. Xiao, "Femtosecond laser fabrication of long period fiber gratings and applications in refractive index sensing," *Optics & Laser Technology,* vol. 43, no. 8, pp. 1420-1423, 11// 2011.

[11] M. Smietana, M. L. Korwin-Pawlowski, W. J. Bock, G. R. Pickrell, and J. Szmidt, "Refractive index sensing of fiber optic long-period grating structures coated with a plasma deposited diamond-like carbon thin film," *Measurement Science and Technology,* vol. 19, no. 8, p. 085301, 2008.

[12] J. Yang, L. Yang, C.-Q. Xu, C. Xu, W. Huang, and Y. Li, "Long-period grating refractive index sensor with a modified cladding structure for large operational range and high sensitivity," *Applied Optics,* vol. 45, no. 24, pp. 6142-6147, 2006/08/20 2006.

[13] F. Ahmed, H.-E. Joe, B.-K. Min, and M. B. G. Jun, "Characterization of refractive index change and fabrication of long period gratings in pure silica fiber by femtosecond laser radiation," *Optics & Laser Technology,* vol. 74, pp. 119-124, 11// 2015.

[14] B. H. Lee *et al.*, "Interferometric fiber optic sensors," *Sensors (Basel),* vol. 12, no. 3, pp. 2467-86, 2012.

[15] R. Correia, S. James, S. W. Lee, S. P. Morgan, and S. Korposh, "Biomedical application of optical fibre sensors," *Journal of Optics,* vol. 20, no. 7, p. 073003, 2018/06/08 2018.

[16] S. S. Chong, A. A. A. Raman, S. W. Harun, and H. Arof, "Dual Output Approach in Dye Concentrations Determination Using Non-Adiabatic Tapered Fiber," *IEEE Sensors Journal,* vol. 15, no. 7, pp. 3903-3908, 2015.

[17] Y. Chen and H. Ming, "Review of surface plasmon resonance and localized surface plasmon resonance sensor," *Photonic Sensors,* journal article vol. 2, no. 1, pp. 37-49, March 01 2012.

[18] A. B. Socorro, I. Del Villar, J. M. Corres, I. R. Matias, and F. J. Arregui, "Lossy mode resonances dependence on the geometry of a tapered monomode optical fiber," *Sensors and Actuators A: Physical*, vol. 180, pp. 25-31, 2012/06/01/ 2012.

[19] L. Tong *et al.*, "Subwavelength-diameter silica wires for low-loss optical wave guiding," *Nature*, 10.1038/nature02193 vol. 426, no. 6968, pp. 816-819, 12/18/print 2003.

[20] Y.-H. Tai and P.-K. Wei, "Sensitive liquid refractive index sensors using tapered optical fiber tips," *Optics Letters*, vol. 35, no. 7, pp. 944-946, 2010/04/01 2010.

[21] O. International Conference on Integrated, C. Optical Fibre, and C. European Conference on Optical, "IOOC-ECOC '85 : 5th International Conference on Integrated Optics and Optical Fibre Communication : 11th European Conference on Optical Communication : Venezia, Italy, October 1-4, 1985 : technical digest," Genova, Italy: Istituto Internazionale Delle Communicazioni.

[22] H. Latifi, M. I. Zibaii, S. M. Hosseini, and P. Jorge, "Nonadiabatic tapered optical fiber for biosensor applications," *Photonic Sensors*, vol. 2, no. 4, pp. 340-356, 2012/12/01 2012.

[23] H. S. MacKenzie and F. P. Payne, "Evanescent field amplification in a tapered single-mode optical fibre," *Electronics Letters*, vol. 26, no. 2, pp. 130-132Available: https://digital-library.theiet.org/content/journals/10.1049/el_19900089

[24] A. Massaro, L. Pierantoni, and T. Rozzi, "Far-field radiation of optical fibers with tapered end," *Journal of Lightwave Technology*, vol. 24, no. 8, pp. 3162-3168, 2006.

[25] E. C. Mägi, P. Steinvurzel, and B. J. Eggleton, "Tapered photonic crystal fibers," *Optics Express*, vol. 12, no. 5, pp. 776-784, 2004/03/08 2004.

[26] C. E. Chryssou, "Theoretical analysis of tapering fused silica optical fibers using a carbon dioxide laser," *Optical Engineering*, vol. 38, no. 10, pp. 1645-1649, 1999.

[27] G. M. Rego, P. V. S. Marques, J. L. Santos, and H. M. Salgado, "Estimation of the fibre temperature during the inscription of arc-induced long-period gratings," *Optics Communications*, vol. 259, no. 2, pp. 620-625, 2006.

[28] W. J. Bock, J. Chen, P. Mikulic, and T. Eftimov, "A Novel Fiber-Optic Tapered Long-Period Grating Sensor for Pressure Monitoring," *IEEE Transactions on Instrumentation and Measurement*, vol. 56, no. 4, pp. 1176-1180, 2007.

[29] Z. Tian *et al.*, "Refractive Index Sensing With Mach-Zehnder Interferometer Based on Concatenating Two Single-Mode Fiber Tapers," *IEEE Photonics Technology Letters*, vol. 20, no. 8, pp. 626-628, 2008.

[30] F. B. a. J.-P. Meunier, "Efficient fabrication of fused-fiber biconical taper structures by a scanned CO2 laser beam techniques," *Applied Optics*, vol. 44, pp. 6402-6411, 2005.

[31] P. Wang, G. Brambilla, M. Ding, Y. Semenova, Q. Wu, and G. Farrell, "High-sensitivity, evanescent field refractometric sensor based on a tapered, multimode fiber interference," *Optics Letters*, vol. 36, no. 12, pp. 2233-2235, 2011/06/15 2011.

[32] R. Nagai and T. Aoki, "Ultra-low-loss tapered optical fibers with minimal lengths," *Opt Express*, vol. 22, no. 23, pp. 28427-36, Nov 17 2014.

[33] M. Z. A. Razak, S. A. Reduan, A. S. Sharbirin, N. Jamaludin, M. Z. Zulkifli, and H. Ahmad, "Noncontact Optical Displacement Sensor Using an Adiabatic U-Shaped Tapered Fiber," *IEEE Sensors Journal*, vol. 15, no. 10, pp. 5388-5392, 2015.

[34] H. L. Sorensen, E. S. Polzik, and J. Appel, "Heater Self-Calibration Technique for Shape Prediction of Fiber Tapers," *Journal of Lightwave Technology*, vol. 32, no. 10, pp. 1886-1891, 2014.

[35] G. Kakarantzas, T. E. Dimmick, T. A. Birks, R. Le Roux, and P. S. J. Russell, "Miniature all-fiber devices based on CO2 laser microstructuring of tapered fibers," *Optics Letters,* vol. 26, no. 15, pp. 1137-1139, 2001/08/01 2001.

[36] D. J. Flannigan and K. S. Suslick, "Plasma formation and temperature measurement during single-bubble cavitation," *Nature,* 10.1038/nature03361 vol. 434, no. 7029, pp. 52-55, 03/03/print 2005.

[37] G. Badenes *et al.*, "Tapered photonic crystal fibres: properties, characterisation, and applications (Invited Paper)," vol. 5840, p. 29, 2005.

[38] D. M. n.-H. n. Joel Villatoro, and Efrain Mejı´a, "Fabrication and modeling of uniform-waist single-mode tapered optical fiber sensors," *Applied Optics,* vol. 42, no. 13, pp. 2278-2283, 2003.

[39] G. Rego, L. M. N. B. F. Santos, and B. Schröder, "Estimation of the fiber temperature during an arc-discharge," *Microwave and Optical Technology Letters,* vol. 50, no. 8, pp. 2020-2025, 2008.

[40] J. M. Ward, A. Maimaiti, V. H. Le, and S. N. Chormaic, "Contributed Review: Optical micro- and nanofiber pulling rig," *Review of Scientific Instruments,* vol. 85, no. 11, p. 111501, 2014.

[41] A. Cronin *et al.*, "Laser-based workstation for the manufacture of fused biconical tapered coupler devices," vol. 5827, p. 505, 2005.

[42] J. M. Ward, D. G. O'Shea, B. J. Shortt, M. J. Morrissey, K. Deasy, and S. l. G. Nic Chormaic, "Heat-and-pull rig for fiber taper fabrication," *Review of Scientific Instruments,* vol. 77, no. 8, p. 083105, 2006.

[43] M. C. Frawley, A. Petcu-Colan, V. G. Truong, and S. Nic Chormaic, "Higher order mode propagation in an optical nanofiber," *Optics Communications,* vol. 285, no. 23, pp. 4648-4654, 2012.

[44] G. Brambilla, "Optical fibre nanowires and microwires: a review," *Journal of Optics,* vol. 12, no. 4, p. 043001, 2010.

[45] F. Ahmed, V. Ahsani, A. Saad, and M. B. G. Jun, "Bragg Grating Embedded in Mach-Zehnder Interferometer for Refractive Index and Temperature Sensing," *IEEE Photonics Technology Letters,* vol. 28, no. 18, pp. 1968-1971, 2016.

[46] F. Ahmed, V. Ahsani, S. Jo, C. Bradley, E. Toyserkani, and M. B. G. Jun, "Measurement of In-Fiber Refractive Index Change Using a Mach–Zehnder Interferometer," *IEEE Photonics Technology Letters,* vol. 31, no. 1, pp. 74-77, 2019.

[47] F. Ahmed, V. Ahsani, L. Melo, P. Wild, and M. B. G. Jun, "Miniaturized Tapered Photonic Crystal Fiber Mach–Zehnder Interferometer for Enhanced Refractive Index Sensing," *IEEE Sensors Journal,* vol. 16, no. 24, pp. 8761-8766, 2016.

[48] V. Ahsani, F. Ahmed, M. B. G. Jun, and C. Bradley, "Tapered Fiber-Optic Mach-Zehnder Interferometer for Ultra-High Sensitivity Measurement of Refractive Index," *Sensors,* vol. 19, no. 7, p. 1652, 2019.

[49] B. H. Lee *et al.*, "Interferometric Fiber Optic Sensors," (in English), *Sensors,* vol. 12, no. 3, pp. 2467-2486, Mar 2012.

[50] K. T. V. Grattan and T. Sun, "Fiber Optic Sensor Technology: Introduction and Overview," in *Optical Fiber Sensor Technol.*: Springer US, 2000, pp. 1-44.

[51] L. C. Li, X. Li, Z. H. Xie, Z. L. Liao, F. Tu, and D. M. Liu, "Simultaneous measurement of refractive index and temperature using thinned fiber based Mach-Zehnder interferometer," (in English), *Optics Communications,* vol. 285, no. 19, pp. 3945-3949,

Sept. 2012.
[52] L. Li, X. Li, Z. Xie, Z. Liao, F. Tu, and D. Liu, "Simultaneous measurement of refractive index and temperature using thinned fiber based Mach–Zehnder interferometer," *Optics Communications,* vol. 285, no. 19, pp. 3945-3949, 2012.
[53] P. Lu, L. Q. Men, K. Sooley, and Q. Y. Chen, "Tapered fiber Mach-Zehnder interferometer for simultaneous measurement of refractive index and temperature," (in English), *Applied Physics Letters,* vol. 94, no. 13, Mar 30 2009.
[54] H. P. Luo, Q. Z. Sun, Z. L. Xu, D. M. Liu, and L. Zhang, "Simultaneous measurement of refractive index and temperature using multimode microfiber-based dual Mach-Zehnder interferometer," (in English), *Optics Letters,* vol. 39, no. 13, pp. 4049-4052, Jul 1 2014.
[55] Y. Cao, H. Y. Liu, Z. R. Tong, S. Yuan, and J. Su, "Simultaneous measurement of temperature and refractive index based on a Mach-Zehnder interferometer cascaded with a fiber Bragg grating," (in English), *Optics Communications,* vol. 342, pp. 180-183, May 1 2015.
[56] Q. Q. Yao *et al.*, "Simultaneous measurement of refractive index and temperature based on a core-offset Mach-Zehnder interferometer combined with a fiber Bragg grating," (in English), *Sensors and Actuators a-Physical,* vol. 209, pp. 73-77, Mar 1 2014.
[57] Y. J. Kim, U. C. Paek, and B. H. Lee, "Measurement of refractive-index variation with temperature by use of long-period fiber gratings," (in English), *Optics Letters,* vol. 27, no. 15, pp. 1297-1299, Aug 1 2002.
[58] H. Y. Choi, M. J. Kim, and B. H. Lee, "All-fiber Mach-Zehnder type interferometers formed in photonic crystal fiber," (in English), *Optics Express,* vol. 15, no. 9, pp. 5711-5720, Apr 30 2007.
[59] F. Ahmed and M. B. G. Jun, "Microfiber Bragg grating sandwiched between standard optical fibers for enhanced temperature sensing," *IEEE Photon. Technol. Lett.,* no. 99, Dec. 2015.
[60] Y. Wang, M. W. Yang, D. N. Wang, S. J. Liu, and P. X. Lu, "Fiber in-line Mach-Zehnder interferometer fabricated by femtosecond laser micromachining for refractive index measurement with high sensitivity," (in English), *Journal of the Optical Society of America B-Optical Physics,* vol. 27, no. 3, pp. 370-374, Mar 2010.
[61] C. R. Liao, Y. Wang, D. N. Wang, and M. W. Yang, "Fiber In-Line Mach-Zehnder Interferometer Embedded in FBG for Simultaneous Refractive Index and Temperature Measurement," (in English), *Ieee Photonics Technology Letters,* vol. 22, no. 22, pp. 1686-1688, Nov 15 2010.
[62] Y. F. Lu, C. Y. Shen, C. Zhong, D. B. Chen, X. Y. Dong, and J. H. Cai, "Refractive Index and Temperature Sensor Based on Double-Pass M-Z Interferometer With an FBG," (in English), *Ieee Photonics Technology Letters,* vol. 26, no. 11, pp. 1124-1127, Jun 1 2014.
[63] V. R. Bhardwaj *et al.*, "Femtosecond laser-induced refractive index modification in multicomponent glasses," *Journal of Applied Physics,* vol. 97, no. 8, p. 083102, 2005.
[64] K. O. Hill, Y. Fujii, D. C. Johnson, and B. S. Kawasaki, "Photosensitivity in optical fiber waveguides: Application to reflection filter fabrication," *Applied Physics Letters,* vol. 32, no. 10, pp. 647-649, 1978.
[65] L. A. Fernandes, O. Sezerman, G. Best, M. L. Ng, and S. Kane, "Direct writing of fiber optic components in photonic crystal fibers and other specialty fibers," in *SPIE LASE*, 2016, vol. 9740, p. 9: SPIE.
[66] K. Minoshima, A. M. Kowalevicz, I. Hartl, E. P. Ippen, and J. G. Fujimoto, "Photonic

device fabrication in glass by use of nonlinear materials processing with a femtosecond laser oscillator," *Optics Letters,* vol. 26, no. 19, pp. 1516-1518, 2001/10/01 2001.

[67] M. Hughes, W. Yang, and D. Hewak, "Fabrication and characterization of femtosecond laser written waveguides in chalcogenide glass," (in English), *Applied Physics Letters,* vol. 90, no. 13, Mar 26 2007.

[68] H. El-Ghandoor, E. Abd El-Ghafar, and R. Hassan, "Refractive index profiling of a GRIN optical fiber using a modulated speckled sheet of light," (in English), *Optics and Laser Technology,* vol. 31, no. 7, pp. 481-488, Oct 1999.

[69] F. Ahmed, H. E. Joe, B. K. Min, and M. B. G. Jun, "Characterization of refractive index change and fabrication of long period gratings in pure silica fiber by femtosecond laser radiation," (in English), *Optics and Laser Technology,* vol. 74, pp. 119-124, Nov 2015.

[70] P. Oberson, B. Gisin, B. Huttner, and N. Gisin, "Refracted near-field measurements of refractive index and geometry of silica-on-silicon integrated optical waveguides," (in English), *Applied Optics,* vol. 37, no. 31, pp. 7268-7272, Nov 1 1998.

[71] A. D. Yablon, "Multi-Wavelength Optical Fiber Refractive Index Profiling by Spatially Resolved Fourier Transform Spectroscopy," (in English), *Journal of Lightwave Technology,* vol. 28, no. 4, pp. 360-364, Feb 15 2010.

[72] Z. Y. Liu, X. M. Dong, Q. H. Chen, C. Y. Yin, Y. X. Xu, and Y. J. Zheng, "Nondestructive measurement of an optical fiber refractive-index profile by a transmitted-light differential interference contact microscope," (in English), *Applied Optics,* vol. 43, no. 7, pp. 1485-1492, Mar 1 2004.

[73] B. L. Bachim and T. K. Gaylord, "Microinterferometric optical phase tomography for measuring small, asymmetric refractive-index differences in the profiles of optical fibers and fiber devices," (in English), *Applied Optics,* vol. 44, no. 3, pp. 316-327, Jan 20 2005.

[74] D. Johlen, H. Renner, A. Ewald, and E. Brinkmeyer, "Fiber Bragg grating Fabry-Perot interferometer for a precise measurement of the UV-induced index change," (in English), *24th European Conference on Optical Communication, Vol 1-3,* pp. 393-394, 1998.

[75] E. Fertein, C. Przygodzki, H. Delbarre, A. Hidayat, M. Douay, and P. Niay, "Refractive-index changes of standard telecommunication fiber through exposure to femtosecond laser pulses at 810 cm," (in English), *Applied Optics,* vol. 40, no. 21, pp. 3506-3508, Jul 20 2001.

[76] L. Jiang, J. Yang, S. Wang, B. Li, and M. Wang, "Fiber Mach-Zehnder interferometer based on microcavities for high-temperature sensing with high sensitivity," (in English), *Optics Letters,* vol. 36, no. 19, pp. 3753-3755, Oct 1 2011.

[77] J. Wo *et al.*, "Refractive index sensor using microfiber-based Mach–Zehnder interferometer," *Optics Letters,* vol. 37, no. 1, pp. 67-69, 2012/01/01 2012.

[78] T. Allsop, R. Reeves, D. J. Webb, I. Bennion, and R. Neal, "A high sensitivity refractometer based upon a long period grating Mach–Zehnder interferometer," *Review of Scientific Instruments,* vol. 73, no. 4, pp. 1702-1705, 2002.

[79] P. S. J. Russell, "Photonic-Crystal Fibers," *Journal of Lightwave Technology,* vol. 24, no. 12, pp. 4729-4749, 2006/12/01 2006.

[80] W. N. MacPherson *et al.*, "Remotely addressed optical fibre curvature sensor using multicore photonic crystal fibre," *Optics Communications,* vol. 193, no. 1–6, pp. 97-104, 6/15/ 2001.

[81] J. N. Wang and J. L. Tang, "Photonic crystal fiber Mach-Zehnder interferometer for refractive index sensing," *Sensors (Basel),* vol. 12, no. 3, pp. 2983-95, 2012.

[82] C. Li, S.-J. Qiu, Y. Chen, F. Xu, and Y.-Q. Lu, "Ultra-Sensitive Refractive Index Sensor With Slightly Tapered Photonic Crystal Fiber," *IEEE Photonics Technology Letters,* vol. 24, no. 19, pp. 1771-1774, 2012.

[83] S.-j. Qiu, Y. Chen, J.-l. Kou, F. Xu, and Y.-q. Lu, "Miniature tapered photonic crystal fiber interferometer with enhanced sensitivity by acid microdroplets etching," *Applied Optics,* vol. 50, no. 22, pp. 4328-4332, 2011/08/01 2011.

[84] Q. Liu and Q. Wang, "Refractive index sensor based on tapered PCF in-line interferometer," *Chinese Optics Letters,* vol. 10, no. 9, pp. 090601-090601, 2012/09/01 2012.

[85] G. A. Cárdenas-Sevilla, V. Finazzi, J. Villatoro, and V. Pruneri, "Photonic crystal fiber sensor array based on modes overlapping," *Optics Express,* vol. 19, no. 8, pp. 7596-7602, 2011/04/11 2011.

[86] H. P. Uranus, "Theoretical study on the multimodeness of a commercial endlessly single-mode PCF," *Optics Communications,* vol. 283, no. 23, pp. 4649-4654, 12/1/ 2010.

[87] R. Jha, J. Villatoro, G. Badenes, and V. Pruneri, "Refractometry based on a photonic crystal fiber interferometer," *Optics Letters,* vol. 34, no. 5, pp. 617-619, 2009/03/01 2009.

[88] J.-l. Kou, J. Feng, Q.-j. Wang, F. Xu, and Y.-q. Lu, "Microfiber-probe-based ultrasmall interferometric sensor," *Optics Letters,* vol. 35, no. 13, pp. 2308-2310, 2010/07/01 2010.

[89] J. Villatoro, V. Finazzi, G. Badenes, and V. Pruneri, "Highly Sensitive Sensors Based on Photonic Crystal Fiber Modal Interferometers," *Journal of Sensors,* vol. 2009, pp. 1-11, 2009.

[90] M. Shao, X. Qiao, H. Fu, Y. Liu, X. Zhao, and N. Yao, "High sensitivity refractive index sensing of Mach–Zehnder interferometer based on multimode fiber core sandwiched between two waist-enlarged fiber tapers," *Optics Communications,* vol. 311, pp. 359-363, 2013.

[91] D. Monzón-Hernández and J. Villatoro, "High-resolution refractive index sensing by means of a multiple-peak surface plasmon resonance optical fiber sensor," *Sensors and Actuators B: Chemical,* vol. 115, no. 1, pp. 227-231, 2006.

[92] L. Li, L. Xia, Z. Xie, L. Hao, B. Shuai, and D. Liu, "In-line fiber Mach–Zehnder interferometer for simultaneous measurement of refractive index and temperature based on thinned fiber," *Sensors and Actuators A: Physical,* vol. 180, pp. 19-24, 2012.

[93] H. Wang *et al.*, "Simultaneous measurement of refractive index and temperature based on asymmetric structures modal interference," *Optics Communications,* vol. 364, pp. 191-194, 2016.

[94] K. Ni, X. Dong, C. C. Chan, T. Li, L. Hu, and W. Qian, "Miniature refractometer based on Mach–Zehnder interferometer with waist-enlarged fusion bitaper," *Optics Communications,* vol. 292, pp. 84-86, 2013.

[95] Z. Tian, S. S. H. Yam, and H.-P. Loock, "Single-Mode Fiber Refractive Index Sensor Based on Core-Offset Attenuators," *IEEE Photonics Technology Letters,* vol. 20, no. 16, pp. 1387-1389, 2008.

[96] F. Ahmed, V. Ahsani, L. Melo, P. Wild, and M. B.-G. Jun, "Miniaturized Tapered Photonic Crystal Fiber Mach-Zehnder Interferometer for Enhanced Refractive Index Sensing," *IEEE Sensors Journal,* pp. 1-1, 2016.

[97] L. Viet Nguyen, D. Hwang, S. Moon, D. Seung Moon, and Y. Chung, "High temperature fiber sensor with high sensitivity based on core diameter mismatch," *Optics Express,* vol. 16, no. 15, pp. 11369-11375, 2008/07/21 2008.

[98] W. Talataisong, D. N. Wang, R. Chitaree, C. R. Liao, and C. Wang, "Fiber in-line Mach–Zehnder interferometer based on an inner air-cavity for high-pressure sensing," *Optics Letters,* vol. 40, no. 7, pp. 1220-1222, 2015/04/01 2015.
[99] J. M. Sierra-Hernandez *et al.*, "Torsion sensing setup based on a three beam path Mach–Zehnder interferometer," *Microwave and Optical Technology Letters,* vol. 57, no. 8, pp. 1857-1860, 2015.
[100] !!! INVALID CITATION !!! {}.
[101] H. Fu *et al.*, "TCF-MMF-TCF fiber structure based interferometer for refractive index sensing," *Optics and Lasers in Engineering,* vol. 69, pp. 58-61, 2015.
[102] Y. Zhao, D. Wu, and Q. Wang, "All-fiber Mach-Zehnder interferometer using a tapered photonic crystal fiber for refractive index measurement," in *IEEE SENSORS 2014 Proceedings*, 2014, pp. 1080-1083.
[103] B. Grunwald and G. Holst, "Fibre optic refractive index microsensor based on white-light SPR excitation," *Sensors and Actuators A: Physical,* vol. 113, no. 2, pp. 174-180, 2004.
[104] A. K. Sharma, R. Jha, and B. D. Gupta, "Fiber-Optic Sensors Based on Surface Plasmon Resonance: A Comprehensive Review," *IEEE Sensors Journal,* vol. 7, no. 8, pp. 1118-1129, 2007.
[105] Q. Rong, X. Qiao, R. Wang, H. Sun, M. Hu, and Z. Feng, "High-Sensitive Fiber-Optic Refractometer Based on a Core-Diameter-Mismatch Mach–Zehnder Interferometer," *IEEE Sensors Journal,* vol. 12, no. 7, pp. 2501-2505, 2012.
[106] Y. Cao, H. Liu, Z. Tong, S. Yuan, and J. Su, "Simultaneous measurement of temperature and refractive index based on a Mach–Zehnder interferometer cascaded with a fiber Bragg grating," *Optics Communications,* vol. 342, pp. 180-183, 2015.
[107] D. Wu, Y. Zhao, and J. Li, "PCF taper-based Mach–Zehnder interferometer for refractive index sensing in a PDMS detection cell," *Sensors and Actuators B: Chemical,* vol. 213, pp. 1-4, 2015.
[108] G. Yin, S. Lou, and H. Zou, "Refractive index sensor with asymmetrical fiber Mach–Zehnder interferometer based on concatenating single-mode abrupt taper and core-offset section," *Optics & Laser Technology,* vol. 45, pp. 294-300, 2013.
[109] Y. Zhao, X.-g. Li, and L. Cai, "A highly sensitive Mach–Zehnder interferometric refractive index sensor based on core-offset single mode fiber," *Sensors and Actuators A: Physical,* vol. 223, pp. 119-124, 2015.
[110] Q. Wang, W. Wei, M. Guo, and Y. Zhao, "Optimization of cascaded fiber tapered Mach–Zehnder interferometer and refractive index sensing technology," *Sensors and Actuators B: Chemical,* vol. 222, pp. 159-165, 2016.
[111] T. K. Yadav, R. Narayanaswamy, M. H. Abu Bakar, Y. M. Kamil, and M. A. Mahdi, "Single mode tapered fiber-optic interferometer based refractive index sensor and its application to protein sensing," *Opt Express,* vol. 22, no. 19, pp. 22802-7, Sep 22 2014.
[112] D. Jauregui-Vazquez, J. W. Haus, A. B. H. Negari, J. M. Sierra-Hernandez, and K. Hansen, "Bitapered fiber sensor: Signal analysis," *Sensors and Actuators B: Chemical,* vol. 218, pp. 105-110, 2015/10/31/ 2015.
[113] A. Ghatak, *Optics*, 4th Edition ed. Tata McGraw-Hill Publishing Company Limited, 2009.
[114] X. Piao, S. Yu, and N. Park, "Control of Fano asymmetry in plasmon induced transparency and its application to plasmonic waveguide modulator," *Optics Express,* vol. 20, no. 17, pp. 18994-18999, 2012/08/13 2012.

Appendix A

Miniature Dual Flame-based Tapering Process and System Development for Fabrication of Optical Fiber Sensors

Published and Presented in the World Congress on Micro and Nono Manufacturing, 2017, Taiwan
Vahid Ahsani, Farid Ahmed, Junghyuk Ko, Colin Bradley, and Martin B. G. Jun

Abstract

A dual flame-based tapering system is designed for optical fiber sensor's development. Micro-scale converging/diverging nozzles with various hole diameters (i.e., 75 µm outside and 30 µm inside) are laser machined using a 120 femtosecond laser to offer miniature flames. Such a flame is ideal for very short tapers with an adiabatic condition and uniform taper waist geometry. Since the hot zone is shrunk and its width is reduced to about 800 µm, the necessity of having two flames to ensure the satisfaction of the above-mentioned conditions for tapering can be predicted. A sliding shutter mechanism is designed and integrated into the system to provide better control over the transferred heat from the flame to the fiber. The shutter is made out of ceramic plates and actuates with a HiTEC HS-7235MH servomotor. This servomotor can open and close the shutter in less than 400 ms. Results of interference-based optical fiber sensor tapering, to increase the sensor sensitivity, are discussed.

1. Introduction

Different types of tapering machines have been developed and investigated [25, 26]. They are mainly categorized into arc-based [27-29], laser-based [30, 31], and flame-

based machines [32-34]. Each design has its advantages and disadvantages. Arc and laser can provide a minuscule and fixed heating volume, which leads to the small tapering region, thus limiting fabrication of different sensor configurations [28, 29]. Heating the fiber with a laser beam is neither easy nor cheap [31, 35]. Another limitation with arc and laser based tapering machines is temperature measurement and control [26, 36], which is a crucial parameter for an adiabatic tapering. To make an adiabatically tapered fiber and reduce the amount of losses, perfect control over the generated heat is required [37]. The temperature of the heating volume can be measured by a thermocouple with an excellent accuracy when heated by torch [38]; however, this simple measurement is not feasible in an arc and laser based tapering machines [27, 39]. Another specific limitation of CO_2 laser-based tapering machines is the complexity of directly heating the fiber when its diameter is less than 1 μm because of the inverse square relationship between fiber radius and heating for a CO_2 laser [40]. This issue can be resolved by using a flame heat source, which has an inverse relationship with fiber radius. Thus fibers can be tapered down to smaller diameters with flame-based tapering machines [41, 42]. Controlling the temperature gradient and fiber geometry are the challenges when tapering fibers below 1 μm, due to the turbulence of the flame and convection [19]. It is even more challenging when miniature tapering with a flame smaller than 1 mm or tapering using oscillating flame is performed [40].

There are three main configurations in which flame-based tapering machines are typically set up for optical micro- or nanofiber (MNF) fabrication. (i) Stacked pulling stages with a fixed flame [34], (ii) independent pulling stages with a fixed flame [43], and (iii) independent pulling stages and an oscillating flame [33, 44]. The schematic of

these flame brushing rigs is presented in Fig. 1.

In this work, we present the development of a dual flame tapering system with micro-scale nozzles. A shutter mechanism with millisecond-scale actuation time is integrated into the system to provide better control over the transferred heat to the optical fiber. The current design of the machine provides the capability for an adiabatic and uniform tapering of optical fibers with a broad range of length (from 0.8 mm to a couple of centimeters).

2. System design and control

2.1 Design Overview

After reviewing the tapering machines, in particular, the flame-based ones [40], the parameters for design and development of a unique flame-based tapering machine, which has the capability to taper fiber with wider ranges of taper lengths has been identified. Therefore, the machine was designed to enable simple nozzle exchange, and various nozzles were developed and machined to have different flame sizes. Moreover, a novel flame shutter mechanism was designed and integrated into the system to provide an excellent accuracy in the geometry of tapered profile when tapering very short length of fiber.

The machine has two linear-motorized stages TSDM60-20X that provide a resolution of 1 μm/pulse. Two fiber holders were mounted on these stages to hold the fiber securely. In this design, it is vital to be able to position different torches properly in the X, Y, and Z directions. Therefore, a micro-positioning stage was used to position torches in the Y and the Z directions. The designed torch-clamp provides the alignment in the X direction.

Besides, another micro-positioning stage was used to finely adjust the focal position of the PointGrey FL3-U3-13E4 CCD camera and its zoom lens in the Z direction (see Fig. 2).

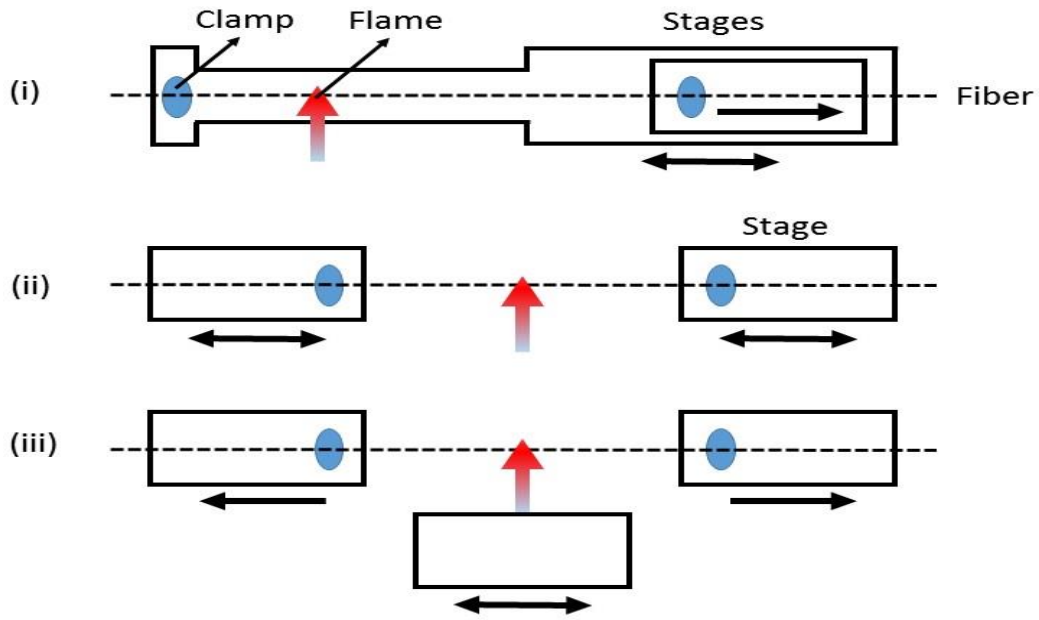

Fig. 1. (i) Stacked pulling stages with a fixed flame, (ii) independent pulling stages with a fixed flame, and (iii) independent pulling stages and an oscillating flame.

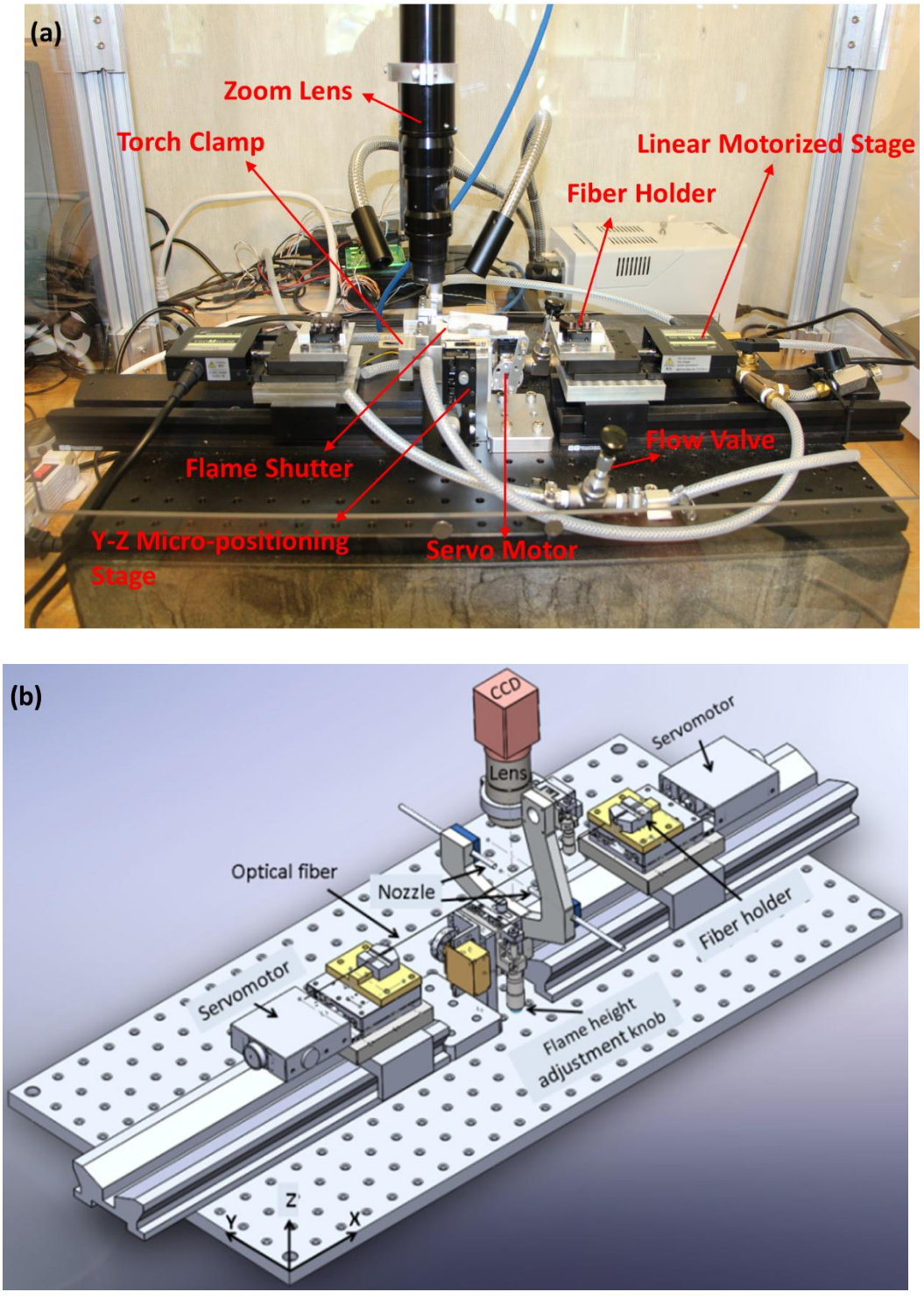

Fig. 2. (a) Manufactured flame-based tapering machine, and (b) 3D model of the designed machine.

2.2 Nozzle Design

Various torches have been designed to offer several flame sizes. The only difference in their designs is the orifice size. Two nozzles with the orifice diameters of 280 µm and 400 µm were designed. Moreover, converging/diverging nozzles with a different combination of inside and outside hole diameters from 30 µm (the smallest) up to 150 µm (the largest) were designed and machined using femtosecond laser. It can be seen how fast and easy one can change nozzles and tune the machine for new flame conditions when considering the design of the system. Fig. 3 shows some of the manufactured nozzles. The smallest flame was achieved using a converging/diverging nozzle with an inside and outside orifice diameters of 30 µm and 75 µm respectively. Clean hydrogen was supplied into the nozzle to avoid pollution on the tapered fiber. Hydrogen at the pressure of 20 psi was injected into the tubes and nozzles. The width of the resultant flames of two nozzles at the heating zone, where fiber is positioned, was measured about 0.8 mm.

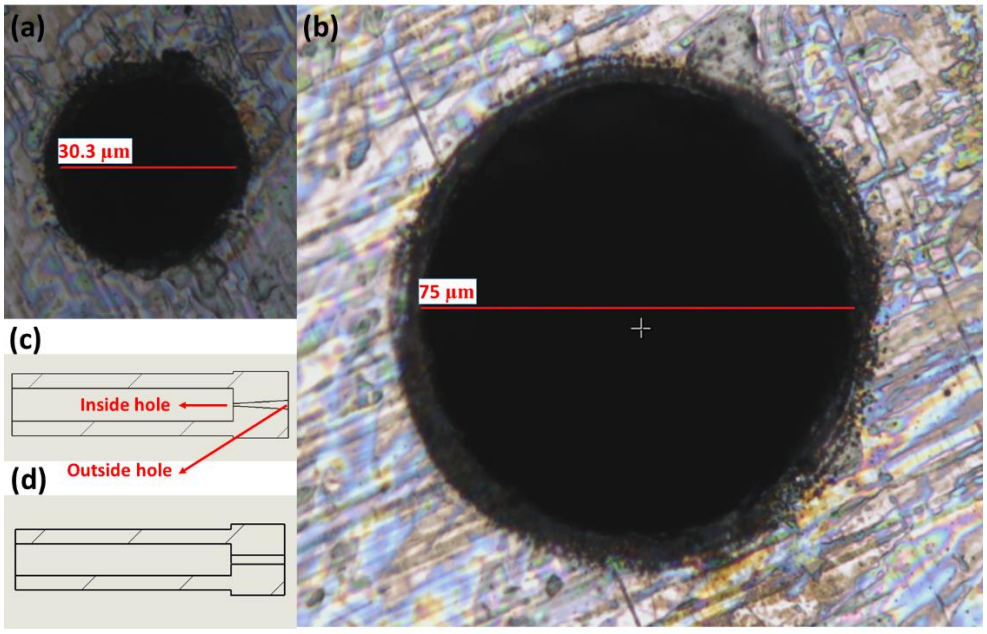

Fig. 3. (a & b) Smallest laser machined inside and outside holes with a diameter of 30 µm and 75 µm respectively, (b) (c) cross section of the converging/diverging nozzles, and (d) cross section of the fixed orifice nozzle (solid stream nozzle).

Fig. 4 shows a flame comparison between two nozzle designs. The flame temperature was controlled to exceed the softening point of fiber while it was not passing the melting point. For standard single mode fiber (SMF) and photonic crystal fiber (PCF), the required temperature of 900 °C and 1100 °C was found respectively for an adiabatic tapering.

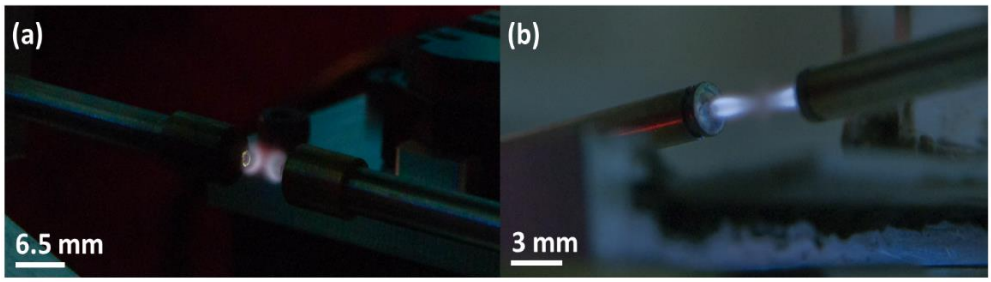

Fig. 4. (a) Flame with the fixed orifice nozzle, and (b) flame with converging/diverging micro nozzle.

2.2 Shutter Design

A novel deign aspect of this tapering machine is the flame shutter. It was determined that in order to have precise control over heat delivery, which is a critical parameter to taper fibers with low losses and uniform geometry, it is crucial to be able to turn on and off the heat in milliseconds. However, it was also found that because of micro-scale orifice sizes, that lead to a very small gas flow rate in the nozzle, it is impossible to shut down the flame in less than a few seconds. Therefore, a shutter mechanism was designed with ceramic plates that can slide back and forth to block and release the flame to the fiber. It is actuated by a HiTEC HS-7235MH servomotor to provide precise timing

control for turning on and off the heat. Fig. 5 illustrates some of the shutter components.

The shutter was integrated into the main control algorithm such that user can specify the opening and closing time of shutter independently. The opening time (delay) determines how many milliseconds before the pulling process starts the shutter will be opened and the closing time (delay) controls how many milliseconds before the pulling process stops the shutter will be closed. It can be observed that this is an important advantage especially for cutting the flame because it significantly reduces the fiber sag due to its weight. Therefore, cutting the flames a few milliseconds before the pulling process stops, provides a uniform taper and avoids bending of fiber because of gravitational force. Also, the significance of having the flame shutter is revealed when multi-cascade tapers are required periodically. Controlling the transferred heat with the shutter can provide an outstanding consistency in the geometry of the taper profiles.

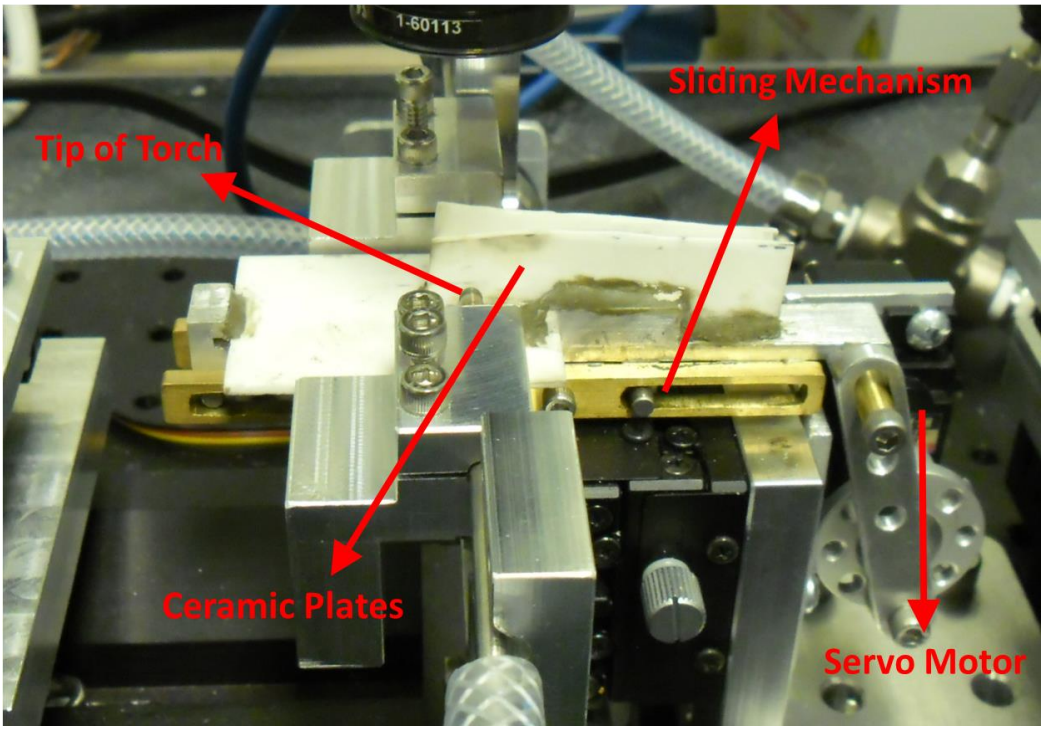

Fig. 5. Shutter mechanism and its components.

2.2 LabVIEW control and run sequence

A LabVIEW program was developed to control the tapering process. This program communicates with GSC-02 two axis stage controller from OptoSigma to send velocity, acceleration, position, and direction of rotation commands and to receive feedback about the current stage position while simultaneously controling the shutter servomotor via NI USB6001 DAQ. When the program runs, stages go to their home position waiting for a command to start. All the required parameters have to be set up by the user prior to selecting one of the tapering algorithms. For a conventional tapering velocity, acceleration, displacement of each motor, and shutter opening and closing time delay have to be selected and followed by hitting the run bottom.

3. Results and Discussion

Fig. 6 shows the tapered PCF Mach-Zehnder interferometer (MZI) sensors with various tapering angles. Tapering this type of fiber is challenging because of it is structure, which consists of an array of micron diameter air holes through the length of fiber. It is vital to preserve the air holes geometry and avoid collapsing any hole. Therefore, the importance of tapering under an adiabatic condition can be seen. Fig. 7 depicts the cross section of the PCF fiber before and after tapering. As can be seen, the holes are intact after tapering.

The fabricated MZI sensors for refractive index (RI) sensing were characterized by numerous RI values. The untapered MZI sensor showed a maximum RI sensitivity of about 172 nm/RIU between RI range of 1.3917 to 1.4204 while the tapered MZI sensor with the taper waist diameter of 50 μm and final sensor length of 8 mm had RI sensitivity of approximately 990 nm/RIU over the same RI range. The sharply tapered MZI sensor

with the waist diameter of 65 µm and final sensor length of 3.8 mm revealed the maximum sensitivity of about 1427 nm/RIU over the same RI range [96]. Fig. 8 describes the characterization results. Also, it can be noticed that the MZI sensor with larger taper waist diameter and sharper tapering angle showed higher RI sensitivity; although, in general the smaller the taper waist diameter, the higher the RI sensitivity. This result proved the significant impact of tapering angle on RI sensitivity of PCF MZI sensor. Therefore, miniature flames are required to taper fibers with sharper tapering angle.

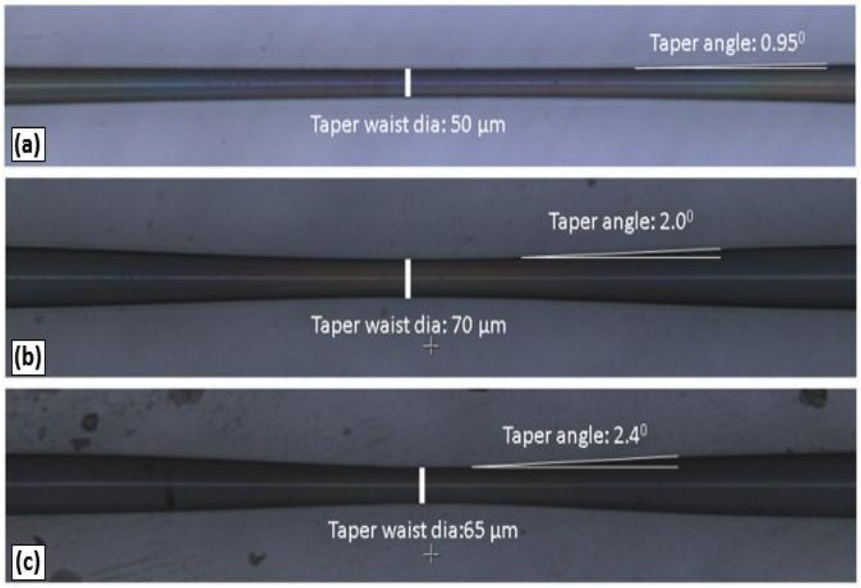

Fig. 6. (a) MZI sensor with the taper waist diameter of 50 µm and a taper angle of 0.95^0, (b,c) the taper diameter of 70 µm with a taper angle of 2^0 and the taper diameter of 70 µm with a taper angle of 2.4^0 were achieved using converging/diverging nozzles.

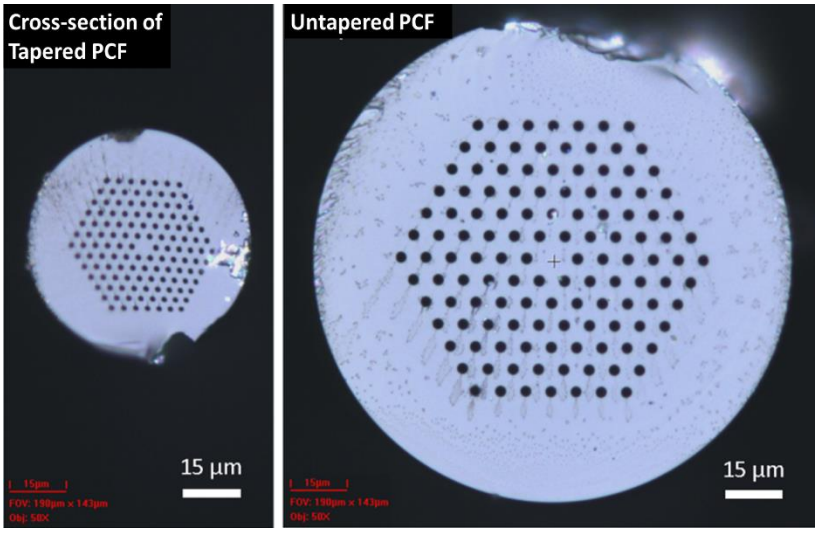

Fig. 7. Cross sections of the PCF showing before and after tapering of the fiber using fixed orifice nozzle flame. The cross section of the tapered fiber is taken at the waist region.

Fibers with various uniform waist diameters have been fabricated using the flame brushing technique. In this method, fiber is pulled from both ends while an oscillating flame heats a portion of the fiber. The limitation is the length of the hot zone generated by traveling flame because uniform heat distribution is essential for an adiabatic tapering. A process was developed to overcome this limitation by heating the fiber very locally with dual miniature flames while one stage pulls and the other one pushes the fiber at different rates. The more the motors can travel, the longer the length of microfiber. Fig. 9 displays the initial result of 20 mm microfiber fabrication.

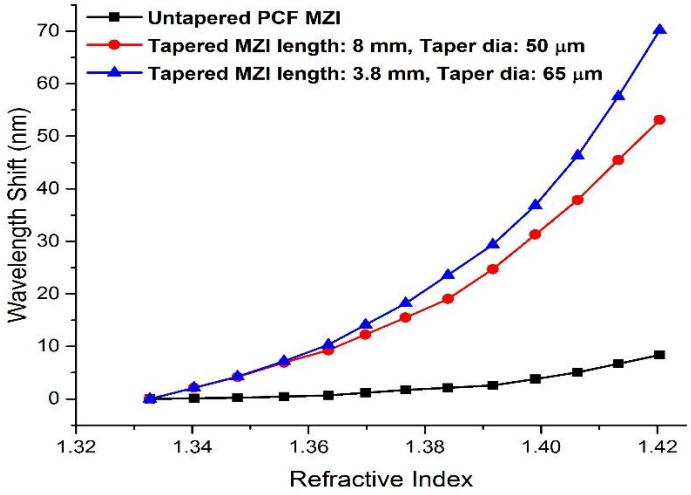

Fig. 8. The overall refractive index sensitivity plots for both untapered and tapered PCF based MZI sensor

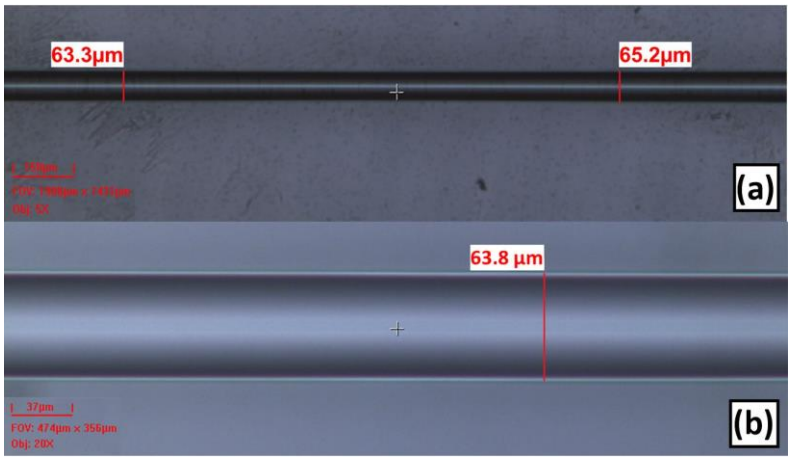

Fig. 9. (a) 20 mm Microfiber fabrication using "pull and push" method, (b) image of the same fiber with higher magnification.

4. Conclusion

In conclusion, we have shown the design and development of a unique flame-based tapering process that is capable of tapering optical fibers with a very short taper length. The machine was designed to work with two torches for miniature tapering. A PCF MZI sensor with initial length of ~ 2 mm that was fabricated by fusion splicing between two

stubs of SMF was tapered down from 125 µm to 65 µm. Its RI sensitivity increased about 44% compared to the one with initial sensor length of ~ 6 mm. An array of micro nozzles with various hole sizes thus many flame sizes was laser machined using a 120 femtosecond laser. A novel shutter mechanism was designed and incorporated into the process to provide an exceptional heat control. Besides, microfibers with uniform waist diameters were fabricated without oscillating the flame underneath the fiber. Instead, one stage pushed the fiber and the other one pulled it at a different rate, while two narrow flames were generating a pointy hot zone.

List of Publications

(https://scholar.google.ca/citations?hl=en&user=coPSLeQAAAAJ&view_op=list_works&sortby=pubdate)

1. **V. Ahsani**, F Ahmed, MBG Jun, C Bradley, *"Tapered Fiber-Optic Mach-Zehnder Interferometer for Ultra-High Sensitivity Measurement of Refractive Index"* in Sensors 19 (7), 1652, 2019. **(IF: 3.031)**
2. F Ahmed, **V Ahsani**, K Nazeri, E Marzband, C Bradley, E Toysekani, and MBG Jun, *"Monitoring of Carbon Dioxide Using Hollow-Core Photonic Crystal Fiber Mach–Zehnder Interferometer"* in Sensors 19 (7), 3357, 2019. **(IF: 3.031)**
3. K Nazeri, **V Ahsani**, F Ahmed, HE Joe, MBG Jun, and C Bradley*, "Experimental comparison of the effect of the structure on MZI fiber gas sensor performance",* in 2019 IEEE Pacific Rim Conference on Communications, Computers and Signal Processing (PACRIM)
4. F Ahmed, **V Ahsani**, S Jo, C Bradley, E Toyserkani, MBG Jun, *"Measurement of In-Fiber Refractive Index Change Using a Mach–Zehnder Interferometer",* IEEE Photonics Technology Letters 31 (1), 74-77, 2018. **(IF: 2.553)**
5. MBGJ Nazeri, K., **V. Ahsani**, F. Ahmed, P.C. Lee, *"Photonic Crystal Fiber Based Refractive Index Sensors"* in TechConnect World Innovation Conference and Expo, May 2017, Washington DC, USA.
6. **Vahid Ahsani**, Farid Ahmed, Junghyuk Ko, Colin Bradley, and Martin B.G. Jun, *"Miniature Dual Flame-based Tapering Process and System Development for Fabrication of Optical Fiber Sensors",* in international Conference on Micro Manufacturing (ICOMM 2017), March 2017, Kaohsiung,Taiwan.
7. Farid Ahmed, **Vahid Ahsani**, Martin BG Jun, *"Interferometric measurement of refractive index modification in a single mode microfiber"*, in Ultrafast Phenomena and Nanophotonics XXI, Feb 2017, SPIE Proceedings, San Francisco, USA.
8. Ko, J., **V. Ahsani**, S.X. Yao, N. Mohtaram, P.C. Lee, and M.B.G. Jun, *"Fabricating and Controlling PCL Electrospun Microfibers using Filament Feeding Melt Electrospinning Technique",* in Journal of Micromechanics and Microengineering, 27 (2), 025007, 2016. **(IF: 2.141)**
9. Farid Ahmed, **Vahid Ahsani**, Luis Melo, Peter Wild, and Martin B.G. Jun, *"Miniaturized Tapered Photonic Crystal Fiber Mach-Zehnder Interferometer for Enhanced Refractive Index Sensing"*, DOI: 10.1109/JSEN.2016.2566663, IEEE Sensors Journal, 2016. **(IF: 3.076)**
10. Farid Ahmed, **Vahid Ahsani,** Akram Saad, and Martin B. G. Jun, *"Bragg Grating Embedded in Mach-Zehnder Interferometer for Refractive Index and Temperature Sensing"*, IEEE PHOTONICS TECHNOLOGY LETTERS, VOL. 28, NO. 18, SEPTEMBER 15, 2016. **(IF: 2.553)**
11. PCL Ko, J., **V. Ahsani,** S.X. Yao, M.B.G. Jun, *"A Novel Fiber Processing Technology Based on Fused Deposition 3D Printing Combined with Melt Electrospinning"*, in 32nd International Conference of the Polymer Processing Society, July 2016, Lyon, France.
12. F. Ahmed, Y. Cho, K. Nazeri, **V. Ahsani**, P. C. Lee, and M. B. G. Jun, *"Refractive Index Sensing by Femtosecond Laser Fabricated Fiber Optic Sensors"*, 11th International Conference on Micro Manufacturing Orange County, California, USA, March 2016.